Universidade de Aveiro Departamento de Química
2009

LUCIANA
SARABANDO DA
ROCHA

ELÉCTRODOS DE FILME DE MERCÚRIO EM ESTUDOS DE ESPECIAÇÃO DINÂMICA DE METAIS

THIN MERCURY FILM ELECTRODES IN DYNAMIC SPECIATION STUDIES OF METALS

Universidade de Aveiro Departamento de Química
2008

LUCIANA SARABANDO DA ROCHA

ELÉCTRODOS DE FILME FINO DE MERCÚRIO EM ESTUDOS DE ESPECIAÇÃO DINÂMICA DE METAIS

THIN MERCURY FILM ELECTRODES IN DYNAMIC SPECIATION STUDIES OF METALS

Dissertação apresentada à Universidade de Aveiro para cumprimento dos requisitos necessários à obtenção do grau de Doutor em Química, realizada sob a orientação científica da Doutora Helena Maria Seixas Carapuça, Professora Auxiliar do Departamento de Química da Universidade de Aveiro e sob a co-orientação do Doutor José Paulo Soares Pinheiro, Professor Associado no Departamento de Química, Bioquímica e Farmácia, da Faculdade de Ciências e Tecnologia da Universidade do Algarve.

Dedico este trabalho em memória da minha professora, a Doutora Helena Carapuça, pelos seus ensinamentos e pelo incansável apoio.

o júri

presidente

Doutor João Manuel Nunes Torrão
Professora Catedrático da Universidade de Aveiro

Doutor Christopher Michael Ashton Brett
Professor Associado com Agregação da Faculdade de Ciências e Tecnologia da Universidade de Coimbra

Doutora Ana Maria Albuquerque Ferreira de Macedo Almeida Mota
Professora Associada com Agregação do Instituto Superior Técnico da Universidade Técnica de Lisboa

Doutor José Paulo Soares Pinheiro
Professor Associado da Faculdade de Ciências e Tecnologia da Universidade do Algarve

Doutora Maria Eduarda da Cunha Pereira
Professora Auxiliar da Universidade de Aveiro

Doutor Alessandro Gandini
Equiparado a Investigador Coordenador do Laboratório Associado do CICECO-Centro de Investigação de Materiais Cerâmicos e Compósitos da Universidade de Aveiro

agradecimentos

palavras-chave

Metais vestigiais, Especiação dinâmica, Eléctrodos de Filme Fino de Mercúrio (TMFE), Eléctrodos Modificados, Polímeros de Troca Catiónica, Voltametria de Redissolução Anódica (ASV), Cronopotenciometria de Redissolução (SCP), Cronopotenciometria de Redissolução por Varrimento (SSCP).

resumo

No presente trabalho, foi avaliado o desempenho e a aplicabilidade do eléctrodo de filme fino de mercúrio, em estudos de especiação dinâmica de metais vestigiais. Para tal, foram utilizadas duas técnicas electroanalíticas de redissolução: a clássica Voltametria de Redissolução Anódica (ASV) e a recentemente desenvolvida, Cronopotenciometria de Redissolução com varrimento do potencial de deposição (SSCP).

As propriedades de troca-iónica e de transporte de massa de películas mistas preparadas a partir de dois polímeros com características distintas, o Nafion (NA) e o 4-Poliestireno sulfonato de sódio (PSS), foram avaliadas, antes da sua aplicação no âmbito da especiação de metais. Estas películas de NA-PSS demonstraram uma elevada sensibilidade, reprodutibilidade, estabilidade mecânica, bem como, propriedades de anti-bloqueio adequadas na modificação química do eléctrodo de filme fino de mercúrio (TMFE) e, na sua aplicação na determinação de catiões metálicos vestigiais em amostras complexas, por ASV.
Para além disso, o desempenho de membranas do polielectrólito PSS em estudos de voltametria de troca-iónica (IEV) foi estudado. O objectivo desta investigação foi reunir as condições ideais na preparação de películas de PSS estáveis e com uma densidade de carga negativa elevada, de modo a aumentar a acumulação electrostática de catiões metálicos no filme polimérico e por conseguinte, conseguir incrementos no sinal voltamétrico.

O desempenho e aplicabilidade do TMFE em estudos de especiação de metais vestigiais foram extendidos à SSCP como técnica analítica. Dada a elevada sensibilidade e resolução evidenciada pelo TMFE, este revelou ser uma alternativa adequada aos eléctrodos de mercúrio convencionais, podendo ser utilizado durante um dia de trabalho, sem degradação aparente do sinal analítico de SCP. As curvas de SSCP obtidas experimentalmente utilizando o TMFE estavam em concordância com aquelas previstas pela teoria. Para além disso, a constante de estabilidade (K) calculada a partir do desvio do potencial de meia-onda, para dois sistemas metal-complexo lábeis, aproxima-se não só do valor teórico, como também daquele obtido utilizando o eléctrodo de mercúrio de gota suspensa (HMDE).
Adicionalmente, o critério experimental de labilidade inerente a esta técnica foi validado e o grau de labilidade para um dado sistema metal-complexo foi determinado, utilizando o filme fino de mercúrio depositado sob um eléctrodo rotativo (TMF-RDE). Este eléctrodo é muito útil na determinação de parâmetros cinéticos, como é o caso da constante de velocidade de associação (k_a), uma vez que as condições hidrodinâmicas, durante a etapa de deposição, se encontram bem definidas.

abstract

In the present work the performance and applicability of the thin mercury film electrode (TMFE) in the dynamic speciation of trace metals was investigated. Two different electroanalytical stripping techniques were used: the classical anodic stripping voltammetry (ASV) and a recent developed technique, scanning stripping chronopotentiometry (SSCP).

The ion-exchange and the mass transport features of novel mixed coatings of two sulfonated cation-exchange polymers with dissimilar characteristics, Nafion (NA) and poly(sodium 4-styrenesulfonate) (PSS) were evaluated, prior to its application in the field of trace metal analysis. Suitable NA-PSS polymer coatings could be used in the modification of TMFE, presenting a high sensitivity, reproducibility, mechanical stability and adequate antifouling properties in the ASV determination of trace metal cations in complex media.
Also the features of the PSS polyelectrolyte layers for ion-exchange voltammetry (IEV) were evaluated. The goal was to search for the best conditions to obtain stable PSS coated electrodes, which could present high negative charge densities in order to enhance the electrostatic accumulation of cations within the film, thus enlarging the ASV signal.

The applicability and performance of the TMFE in the trace metal speciation studies, by SSCP, were for the first time exploited. The optimized TMFE presented a high sensitivity and resolution, being an excellent complement to the conventional mercury electrodes and could be use for 1-day term with no significant variation in the SCP analytical signal and no apparent degradation. The calculated SSCP curves were in excellent agreement with experimental data at the TMFE and the stability constant (K), calculated from the shift in the SSCP half-wave potential, of two labile metal-complex systems were in good agreement with the ones obtained using the conventional Hanging mercury drop electrode (HMDE) and those predicted by theory .
Additionally, the experimental lability diagnosis inherent to the SSCP technique was validated and a rigorous quantification of the lability degree was made. Due to the well defined hydrodynamic conditions at the thin mercury film rotating disk electrode (TMF-RDE), during the deposition step, this electrode is quite valuable in the determination of kinetic parameters, like the association rate constants (k_a).

CONTENTS

CHAPTER 1   Introduction

CHAPTER 2   Incorporation, partition and transport features at Nafion/ Poly(sodium 4-styrenesulfonate) mixed coatings

CONTENTS

CHAPTER 3   Ion-exchange voltammetry with Nafion/ Poly(sodium 4-
styrenesulfonate) mixed coatings on mercury film electrodes

CONTENTS

CHAPTER 4   Modification of glassy carbon electrodes with Poly(sodium 4-styrenesulfonate): improvement of the experimental preparation conditions

CONTENTS

CONTENTS

Figure 1.1. Schematic representation of the reactions of a metal ion, M, with different types of aquatic constitutes.

Figure 1.2. Figure 1.2. Schematic representation of the characteristic regimes of metal complex systems as determined by the ratio between the time scale of the experiment, *t*, and the association/dissociation kinetics of the complex involved. k_a' denotes product between the association constant (k_a) and the concentration of the ligand; k_d is the dissociation rate constant; J_{kin} and J_{dif} denotes the contribution to the flux under purely kinetic and purely diffusion controlled conditions, respectively.

Figure 1.3. Schematic representation of: (A.) preconcentration of a favourably ion-exchange electroactive cation (blue circle), that exchanges with the electrochemically inert couter-ion (yellow circle) of the polyanionic film, (B.) exclusion of an organic molecule and (C.) exclusion of an anionic specie.

Figure 1.4. Chemical structure of acidic form of NA 115 monomeric unit and its equivalent mass weight (M_w).

Figure 1.5. Chemical structure of acidic form of PSS–Na$^+$ monomeric unit and its equivalent mass weight (M_w).

Figure 1.6. Schematic representation of the stripping signal obtained for direct current ASV (*I vs E*).

Figure 1.7. Schematic representation of the SCP *t, E* transient (---) and the ensuing *dE/dt vs E* peak (—). The transition time, τ, is indicated on the plateau of the *t,E* curve, and corresponds to the shaded area under the *dE/dt vs E* peak.

Figure 2.1. Incorporation of DA into the 9.2 μm NA-coated electrode: cyclic voltammograms in 1.00×10^{-4} mol dm^{-3} DA / pH 7.4 phosphate buffer (ionic strength 0.12_4 mol dm^{-3}) recorded in 5 min. time intervals. The first voltammogram was taken immediately after transferring the NA-coated electrode to the DA solution. Scan rate: 0.25 V s^{-1}. Inset: variation of the DA oxidation peak current with time.

Figure 2.2. Incorporation of DA (1.00×10^{-4} mol dm^{-3} at pH 7.4 phosphate buffer) into the 5.4 μm PSS-coated electrode: variation of the DA oxidation peak current with time. Experimental conditions as in Fig. 2.1.

Figure 2.3. Variation of the DA concentration in the 9.2 μm NA-film as a function of the DA concentration in the sodium phosphate electrolyte solution (ionic strength 0.12_4 mol dm^{-3}). The concentration of DA in solution used in this experiment range between [0-1.02×10^{-3}] mol dm^{-3}.

Figure 2.4. Calibration plot of DA concentration in NA-film *vs* DA concentration in the electrolyte solution, for a concentration of DA within the interval [0-4.86×10^{-5}] mol dm^{-3}.

Figure 2.5. Concentration of dopamine in the NA/PSS films, c_{DA}^{film}, as a function of $c_{DA}^{so\ln}$, the DA concentration in the phosphate electrolyte solution (ionic strength 0.12_4 mol dm^{-3}). Black markers: NA/PSS r_m 5.3, white markers: NA/PSS r_m 1.1. The concentration of DA in the solution used range between [0-5.05×10^{-4}] mol dm^{-3}.

Figure 2.6. Calibration plot of DA concentration in NA-film *vs* DA concentration in the electrolyte solution, for a concentration of DA within the interval [0-5.00×10^{-5}] mol dm^{-3}.

Figure 3.1. Mass loading characteristics of the ion-exchange NA/PSS films. The NA/PSS mixed coatings presents the following values for total mass loading: 5.1, 5.8 and 9.5 μg mm^{-2} for a mass ratio (r_m) of 27, 5.3 and 1.1, respectively.

Figure 3.2. Linear sweep voltammograms, normalized for concentration, for the oxidation of (A) cathecol, (B) uric acid ($\sim 1 \times 10^{-3}$ mol dm^{-3} solutions in pH 7.4 phosphate buffer) (C) dopamine (5×10^{-4} mol dm^{-3} solution in pH 7.4 phosphate buffer): GCE (a), NA/PSS; r_m 1.1 (b), NA/PSS; r_m 5.3 (c) and NA/PSS; r_m 27 (d). Scan rate 0.050 V s^{-1}.

Figure 3.3. Scanning electron micrographs ($\times 500$ or $\times 5000$) of different NA/PSS coatings on GGE: NA:PSS, molar ratios 27, 5.3 and 1.1. For r_m 5.3 and r_m 1.1 two micrographs are displayed (A and B) corresponding to different magnifications.

Figure 5.1. Evaluation of the SCP stripping regime for a TMFE (thickness 7.6 nm) by plotting: (A.) $I_s\tau$ *vs.* I_s (conditions of complete depletion), and (B.) $I_s\tau^{1/2}$ *vs.* I_s (conditions of semi-infinite linear diffusion) within the I_s interval of $[0\text{-}500]\times10^{-9}$ A. The transition times (τ) were measured in a solution of lead(II) (1.19×10^{-7} M in 0.01 M NaNO$_3$) and for a deposition time of 40 s.

Figure 5.2. Effect of the oxidizing current (I_s) in the SCP signal of Pb(II) (1.19×10^{-7} M in 0.01 M NaNO$_3$) for a TMFE (thickness 7.6 nm). Deposition time: 40 s. The data are plotted as: τ *vs* $1/I_s$ for I_s values ranging: (A.) $[5 - 500]\times10^{-9}$ A and (B.) $[20- 500]\times10^{-9}$ A.

Figure 5.3. Effect of the deposition time (t_d) in the SCP signal of lead (τ) at the TMFE (7.6 nm thickness) and for t_d values of: 20, 40, 60, 80, 100, 200 and 300 s at a deposition potential of -0.65 V. Calibration plot (A.) and SCP signals for t_d within the interval of $[20\text{-}100]$ s (B.). Experiments performed in 0.01 M NaNO$_3$ using a Pb(II) concentration of 1.19×10^{-7} M and a I_s of 75×10^{-9} A.

Figure 5.4. Variation of the SCP signal (τ) as a function of the concentration of Pb(II) at the TMFE (7.6 nm thickness), for a Pb(II) concentration (x10^{-9} M): 15, 45, 60, 89, 120, 240, 360. Calibration plot (A.) and respective SCP signals (B.) for a concentration range $[0\text{-}240]\times10^{-9}$ M. The experiments were performed in 0.01 M NaNO$_3$ using t_d of 40 s and a I_s of 75×10^{-9} A.

Figure 5.5. SCP signal (τ) for repeated measurements (N'=60) in a test solution of $1.19\text{x}10^{-7}$ mol dm^{-3} of lead(II) in 0.01 mol dm^{-3} NaNO$_3$, at the TMFE (7.6 nm thickness). The other experimental conditions used were: $I_s = 75\times10^{-9}$ A and t_d of 40 s.

Figure 5.6. Experimental (diamonds) and fitted (full line) SSCP waves for a Pb(II) concentration of 1.19×10^{-7} M at the TMFE (thickness of 7.6 nm). Experimental data was obtained in 0.1M NaNO$_3$ media at a pH 3.4, using the following SCP experimental parameters: t_d=40 s and I_s=7.5×10^{-8} A.

Figure 5.7. Log analysis of the experimental SSCP wave (♦ and ◊) for Pb(II) at the TMFE (data presented in figure 5.6). The slope for experimental SSCP curve was determined in the steepest region (♦). Dashed line on the SSCP wave indicates the region of the steepest slope at the foot of the wave.

Figure 6.3. Experimental ($\bullet$, $\Diamond$) and fitted (full line) SSCP waves for Cd(II) and Cd(II)-NTA system at pH 8 at the TMFE (thickness of 9.1 nm). Experimental curves were measured for a Cd(II) concentration of 4.75×10^{-7} mol dm^{-3} in the absence ($\bullet$) and presence of 2.23×10^{-6} mol dm^{-3} nitriloacetic acid ($\Diamond$) in 0.1 mol dm^{-3} NaNO$_3$, using the following SCP experimental parameters: t_d=80 s and I_s=7.5$\times10^{-8}$ A. Other parameters: E^0 in the interval [-0.376;-0.374] V, n=2, V_{Hg}=2.82$\times10^{-14}$ m^3, D_M= D_{ML}=7.19$\times10^{-10}$ m^2 s^{-1}, δ_M=4.44$\times10^{-5}$ m and v=9.78$\times10^{-4}$ m^2 s^{-1}.

Figure 6.4. Experimental ($\bullet$, $\Diamond$) and fitted (lines) SSCP waves for Pb(II) and Pb(II)-IDA assuming a fully labile (dash line) and quasi-labile system (full line) at pH 5.5 at the TMFE (thickness of 9.1 nm). Experimental curves were measured for a Pb(II) concentration of 1.19×10^{-7} mol dm^{-3} in the absence ($\bullet$) and presence of: (A.) 2.44×10^{-5} mol dm^{-3}, (B.) 3.75×10^{-4} mol dm^{-3} and (C.) 2.82×10^{-3} mol dm^{-3} iminodiacetic acid ($\Diamond$) in 0.01 mol dm^{-3} NaNO$_3$. The SCP experimental parameters used were: t_d=80 s and I_s=7.5$\times10^{-8}$ A. Other parameters: E^0 in the interval [-0.386;-0.381] V, n=2, V_{Hg}=2.82$\times10^{-14}$ m^3, D_M=9.85$\times10^{-10}$ m^2 s^{-1}, δ_M=4.44$\times10^{-5}$ m, D_{ML}=7.19$\times10^{-10}$ m^2 s^{-1} and v=9.78$\times10^{-4}$ m^2 s^{-1}.

Figure 6.5. Log analysis of the experimental SSCP wave at the TMFE (data presented in Fig. 6.4) for Pb(II) ($\bullet$) and for Pb-IDA complex, using the following ligand concentrations: 3.75×10^{-4} mol dm^{-3} ($\Diamond$) and 2.82×10^{-3} mol dm^{-3} ($\blacklozenge$). Other conditions as indicated in Fig. 6.4.

Table 6.3. Stability constants (mean values) of the Cd-NTA and Pb-IDA systems, obtained at the TMFE using different experimental conditions: pH, ionic strength (I) and total ligand concentration. All the experiments were performed in $NaNO_3$ media, for concentrations of Cd and Pb of 4.75×10^{-7} mol dm^{-3} and 1.19×10^{-7} mol dm^{-3}, respectively.

Table 6.4. Degree of lability and association rate constants obtained at the TMF-RDE for the system Cd-NTA. Other conditions as indicated in Fig. 6.3.

 Table 6.5. Degree of lability and association rate constants obtained at the TMF-RDE for the system Pb-IDA using different concentrations of the ligand. Other conditions as indicated in Fig. 6.4.

Table 6.6. Degree of lability and association rate constants obtained at the TMF-RDE for the system Pb-IDA at pH 6.0 and using a concentration of 2.82×10^{-3} mol dm^{-3}. Other conditions as indicated in Fig. 6.4.

Abbreviations

ASV - Anodic Stripping Voltammetry

BSA - Bovine Serum Albumine

CME - Chemically Modified Electrode

C - Cathecol

DA - Dopamine

DOC - Dissolved Organic Carbon

EDS - Electron Dispersive Spectroscopy

GC - Glassy Carbon

GCE - Glassy Carbon Electrode

HMDE - Hanging Mercury Drop Electrode

HYA - Hyamine

MFE - Mercury Film Electrode

IDA - Iminodiacetic acid

LOD - Limit of detection

MES - 2-(N-morpholino-ethanesulfonic acid)

NA - Nafion

NA/PSS - Nafion/ Poly(sodium 4-styrenesulfonate) mixed coating

NTA - Nitriloacetic acid

 PDCA - Pyridine-2,6-dicarboxilic acid

PSS - Poly(sodium 4-styrenesulfonate)

RDE - Rotating Disk Electrode

SCP - Stripping Chronopotentiometry

SDS - Sodium Dodecyl Sulphate

SEM -Scanning Electron Microscopy

SSCP - Scanning Stripping Chronopotentiometry

SWASV - Square-Wave Anodic Stripping Voltammetry

TMFE - Thin Mercury Film Electrode

TMF-RDE - Thin Mercury Film deposited in the Rotating Disk Electrode

UA - Uric Acid

Symbols

A - Area of the mercury film

c_{DA}^{film} - Concentration of DA in the polymeric film

$c_{DA}^{MAX(film)}$ - Total concentration of ion-exchange sites in the polymeric film

$c_{DA}^{so\,ln}$ - Concentration of DA in the solution

C_{Hg} - Concentration of the metal in the mercury amalgam

C_{L}^{*} - Ligand concentration in the bulk solution

$c_{L,t}$ - Total concentration of the ligand L

$c_{L,t}^{*}$ - Total concentration of L in the bulk solution

c_{M}^{*} - Metal Concentration in the bulk solution

$C_{M^0}^{0}$ - Concentration of reduced metal at the electrode surface

$C_{M,t}^{0}$ - Concentration of the total metal ion at the electrode surface

c_{M}^{0} - Metal surface concentration

$c_{M,t}$ - Total concentration of the metal M

c_{ML}^{*} - Bulk concentration of the complex ML

cO_{pol}^{m+} - Concentration of the analyte in the polymeric phase

cO_{sol}^{m+} - Concentration of the analyte in the solution phase

C_{Pb} - Concentration of lead

D - Diffusion coefficient in solution

$\overline{D}$ - Mean diffusion diffusion coefficient

D_{app} - Apparent diffusion coefficient

D_{M} - Diffusion coefficient of the free metal ion M

D_{ML} - Diffusion coefficient of the complex species ML

E - Potential

E_{clean} - Potential applied during a cleaning step

E_{i} - Initial potential

E_{f} - Final potential

E_{d} - Deposition potential

$E_{d,1/2}$ - Half-wave deposition potential

E_p - Peak potential

E^0 - Standard potential

I_p - Peak current of the metal

I_d^* - Limiting value of the deposition current

$I_{d,M+L}^*$ - Limiting value of the deposition current for the complex ML

I_s - Oxidizing current

J_{dif} - Flux for the ML system under diffusion controlled conditions

J_{free} - Flux for the inert ML system

J_{kin} - Flux for the ML system under kinetic controlled conditions

J_{lab} - Flux for the labile ML system

K - Stability constant

k_a - Rate constant of complex association

k_D - Distribution coefficient

k_d - Rate constant of complex dissociation

K_{os} - Stability constant for the formation of the outer-sphere complex

k_{-w} - Stability constant for the removal of water from the inner coordination sphere

l - Thickness of the mercury film

M_w - Equivalent mass weight

n - Number of transferred electrons

n' - Number of polymeric coated electrodes

n_α - Number of electrons transferred up to, and including the rate determining step

N - Number of experimental points

N' - Number of repeated measurements

$N_{deposited}$ - Number of moles deposited

Q - Electric charge

Q_{Hg} - Charge associated to the deposited mercury

p - Hydrodynamic parameter

r_{Hg} - Hg atomic radius

r_m - Mass ratio

T – Temperature

t – Time

t_d - Deposition time

v - Stripping rate

v_{rot} - Speed of rotation

$V_{Hg\,dep}$ - Volume of the thin film mercury electrode

$w_{1/2}$ - Peak half-width

Greek Symbols

τ - Transition time

τ_d - Characteristic time constant of the deposition process

τ^* - Limiting value for the transition time

τ^*_{M+L} - Limiting transition time for the complex ML

$\tau^*_{ML,kin}$ - Limiting transition time for the kinetically controlled ML system

$\tau^*_{ML,lab}$ - Limiting transition time for the labile ML case

τ^*_{freeM} - Limiting transition time for the amount of free metal in the system

α - Proportional

α_c - Transfer coefficient for the rate determining step

δ_M - Diffusion layer thickness

$\overline{\delta}$ - Mean diffusion layer thickness

ω - Angular speed rotation

υ - Viscosity coefficient of the solution

θ - Free metal surface concentration ratio

$\Delta E_{d,1/2}$ - Shift in the half-wave potential

μ - Mobility and mean lifetime of a given free metal

Constants

F - Faraday constant (96485 C mol^{-1})

R - Gas constant (8.314472 J K^{-1} mol^{-1})

CHAPTER 1

Introduction

CHAPTER 1   Introduction

1.1. Metal speciation in aquatic systems

1.2. Trace metal dynamic speciation

1.3. Analytical techniques in trace metal speciation

1.4. Electrochemical stripping techniques

      1.4.1. Thin mercury film electrodes in stripping analysis

      1.4.2. Chemically modified electrodes in stripping analysis

      1.4.3. Anodic Stripping Voltammetry

      1.4.4. Stripping Chronopotentiometry

      1.4.5. Scanning Stripping Chronopotentiometry

1.5. Outline of this thesis

1.1. Metal speciation in aquatic systems

A major category of globally-distributed pollutants are the heavy metals. These are natural elements that have been extracted from the earth and harnessed for human industry and products. They are notable for their wide environmental dispersion from such activity and their tendency is to accumulate in select tissues of the human body [1]. Perhaps the most important features which distinguish metals from other toxic pollutants are that they are not biodegradable and that, once they have entered in the environment, their potential toxicity is controlled by their physicochemical form [2].

In natural waters only a small portion of the overall dissolved metal may be presented as free hydrated cations because metal ions forms stable complexes with a large variety of inorganic and organic ligands, which influence the bioavailability, toxicity and mobility of the metal. Therefore, the total metal concentration in a water sample is rarely adequate to interpret the reactivity of the metal in biological or environmental processes. Metal speciation is a well-known term used for the determination of the distribution of metal ions over different chemical and/or physical forms, and for the distribution itself, and this, is the real key to a better understanding of the metal availability to the biota in aquatic media [3].

Among the different types (physico-chemical) of metal species present in natural waters, the following ones should be taken into consideration [3,4]:

- Hydrated free metal ion
- Dissolved inorganic complexes
- Dissolved organic complexes
- Metal species in the form of dispersed colloids
- Metal species adsorbed on a variety of colloidal particles or suspended matter

All of these species co-exist (Fig. 1.1), hence, the prediction of the metal ion distribution in these systems may be quite complicated. With respect to the bioavailability of (heavy) metals, knowledge of their speciation is of great significance, both from the viewpoint of their essentiality for various life forms, which is the case for e.g. zinc,

potassium and cadmium, and with respect to their toxicity, as in the case of e.g. cadmium and lead. The toxic effects of heavy metals may be reduced in the presence of complexing agents, since, under these conditions, the metals may be less available to the organisms [5].
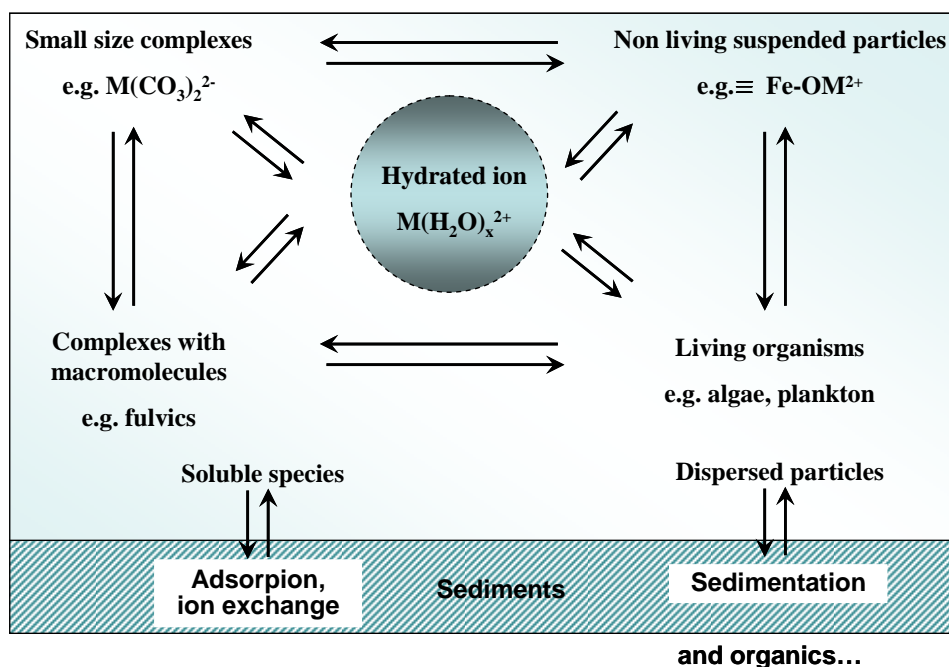
Figure 1.1. Schematic representation of the reactions of a metal ion, M, with different types of aquatic constitutes [4].

Given that each of these species behaves differently in terms of mobility and bioavailability, the aquatic systems are subject to changing conditions and practically never reach chemical equilibrium. This renders the study of metal speciation much more complicated, since it makes necessary a rigorous quantitative understanding of the metal speciation in the aquatic medium to elucidate the relationships between the different physicochemical forms and reactivities, mobilities and bioavailabilities in the biological and environmental process, i.e. kinetic features of the metal complex species interconversion [3].

In fact, the term speciation, strictly refers to the proportion of each species (M, ML_1, ML_2,…) with respect to the total concentration of M, that includes the complexes of M with the binding sites present in suspended particles or dissolved ligands. However, to

measure the distribution of M amongst its chemical species, requires the prior determination of the properties of certain species, such as [4]:

♦ size, electric charge, structure and hydratation degree;
♦ molecular diffusion coefficients;
♦ thermodynamics and kinetic constants.

The experimental determination of trace metal equilibrium and dynamic speciation in natural waters is a very difficult task because of the very low concentrations to be measured on attempting to resolve component species. Therefore, very sensitive methods are required and there is a high risk of contamination, alteration and/or adsorption losses. The ideal speciation method would be sufficiently sensitive and selective to be used directly on natural water samples, would involve minimal perturbation of the samples and would furnishing signal directly dependent on the (chemical) reactivity of the element of interest [2,6].

1.2. Trace metal dynamic speciation

The understanding of the kinetic features of the interconversion of metal complex species, is fundamental for establishing a rigorous quantitative basis for the relationship between metal ion speciation, bioavailability and biouptake, and thus for establishing the foundations for dynamic risk assessment [7,8,9].

Considering the formation of a 1:1 metal complex, ML, between the electroactive metal ion M and the ligand L:

$$\text{M+L} \underset{K_d}{\overset{K_a}{\rightleftharpoons}} \text{ML}$$
$$\big\downarrow\big\uparrow n\bar{e}$$
$$\text{M}^0$$

(1.1)

The rate constants are related with the stability constant of the complex ML, K (m^3 mol^{-1}), by:

$$K = c^*_{ML}/(c^*_M c^*_L) = k_a/k_d \qquad (1.2)$$

where c^*_i denotes the bulk concentration (mol m^{-3}) of the species i.

The association rate constant can be defined, under conditions of sufficient ligand excess ($c^*_{L,t} >> c^*_{M,t} \rightarrow c^*_L \approx c^*_{L,t,}$, where $c^*_{L,t}$ and $c^*_{M,t}$ are the total ligand and metal concentrations in the bulk, respectively), as [7,9]:

$$k'_a = k_a c^*_{L,t} \text{ and } K' = k'_a/k_d = K c^*_{L,t} \qquad (1.3)$$

The rate constant of complex formation, k_a (m^3 mol^{-1} s^{-1}) is generally consisted with a mechanism in which the formation of an outer-sphere complex between the metal and the ligand, with an electrostatically determined stability constant, K_{os} (m^3 mol^{-1}), is followed by a rate-limiting removal of water from the inner coordination sphere of the metal, k_{-w} (s^{-1}), commonly known as the Eigen mechanism. According to this mechanism, the overall association rate constant is defined by:

$$k_a = k_{-w} K_{os} \qquad (1.4)$$

For a given complex system, the value of K_{os} is usually estimated on the basis of the Debye-Hückel electrostatic for the charge interaction metal-ligand [9,10].

The complexes can be considered dynamic or static (inert), depending on whether they are able to dissociate/associate within the timescale of the technique. The contribution of dynamic complexes for the overall metal flux towards the electrode depends on the relative magnitudes of the diffusive and kinetic fluxes, which can change from fully labile (diffusion control) to non-labile (kinetic control), Fig. 1.2 [7].
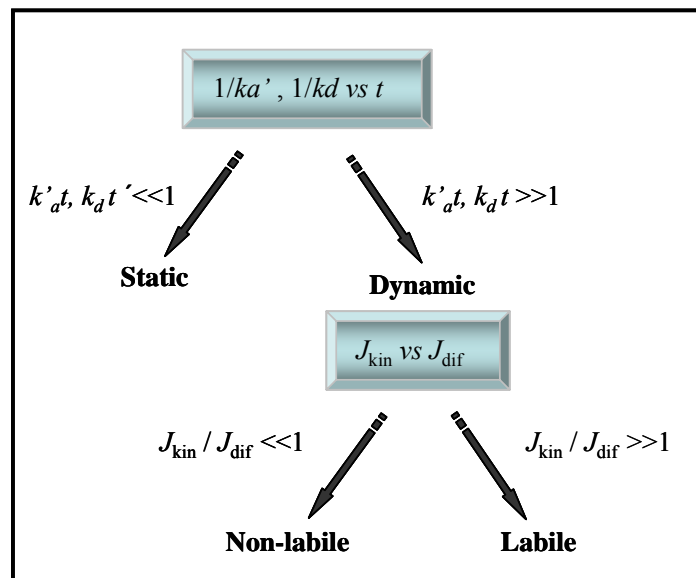
Figure 1.2. Schematic representation of the characteristic regimes of metal complex systems as determined by the ratio between the time scale of the experiment, t, and the association/dissociation kinetics of the complex involved. k_a' denotes product between the association constant (k_a) and the concentration of the ligand; k_d is the dissociation rate constant; J_{kin} and J_{dif} denotes the contribution to the flux under purely kinetic and purely diffusion controlled conditions, respectively [8].

1.3. Analytical techniques in trace metal speciation

The ideal speciation method would be sufficiently sensitive and selective to be used directly on natural water samples, would involve minimal perturbation of the samples and would furnishing signal directly dependent on the (chemical) reactivity of the element of interest [2,6].

Techniques can be divided into main categories [3,4]:

i)   Techniques that detect total metal concentrations but with no inherent speciation capabilities and, as a result, they must be coupled with separation techniques to allow de detection of different species;

ii)   Techniques that detect some operationally defined fractions of the total metal, i.e. the free (reactive) metal ion and physicochemical parameters

(diffusion coefficient, stability and kinetic complexation constants), and do not require the sample pre-treatment (avoids the contamination and/or losses of trace constituents).

The separation techniques described in point i) are based on the fractionation of the sample by size (e.g. filtration/ultrafiltration and gel filtration) or by size and charge (e.g. dialysis, ion-exchange and solvent extraction) [3,4]. The Permeable Liquid Membrane (PLM) and Donnan Membrane Technique (DMT) are two examples of these separation methods. The PLM technique is based on the pre-concentration of the analyte (target elements or species) from the source into a strip solution. In the case of DMT the discrimination between species is primarily based on their charge and the measurement is typically made after equilibrium has been attained, but recent developments also consider a faster steady-state flux-based mode [8]. Both techniques must be coupled with sensitive detectors (low limits of detection) in the determination of metal ion concentrations. In the case of DMT, the graphite furnace atomic absorption spectroscopy (GF-AAS) is currently used, whilst the PLM technique is coupled with the inductively coupled plasma atomic emission spectrometry (ICP-AES) and the inductively coupled plasma mass spectrometry (ICP-MS) [11].

Among the techniques mentioned in point ii) are the electrochemical techniques, which can be subdivided in two classes:

♦ *Techniques that are based on thermodynamic processes*: such as the traditional equilibrium speciation method of ion selective electrodes potentiometry (ISE), which measure directly the free metal ion activity. In the past, the use of most polymer membrane ISEs, in trace metal speciation complexation in natural waters, was limited by the lower detection limits in the micromolar range [2,3,4]. Recently, a new generation of ISE's was developed by Pretchs *et al*., in which the detection limits were improved, by controlling the inner solution [12].

♦ *Techniques that are dynamic in nature*: where the analytical signals contains direct speciation information on both the thermodynamic stability and kinetic lability of metal complex species [13]. Examples of these are the electrochemical stripping methods, the

ones being extremely sensitive and highly suitable in multi-element analysis [2,3,4,6]. This work relies on the use of these techniques in the speciation studies of trace metals and for that reason, they will be further described in the following chapter.

1.4. Electrochemical stripping techniques

The electrochemical stripping techniques essentially comprises two steps: deposition and quantification. The first or deposition step involves the electrolytic deposition of a small portion of the metal ions into the working electrode, usually the mercury electrode. This step is followed by the stripping (measurement) step, where the metals are dissolved ("stripped") from the deposit [14,15]. Their remarkable sensitivity is attributed to the combination of a pre-concentration step with advanced measurements procedures that generates a particularly favourable signal-to-background ratio. Therefore, the detection limits of these techniques can be lowered by 2 or 3 orders of magnitude at concentrations levels down to 10^{-10} M [2,3,4,6,14].

Different versions of stripping analysis can be employed, depending upon the nature of the deposition and measurement steps [14]. Examples of these electrochemical stripping methods are: anodic stripping voltammetry (ASV) and stripping chronopotentiometry (SCP), which are dynamic in nature and thus, are able to provide kinetic data information [8]. The understanding of the kinetic features of the interconversion of metal complex species, is fundamental for establishing a rigorous quantitative basis for the relationship between metal ion speciation, bioavailability and biouptake, and thus, for establishing the foundations for dynamic risk assessment [8,7,9]. The ASV and SCP techniques will be further described in the following sections.

Mercury electrodes play a central role in the success of stripping analysis, due to its highly reproducible, smooth and readily renewable surface. There are several types of mercury electrodes, like the hanging mercury drop electrode (HMDE), the thin mercury film electrode (TMFE) and the mercury microelectrodes. This work will focus on the application of the TMFE [14,16].

1.4.1. Thin mercury film electrodes in stripping analysis

The TMFE is particularly attractive in stripping analysis due the higher surface-to-volume ratio exhibited, when compared with the HMDE. Consequently, the pre-concentration is more efficient, resulting in an improvement in the sensitivity. Besides, due to the small volume and thickness of the TMFE, the stripping step follows thin-layer behaviour, and depletion effects predominate. The total exhaustion of thin mercury films results in sharper peaks and hence improved peak resolution in multicomponent analysis [14,16].

In what concerns TMFEs their use may be quite complicated due to the eventual irreproducibility of the mercury film morphology, to the incomplete removal of the film at the end of an experiment or even to the formation of insoluble mercury(I) compounds. Also, mechanical deterioration had been reported after excessive hydrogen evolution during deposition in acidic solutions and lack of stability during the experimental course [17,18,19]. Recently, a simple preparation procedure was developed, where the pre-plating of the thin mercury coatings (in-situ and ex-situ produced) was performed by a single electrodeposition step of high overpotential, in acidic solutions with or without the thiocyanate anion (depending on the solution pH). The result was the formation of homogeneous and stable mercury deposits of high reproducibility [20].

The application of the thin mercury film deposited over a glassy carbon electrode (CGE), in speciation studies of trace metals by ASV is widespread [2]. In SCP and SSCP speciation studies, the mercury electrodes currently used are the hanging mercury drop electrode (HMDE) and the mercury microelectrode over a supporting iridium micro-disk. There are some disadvantages associated with these electrodes when performing speciation studies, namely the ill-defined hydrodynamic regime during the deposition step for the HMDE and the lower sensitivity of the mercury microelectrode. So far, the application of a micrometer tick MFE, in SCP experiments was only reported by Serrano *et al.* [21]. Despite of the well defined hydrodynamic conditions during the deposition step and the wide range of oxidation currents that could be applied (with the total depletion of the

metal), there were significant disadvantages, namely the lack of reproducibility and a complex preparation procedure [21,22].

1.4.2. Chemically modified electrodes in stripping analysis

One of the most common problems in stripping techniques, when applied to the direct analysis in natural aquatic media, is the interference effects caused by organic constituents of the sample matrix. Adsorption of surface-active compounds onto the working electrode can interfere with the diffusional transport of the analyte and usually results in peak depression. Additionally, adsorption/desorption processes of organic compounds can yield tensammetric peaks which can interfere with or be mistaken for the metal peaks. Obviously, these effects hinder data interpretation, since the analytical signal is not a reliable representation of the speciation in sample solution and this is very problematic in speciation analysis, where sample pre-treatment must be kept to a minimum [23,24,25].

The deliberate alteration of the electrode surface, through the incorporation of an appropriate surface modifier, can meet the needs of several electroanalytical applications. There are different directions by which the chemically modified electrodes (CME's) can benefict, including the acceleration of electron-transfer reactions, preferential accumulation or selective membrane permeation. Such steps can impart higher selectivity, sensitivity or stability to the electrochemical devices. One of the most common approaches for the incorporation of a modifier onto the surface, has been with an appropriate polymer film, often prepared by casting a solution containing the dissolved polymer onto the surface and allowing the solvent to evaporate [14].

A special attention has been given to negatively charged (polyanionic) polymers, where the discrimination properties are on the basis of charge, i.e. positive or neutral species will be incorporated, while anions are excluded [14]. A schematic representation of these phenomena is given in Figure 1.3.

Electrode   Polyanionic film   Solution

Figure 1.3. Schematic representation of: (A.) pre-concentration of a favourably ion-exchange electroactive cation (blue circle), that exchanges with the electrochemically inert couter-ion (yellow circle) of the polyanionic film, (B.) exclusion of an organic molecule and (C.) exclusion of an anionic specie [26].

Also the advantage of coating the electrode surface with a thin film of an ion-exchange polymer lies in the possibility of exploiting the ion-exchange equilibrium taking place at the polymer-solution interface as a way of non-faradaic pre-concentration of electroactive counter-ions. The preconcentrating capability of the coating is ruled by the ion-exchange equilibrium between the electroactive counter-ion (analyte) and nonelectroactive counter-ions present in solution or already incorporated into the coating. In the case of a cation-exchange polymer the following ion-exchange reaction is operative:

$$O^{m+} + m(P^-X^+) \rightleftarrows P_m^-O^{m+} + mX^+ \tag{1.5}$$

where, P^- is the ion-exchange sites in the polymer, $\mathbf{X^+}$ is the electrochemically inert counter-ion (again, for simplicity we examine a monocharged cation, which generally is the supporting electrolyte cation) and O^{m+} is the multiply charged electroactive counter-ion (analyte).

The pre-concentration ability of the coating is ruled by the partitioning of the O^{m+} between the solution and polymer phases, that in the case of trace amounts of the analyte, is expressed quantitatively by the distribution coefficient k_D:

$$k_D = \frac{cO^{m+}_{pol}}{cO^{m+}_{sol}} \tag{1.6}$$

where cO^{m+}_{pol} and cO^{m+}_{sol} is the concentration (mol dm^{-3}) of the analyte in the polymeric and solution phase, respectively. Since O^{m+} is an electroactive specie, it can be reduced at the polymer-electrode interface according to reaction (1.6) and a voltammetric signal is correspondingly recorded:

$$(\text{P}^-)_m\text{O}^{m+} + n\bar{\text{e}} + n\text{X}^+ \leftrightarrow (\text{P}^-)_{(m-n)}\text{O}^{(m+n)}\text{ X}^+) + n(\text{P}^-\text{X}^+) \tag{1.7}$$
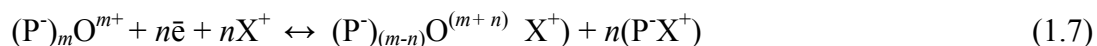
Besides the above mentioned considerations on the ion-exchange features and from the occurrence of short range molecular interactions between the polymer matrix and the target species, the actual mass transport features of analyte throughout the polymer layer, play an important role. Regardless of the actual mechanism of mass transport, the rate of the electrode reaction obeys Fick's laws of diffusion and may be characterized by the apparent diffusion coefficient, D_{app} (cm2 s^{-1}), which in most cases differs from the diffusion coefficient for the species in solution, thus influencing the magnitude of the electrochemical signal [27].

To achieve suitable ion-exchange features for polymeric coating requires the control of the film thickness, since mass transport limitations can arise, leading to a decrease in the sensitivity in the analytical determinations. This depends mainly on the size of the analyte but also on the morphologic properties of the coating [28,29].

Examples of these cation-exchange polymers are: the ionomer Nafion, the most commonly used in ASV determinations of trace metals studies [27,30,31,32,33,34,35,36], and most recently, the polyelectrolyte poly(sodium 4-styrenesulfonate) [37,38].

i) Nafion

Nafion is constituted by a population of hidrophylic nanoclusters, which include the ionized sulfonate groups, its counter-ion and hydration water/electrolyte ions, randomly distributed into a hydrophobic phase of the Nafion fluorinated backbone (Fig. 1.4) [39]. This structural conformation contributes to the rigidity and insolubility of Nafion. The ion-

exchange capacity of Nafion is about four times smaller than that for other typical sulfonate resins, which is related with the rather low content of ion-exchange groups of this ionomer [25,29,39]
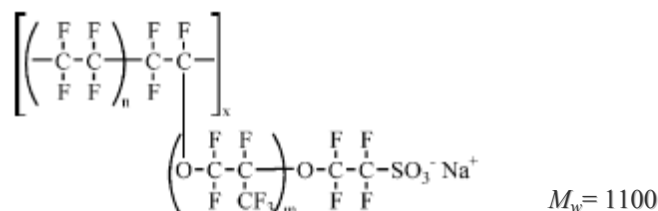
$M_w = 1100$

Figure 1.4. Chemical structure of acidic form of NA 115 monomeric unit and its equivalent mass weight (M_w) [29].

This polymer is chemically inert, nonelectroactive, hydrophilic and insoluble in water, thus it presents almost ideal properties for the modification of electrode surfaces [25,29]. However, the easier coating procedure, performed by recasting from a solution without adding any casting solvents, often present lack of reproducibility [23,32]. This may be related to the internal structure of the film, which is very difficult to control [23].

ii) PSS

Poly(sodium 4-styrenesulfonate) is a water soluble, thermally stable polyelectrolyte [40], with both hydrophilic parts (sulfonate groups and their counterions) and hydrophobic parts (hydrocarbon backbone and phenyl groups) . The chemical structure of this polymer is displaced in Fig. 1.5.
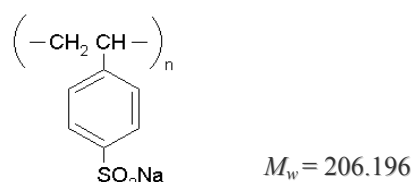
$M_w = 206.196$

Figure 1.5. Chemical structure of acidic form of PSS–Na^{+} monomeric unit and its equivalent mass weight (M_w) [29].

In pure water PSS presents a linear conformation [41] but highly coiled structures are observed in ionic solutions or in coatings whenever deposition proceeds from solutions

of relatively high ionic strength e.g., 0.1 – 2 M, due to shielding of the polyelectrolyte charges [42,43]. The considerable film charge density evidenced by these polyelectrolyte films leads to an effective accumulation of metal ions. Electrostatic effects have long been recognised as a major contribution to metal binding, at least since Manning [44] introduced the concept of "counterion condensation" which treats the counterions as being in strong correlation with the macromolecule ionic groups in the case of strong polyelectrolytes.

The main advantage of ionomers over polyelectrolytes is their higher insolubility in the aqueous media generally used for the determinations. However, as a drawback the volume concentration of ion-exchange groups for ionomer coatings is much lower than in typical polyelectrolytes. Although being water soluble, PSS was successfully used to coat a glassy carbon/thin mercury electrode (GC/TMFE) and applied to the square-wave anodic stripping voltammetry (SWASV) of trace metals in estuarine waters. No leakage of PSS was detected within a one-day work [37,38].

1.4.3. Anodic Stripping Voltammetry

Anodic stripping voltammetry (ASV) is the most widely used form of stripping analysis. In this case, the metals are preconcentrated by cathodic deposition at a controlled time and potential, into a small volume mercury electrode (a thin mercury film or a hanging mercury drop). The metal ions reach the electrode by diffusion or convection, where they are reduced and concentrated as an amalgam [14,45]:

$$M^{n+} + n\bar{e} + Hg \rightarrow M(Hg) \tag{1.8}$$

The concentration of the metal in the amalgam, C_{Hg} (mol m^{-3}) is given by the Faraday law, that in the case of the mercury film electrode (the working electrode of interest in this thesis), MFE, is expressed by:

$$C_{Hg} = \frac{2.7RTI_p}{n^2F^2vA\,l} \tag{1.9}$$

where I_p (A) is the peak current of the metal, v (V s^{-1}) is the stripping rate and A (m^2) and l (m) are the area and the thickness of the mercury film, respectively. The total amount of metal plated represents a small (and yet reproducible) fraction of the total metal present in the bulk solution [14].

In the second step, i.e. the stripping step, the potential is scanned anodically (linearly or in a more sensitive pulse waveform), where the amalgamated metals are reoxidized, i.e. stripped out from the electrode (the deposition scan applied depends on the standard potential of each metal) [14,45]:

$$M(Hg) \rightarrow M^{n+} + n\bar{e} + Hg \tag{1.10}$$

The analytical signal (Fig 1.6.) is expressed by the peak current, which depends upon various parameters of the deposition and stripping steps, as well on the characteristics of the metal ion in solution and on the electrode geometry.
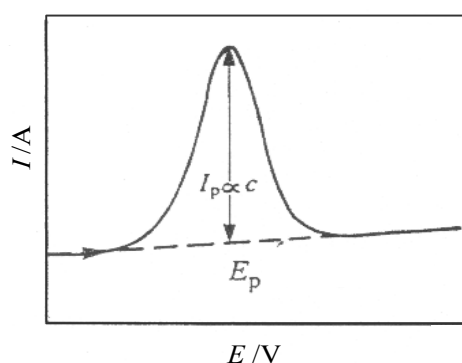
Figure 1.6. Schematic representation of the stripping signal obtained for direct current ASV (*I vs E*) [46].

In the case of the mercury film electrode, the electrode used in the present work, the peak current is given by:

$$I_p = \frac{n^2 F^2 v^{1/2} A l C_{Hg}}{2.7 RT} \tag{1.11}$$

For very thin mercury films, the diffusion in the film can be ignored and the peak current is directly proportional to the scan rate.

Different voltammetric waveforms can be employed during the stripping step, including linear scan, differential pulse, square-wave, staircase, or alternating-current operations. Anodic stripping voltammetry when combined with square-wave stripping mode offers not only a compensation against the charge current contributions, but also a significant speed advantage and a better resistance against dissolved oxygen. Such ability to conduct trace metal determinations in the presence of dissolved oxygen is attributed to the fast scanning ability [14,45].

Several problems have been reported in the ASV determinations of trace metals in environmental matrices containing high levels of organic matter, mainly due to the adsorption of different species onto the electrode surface. This, hinder data interpretation, since the analytical signal, that is altered or even suppressed, is not a reliable representation of the speciation in sample solution [14,47,48]. Some techniques have been proposed to minimize the interferences in ASV determination, in particular, coating the mercury film electrode with a thin permselective membrane, which prevents the diffusion of interfering compounds towards the voltammetric sensor surface, i.e. excludes the fouling material by size exclusion and/or electric charge exclusion [23]. A compromise between the exclusion of the organic matter and the unhindered transport of the metal ions is required and this is obviously dependent on the thickness of the membrane used [25].

Although, the modification of the electrode surface in a reproducible and well-characterised manner, it is not always possible. In addition, since most of the materials used are negatively charged, they confer some ill defined ion-exchange character on the electrode, which may perturb the original equilibria and further confound data interpretation [13].

Additionally, depressions in the stripping peaks of interest may occur from the formation of intermetallic compounds between metals (e.g. Cu-Zn and Cu-Cd) deposited in the mercury electrode [14,45]. These effects are much more serious with the mercury films than with hanging drops, because MFE's feature fairly concentrated amalgams and a high

ratio of substrate area to film volume [16]. Also the resolution of overlapping peaks with similar potentials (e.g. Tl/Cd, Sn/Pb and Bi/Cu) can be a problem in ASV determinations of metals. Many strategies are available to successfully avoid both these problems, including the preferential formation of another intermetallic compound, the selective masking of an interfering metal or a rigorous choice of the deposition potential [45].

1.2.4. Stripping Chronopotentiometry

Stripping chronopotentiometry (SCP) is also a two step technique. The first (deposition) step is the same as that for stripping voltammetry (Eq. 1.8), but the quantification of the accumulated metal is achieved by chronopotentiometry, i.e., the application of a constant oxidizing current, I_s, and following the variation of potential with time. Thus, the analytical signal is the time taken to reoxidize the amalgamated metal, i.e. the transition time, τ. In order to simplify the transition time determination the original E/t data is derivered (dE/dt format) (Fig.1.7). The area under the peak in such plots corresponds to the time taken for the oxidation process, while the area under the baseline is the time of the double-layer charging [49].
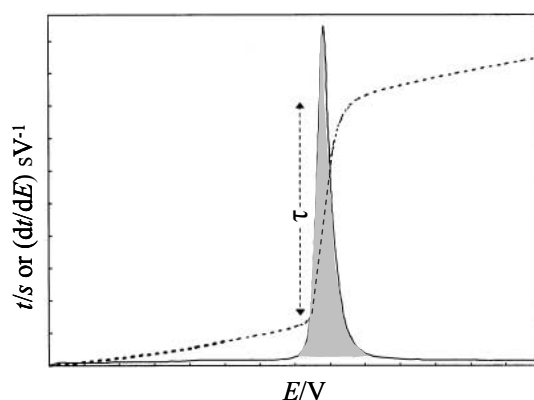
Figure 1.7. Schematic representation of the SCP t,E transient (---) and the ensuing dE/dt vs E peak (—). The transition time, τ, is indicated on the plateau of the t,E curve, and corresponds to the shaded area under the dE/dt vs E peak [50].

The SCP measurements can be performed under two different time regimes, depending on the stripping current magnitude. At low applied oxidizing currents,

reoxidation occurs slowly and practically all of the accumulated metal is fully depleted from the electrode ($I_s\tau$ constant, $\tau \propto C$). The resulting analytical signal is relatively large [49]. Under these conditions, SCP is a straightforward application of the Faraday's law and yields a direct relationship between the analytical signal and the concentration of the species in the sample [51]. For larger stripping currents, conditions approach to those of semi-linear diffusion ($I_s\tau^{1/2}$ constant, $\tau \propto C^2$), i.e., the stripping step is incomplete and the post-peak baseline is influenced by the ongoing faradaic process that follows incomplete depletion of the mercury electrode (the HMDE and the mercury microelectrode over a supporting iridium micro-disk are the currently used electrodes in SCP studies) [49]. In this work only the depletion mode will be used.

For improving sensitivity in SCP (depletion mode) low stripping currents must be used. In this situation, a significant contribution of traces of dissolved oxygen to the metal oxidation may occur, leading to a decrease in SCP transition time. This can be explained by the competition between the chemical oxidation of the metal reduced in the amalgam promoted by the oxygen and the electrochemical oxidation by the application of a constant oxidizing current. This problem can be minimised applying relatively large oxidation currents, producing not too long transition times [21,49]. Therefore, there must be a careful selection in the oxidizing current applied in SCP experiments.

SCP is a valuable alternative to ASV. The main advantage of SCP over ASV is the capacitive charge discrimination, by measuring the area under the dt/dE vs E peak that allows the elimination of adsorption complications [49,52]. The use of the peak area in SCP under conditions of full depletion provide the correct measure of the analytical signals in those cases where peak broadening arises from heterogeneity of metal complexes and/or adsorption of organic matter on the electrode surface during the stripping step [52,53].

1.4.5. Scanning Stripping Chronopotentiometry

Despite of the advantages of SCP when compared with other stripping techniques, the relation between the peak parameters (peak potential, E_p, and peak half-width, $E_{1/2}$) and the metal speciation in the bulk solution (thermodynamic stability and kinetic lability of the metal complex species) are not straightforward [13,54]. These limitations associated with reliable determination of stripping peak parameters for individual depletive SCP stripping curves, at any t_d, can be overcome by constructing curves from the transition time measured as a function of deposition potential, E_d (i.e., the only information taken from a given measurement is the stripping peak area). We denote this technique as scanned deposition potential SCP (SSCP) [50,55]. The detection limit of depletive SSCP is comparable to that of pulsed stripping voltammetric modes [9].

SSCP curves (plots of τ vs E_d) are inherently rich in information, providing data on the stability distribution spectrum and, if applicable, on the corresponding fraction of the rate constant distributions [50,55,56]. The most important development is that the complex stability constant can be calculated from the shift in the half-wave deposition potential ($\Delta E_{1/2}$) irrespective of the degree of lability, while the variation in the limiting transition time in the presence and in the absence of complex ligands will provide information about the lability and diffusion coefficients of the metal species in solution [9].

The theoretical basis of this technique considering the following aspects: metal only case, labile metal complexes and the kinetic current regime and respective limits, will be discussed on chapter 5 and 6 of this thesis. This explanation will be restricted to the thin mercury film electrode (TMFE) deposited in a carbon rotating disk electrode, the working electrode used in the present work.

1.5. Outline of this thesis

Dynamic metal speciation analysis remains a challenging problem since very few techniques combine the potential to perform dynamic speciation and high sensitivity. The electroanalytical methods, in particular ASV and most recently SSCP, fulfil these requirements [57,58]. The aim of the present study is to investigate the applicability of the thin mercury film electrode (TMFE) in the dynamic speciation of trace metals, using the previous techniques. The content of the different chapters are given below.

This thesis is organized in three parts. The first part consists in the introduction (chapter 1), where a general approach on the importance of the dynamic speciation studies of trace metals, in aquatic media, is given and also on the electroanalytical techniques that can be used to provide this information. The second one (chapter 2, 3, 4, 5 and 6) presents the several issues exploited and investigated in this work, each of them with a brief introduction, the chemicals and methods used, the results and its interpretation and finally the conclusions. The third and last part (chapter 7) presents a general conclusion of the global work and some issues that would be relevant to investigate in the future.

Following this general introduction, chapter 2, 3 and 4 focuses on the development of polymeric membranes, suitable to coat a glassy carbon/thin mercury film electrode and applied to the square-wave anodic stripping voltammetric determination of trace lead in aquatic media. Chapter 5 and 6 explores the applicability, the performance and the potentialities of the thin mercury film electrode in the trace metal speciation studies, by a recent developed technique, SSCP.

Chapter 2, assesses the ion-exchange and the mass transport features of dopamine (positively charged specie) within cationic exchange polymers of dissimilar characteristics, nafion (NA), poly(sodium 4-styrenesulfonate) (PSS) and novel mixed coatings of this two sulfonated polymers (different mass ratios). The main objective was to understand some of the semi-permeability properties of film coated electrodes, prior to its application in the field of trace metal analysis.

Chapter 3 describes the preparation and characterization of the NA/PSS mixed coatings, produced by solvent evaporation onto glassy carbon electrodes. The effects of the NA/PSS mass on the perm-selectivity (inclusion and exclusion) properties towards different charged species and on the morphologic features of these films were evaluated. Also, the analytical performance of the TMFE plated throughout the NA/PSS coatings, with different mass ratio, was evaluated based on the reproducibility, the sensitivity and the anti-fouling features in the square-wave anodic stripping voltammetric determination of trace lead. Finally, the efficiency of the NA/PSS modified TMFE, was tested in a real sample, i.e. was applied in the SWASV detection of trace metals of untreated polluted estuarine water.

In chapter 4, the properties of an adsorbed layer of PSS coatings assembled on glassy carbon/thin mercury film electrodes were studied. Due to the highest content of sulfonic groups in these polyelectrolyte coatings, when compared with the Nafion ionomer and the NA/PSS mixed films, the electrostatic effect created by the considerable film charge density leads to an effective accumulation of metal ions in polyelectrolyte films. Therefore, the influence of the composition of the PSS solution, the amount of deposited PSS, molecular weight and of the ionic strength of the external solution electrolyte on the features of the PSS coatings for ion-exchange voltammetry was studied. The goal was to search for the best conditions for the production of stable and with high negative charge densities PSS coated electrodes, in order to obtain the maximum electrostatic accumulation of divalent metal cations within the film, thus enlarging the voltammetric signal.

Chapter 5 investigate the features of the TMFE, in studies of metal ion speciation by SCP/SSCP and elucidates the complementary information that it can provide. Prior to its application in the SCP/SSCP experiments, the thickness of the mercury film was optimized, in order to produce a mechanically stable TMFE. Afterwards, the SCP complete depletion regime was established and the experimental conditions were optimized (oxidizing current, deposition time and metal concentration). The TMFE was used for the first time in SSCP experiments, where the repeatability and reproducibility of SSCP experimental waves has been evaluated. Finally, the applicability and the viability of the results obtained in the determination of metal speciation parameters, like the stability

constant (K), of two metal-complex systems, i.e. Pb(II)-carboxylated latex nanospheres and Pb(II)-pyridine-2,6-dicarboxylic acid, at the TMFE was assessed.

Chapter 6 explores the potentialities of the thin mercury film rotating disk electrode (TMF-RDE) in SSCP trace metal dynamic speciation studies, to fully take advantage of the well defined hydrodynamic features of this electrode. The mechanical stability of the working electrode to the application of higher rotation speeds in the RDE was studied, by evaluating the repeatability of the SSCP experimental waves in the course of the experiments. The experimental lability diagnosis inherent to the SSCP technique was validated at the TMF-RDE and a rigorous quantification of the lability degree was made. The classical and well known cadmium(II)-nitriloacetic acid (Cd-NTA) system was used to critically evaluate the potential of SSCP, in the determination of association rate constant (k_a) values in the kinetic current regime and, than extended to the lead(II)- iminodiethanoic acid (Pb-IDA) complex.

References

[1] E. Berman, Toxic metals and their analysis, Heyden & Son Ltd, ch. 1, 1980.

[2] T. M. Florence, Talanta 29-5A (1982) 345.

[3] Tessier and D. R. Turner, *Metal Speciation and Bioavailability in Aquatic Systems*, John Wiley & Sons, 1995, vol. 3, chap. 5.

[4] J. Buffle, Complexation Reactions in Aquatic Systems, Ellis Horwood, Chichester, 1988.

[5] N. Corp, A. J. Morgan, *Environ. Pollut.* 74 (1991) 39

[6] A. M. Ure and C. M. Davidson, *Chemical Speciation in the Environment*, Blackie Academic & professional, Chapman & Hall, 1995, chap. 2.7.

[7] J. P. Pinheiro, H. P. van Leeuwen, *J. Electroanal. Chem.* 570 (2004) 69

[8] H. P. van Leeuwen, R. M. Town, J. Buffle, Rob. F. M. J. Cleven, W. Davison, J. Puy, W. H. van Riemsdijk, L. Sigg, *Environmental Science & Technology*, 39-22 (2005) 8545.

[9] H. P. van Leeuwen, R. M. Town, *J. Electroanal. Chem.* 561 (2004) 67.

[10] F. M. M. Morel, J. G. Hering, *Principles and Applications of Aquatic Chemistry*, Wiley, New York, 1993, pg. 400.

[11] A. D. Skoog, F. J. Holler, T.A. Nieman, *Principles of Instrumental Analysis*, (5th Ed.), Sauders College Publisihing, ch. 10-11, 1994.

[12] A. Ceresa, T. Sokalski, E. Pretsch, *J. Electroanal. Chem.* 501 (2001) 70.

[13] R. M. Town, H. P. van Leeuwen, *J. Electroanal. Chem.* 523 (2002) 1.

[14] J. Wang, *Analytical electrochemistry*, VCH Publishers Inc., 1994, chap. 2.5.

[15] T. M. Florence, *Analyst* 111 (1993) 489.

[16] A. J. Bard, L.R. Faulkner, *Electrochemical Methods: Fundamentals and Applications* (2nd ed.), John Wiley & Sons, Inc., New York, 2001, chap. 11-12.

[17] W. Frenzel, *Anal. Chim. Acta* 273 (1993) 123.

[18] J. Wang, B. Greene, *Anal. Chim. Acta* 144 (1982) 137.

[19] E. Sahlin, D. Jagner, R. Ratana-ohpas, *Anal. Chim. Acta* 346 (1997) 157.

[20] S.C.C. Monterroso, H. M. Carapuça, J. E. J. Simão, A. C. Duarte, *Anal. Chim. Acta* 503 (2004) 203.

[21] N. Serrano, J. M. Díaz-Cruz, C. Ariño, M. Esteban, *J. Electroanal. Chem.* 560 (2003) 105.

[22] D. Jagner, M. Josefson, S. Westerlund, *Anal. Chem.* 53 (1981) 1406.

[23] M.- L. Tercier, J. Buffle, *Anal. Chem.* 68 (1996) 3670.

[24] G. E. Batley, T. M. Florence, *Electroanal. Chem. and Interf. Electrochem.* 55 (1974) 23.

[25] B. Hoyer, T. M. Florence, G. E. Batley, Anal. Chem. 59 (1987) 1608.

[26] R. W. Murray, A. G. Ewing, R. A. Durst, *Analytical Chemistry* **59** (1987) 379.

[27] P. Ugo, L. M. Moretto, *Electroanalysis* 7 (**1995**) 1105.

[28] M. N. Szentirmay, C. R. Martin, *Anal. Chem* 56 (**1984**) 1898-1902

[29] M. W. Espenscheid, A. R. Ghatak-Roy, R. B. Moore, R. M. Penner, M. N. Szentirmay, C. R. Martin, J. Chem Soc., Faraday Trans. 1, 82 (1986) 1051.

[30] P. Ugo, L.M. Moreto, F. Vezzá, *Chem.Phys.Chem* 3 (2002) 917.

[31] C. M. A. Brett, D. A. Fungaro, J. M. Morgado, M.H. Gil, *J. Electroanal. Chem*. 468 (1999) 26.

[32] M. E. R. Dam, K. N. Thomsen, P. G. Pickup, K. H. Schroder, *Electroanalysis*, 7 (1995) 70.

[33] M. Buckova, M.Vanickova, J. Labuda, *Chem. Papers*, 50 (1996) 279.

[34] F-M. Matysik, S. Matysik, A. M. O. Brett, C. M. A. Brett, *Anal. Chem*. 69 (1997) 1651.

[35] J. Murimboh, T. M. Lam, M. N. Hassan, C. L. Chakrabarti, *Anal. Chim. Acta* 423 (2000) 205.

[36] H. –J. Kim, K. –S. Yun, E. Yoon, J. Kwak, *Electrochim. Acta* 50 (2000) 4471.

[37] S. C. C. Monterroso, H. M. Carapuça, A. C. Duarte, *Electroanalysis* 15 (2003) 1878.

[38] S. C. C. Monterroso, H. M. Carapuça, A. C. Duarte, *Talanta* 64 (2005) 644.

[39] A. Vishnyakov, A.V. Neimark, *J. Phys. Chem. B* 104 (2000) 4471.

[40] Sigma-Aldrich On-Line Catalogue, Product No. 243051 (CAS number 257 04-18-1).

[41] N. J. Turro, T. Okubo, *J. Phys. Chem*. 86 (1982) 1485-1487.

[42] Y. Lvov, R. Price, B. Gaber, I. Ichinose, *Colloids and Surf. A: Physicochem. Engineer. Aspects* 198 (2002) 375

[43] J. Ruths, F. Essler, G. Decher, H. Riegler, *Langmuir* 16 (2000) 8871.

[44] G. S. Manning, *J.Chem.Phys*. 51 (1969) 924.

[45] P. T. Kissinger, W. R. Heineman, Laboratory techniques in electroanalytical chemistry (2nd ed.), Marcel Dekker Inc., 1993, chap. 24.

[46] C. M. Brett e A. M. Brett, *Electroquímica, Princípios, Métodos e Aplicações*, Oxford Univ. press, 1993, chap. 14.

[47] M. L. Tercier, J. Buffle, *Anal. Chem.* 68 (1996) 3670.

[48] G. E. Batley, T. M. Florence, *Electroanal. Chem. and Interf. Electrochem.* 55 (1974) 23.

[49] R. M. Town, H. P. van Leeuwen, *J. Electroanal. Chem.* 509 (2001) 58.

[50] H. P. van Leeuwen, R. M. Town, *Environ. Sci. Technol.* 37 (2003) 3945.

[51] H. P. van Leeuwen, R. M. Town, *J. Electroanal. Chem.* 535 (2002) 1.

[52] H. P. van Leeuwen, R. M. Town, *J. Electroanal. Chem.* 523 (2002) 16.

[53] R. M. Town, H. P. van Leeuwen, *J. Electroanal. Chem.* 523 (2002) 1

[54] R. M. Town, H. P. van Leeuwen, *J. Electroanal. Chem.* 535 (2002) 11.

[55] H. P. van Leeuwen, R. M. Town, *J. Electroanal. Chem.* 536 (2002) 129.

[56] R. M. Town, H. P. van Leeuwen, *J. Electroanal. Chem.* 541 (2003) 51.

[57] R. F. Domingos, M. F. Benedetti, J. P. Pinheiro, *Anal. Chim. Acta* 589 (2007) 261.

[58] R. M. Town, H. P. van Leeuwen, *Electroanalysis* 16 (2004) 458.

CHAPTER 2

Incorporation, partition and transport features at Nafion/Poly(sodium 4-styrenesulfonate) mixed coatings

CHAPTER 2   Incorporation, partition and transport features at Nafion/Poly(sodium 4-styrenesulfonate) mixed coatings

2.1. Introduction

2.2. Experimental section

    2.2.1. Apparatus

    2.2.2. Reagents and solutions

    2.2.3. Electrode conditioning procedure

    2.2.4. Electrode preparation

    2.2.5. Voltammetric procedures

2.3. Results and Discussion

    2.3.1. Determination of incorporation isotherms of NA-, PSS- and NA/PSS- mixed films

    2.3.2. Distribution coefficients and diffusion features of NA-, PSS- and NA/PSS- films

2.4. Conclusions

2.1. Introduction

The evaluation of the ion-exchange and the mass transport features is essential to understand some of the semi-permeability properties of film coated electrodes [1], prior to its application in the field of trace metal analysis (*cf.* Chapter 3). For that reason, the data on the incorporation, partition and transport of dopamine (DA) within cationic exchange polymers, specifically NA-, PSS- single coatings and also novel mixed coatings of this two sulfonated polymers, NA/PSS- mixed coatings (different mass ratios), are provided in the present chapter.

2.2. Experimental section

2.2.1. Apparatus

All the voltammetric measurements were performed with a BAS 100B/W electrochemical analyser (Bioanalytical Systems) connected to a Cell Stand BAS-C2. The working electrode was a glassy carbon disc (BAS, MF-2012; 3 mm diameter), the auxiliary electrode was a Pt wire and the reference electrode was Ag/AgCl (sat. KCl). A combined glass electrode (Orion 9104SC) connected to a pH meter (Cole Parmer, Model 05669-20) was used for pH measurements.

2.2.2. Reagents and solutions

Nafion perfluorinated ion-exchange resin, NA (5 wt. % solution in a mixture of lower aliphatic alcohols and water) and Poly(sodium 4-styrenesulfonate), PSS (M_w 70,000; degree of sulfonation 1.0) were purchased from Sigma-Aldrich and used as received. All chemicals were of analytical reagent grade and all solutions were prepared with ultra-pure water (18.2 MΩ cm, Milli-Q systems, Millipore-waters). Stock solutions of NA (39.7×10^{-3} mol dm^{-3} in monomer units) were prepared in phosphate buffer solution (0.022 mol dm^{-3} NaH$_2$PO$_4$ / 0.041 mol dm^{-3} NaH$_2$PO$_4$, pH 7.4, ionic strength 0.12$_4$ mol dm^{-3}) and stored at 4 ºC. Dopamine standard solutions (approximately 5.000 $\times 10^{-4}$ or 5.000 $\times 10^{-3}$ mol dm^{-3})

were also prepared in phosphate buffer. Biohit Proline pipettes equipped with disposable tips were used for appropriate dilutions.

2.2.3. Electrode conditioning procedure

The glassy carbon electrode (GCE) was conditioned following a reported polishing/cleaning procedure [2]. The GCE was polished with an alumina slurry (grain size 0.3 μm, Metrohm) and sonicated in pure water for 60 seconds, to obtain a renewed electrode surface. Then, an electrochemical pre-treatment was carried out with a multicycle voltammetric scanning (50×) between -0.8 and +0.8 V at 0.1 V s^{-1}, in NH$_4$Ac-HCl solution. These polishing and electrochemical pre-treatments were repeated daily.

The electrochemically active surface area of the glassy carbon electrode, (7.192 ± 0.065) mm^2, was measured by chronoamperometry in 9.854 × 10^{-4} mol dm^{-3} ferricyanide/1.0 mol dm^{-3} KCl solution (3 polishing experiments, each one with 4 replicate determinations).

2.2.4. Electrode preparation

The NA coatings on the GCE were obtained by the droplet evaporation method, by application of 3 μL of the NA 39.7×10^{-3} mol dm^{-3} polymeric solution directly on the electrode surface and evaporating the solvent under a low flux warm air stream (*ca.* 60ºC).

The PSS and NA single coatings on the GCE were obtained by the droplet evaporation method [3], by application of 5 and 3 μL, correspondingly, of the polymeric solution (30 m mol dm^{-3} in monomeric units for PSS and 40 m mol dm^{-3} in monomeric units for NA) directly on the electrode surface. Then, the solvent was evaporated under a low flux warm air stream (*ca.* 60ºC). The film thickness was estimated using the recast density of 1.58 g cm^{-3} [4,5,6,7] and 0.801 g cm^{-3} [8] in monomeric units for Na and PSS, respectively. As a result the film thickness (calculated by the ratio between the loading of the polymeric coating and its density) was of 11 μm (corresponding to mass loadings of

18.2 µg mm^{-2}) and 5.4 µm (mass loadings of 4.30 µg mm^{-2}) for NA and PSS, correspondingly.

For assembling the NA-PSS mixed coatings, a 25×10^{-3} mol dm^{-3} NA ethanolic solution was mixed with suitable amounts of 120×10^{-3} mol dm^{-3} PSS solution in order to obtain different NA/PSS mass ratios, r_m, (5.3 and 1.1), maintaining the NA volume constant (Table 2.1). A 3 µL microdroplet was then applied on the electrode surface and the solvents were evaporated as mentioned above.

Table 2.1. Loading characteristics of NA and PSS coatings on GC electrodes, with an electrochemically active surface area of 7.192 mm^2.

Mass loading (µg mm^{-2})		Mass ratio (NA/PSS)	Total mass loading (µg mm^{-2})
PSS	NA		
0.92	4.9	5.3	5.8
4.6	4.9	1.1	9.5

2.2.5. Voltammetric procedures

The incorporation of DA (1.00×10^{-4} mol dm^{-3}, in pH 7.4 phosphate buffer, ionic strength 0.12$_4$ M) into the NA, PSS and NA/PSS films (r_m 5.3 and 1.1) was assessed firstly by successively recording the cyclic voltammograms of DA for selected time intervals. All voltammetric experiments were carried out in 10 mL of pH 7.4 sodium phosphate buffer solution and the solutions were purged with nitrogen for 5 min prior to the voltammetric experiments.

The determination of DA concentration incorporated in the several NA, PSS and NA/PSS coatings was done by measuring the electric charge due to the oxidation of DA by exhaustive electrolysis conducted at a constant potential of +0.6 V, for *ca.* 1 h. (i.e. until the electrolysis current reached 0.05 % of its initial value). The polymeric films were initially equilibrated in an unstirred DA solution (in pH 7.4 phosphate buffer, ionic strength 0.12$_4$ mol dm^{-3}) for an equilibration time ranging from 25 and 30 min for DA

solution concentrations above 10^{-5} mol dm^{-3} and for 24h and 12h for the lower concentrations, for the NA single and NA/PSS mixed coatings, respectively. Then, the electrode was removed from the equilibration solution, briefly rinsed with pure water and placed in the electrochemical cell containing merely the supporting electrolyte (a diluted pH 7.4 phosphate buffer, ionic strength 0.025 mol dm^{-3}, no added DA). The charges for DA were all corrected from blank values obtained by exhaustive electrolysis experiments conducted at the same experimental conditions. No DA was detected in the electrolyte solution, meaning that ejection of the incorporated species did not occur in the present time scale, under the application of a constant positive potential. Measurements were carried out at room temperature (18-20 ºC).

2.3. Results and Discussion

2.3.1. Determination of incorporation isotherms of NA-, PSS- and NA/PSS- mixed films

At the working pH of 7.4 dopamine (pK_b= 8.87) is a cationic specie, that is electroactive at the glassy carbon electrode (GCE) within the potential window [0.2 V; +1 V] [9]. Protonated dopamine (DA$^+$) is incorporated into the negatively charged polymeric films (both NA and PSS) *via* ion-exchange reaction with the polymer Na$^+$ counter-ions from the film, in a 1:1 charge proportion [1,9]:

$$GC/NA(\sim SO_3^-)(Na^+)^{film} + (DA^+)^{soln} \rightleftharpoons GC/NA(\sim SO_3^-)(DA^+)^{film} + (Na^+)^{soln} \qquad (2.1)$$

The incorporation of DA (1.00×10^{-4} mol dm^{-3} in pH 7.4 sodium phosphate buffer, ionic strength 0.12_4 mol dm^{-3}) into a 11 μm NA film, a 5.4 μm PSS film and NA/PSS films (r_m 5.3 and 1.1) was assessed by consecutively recording the cyclic voltammograms of DA for selected time intervals. Figure 2.1 presents the cyclic voltammograms and the incorporation isotherms into the NA coatings.
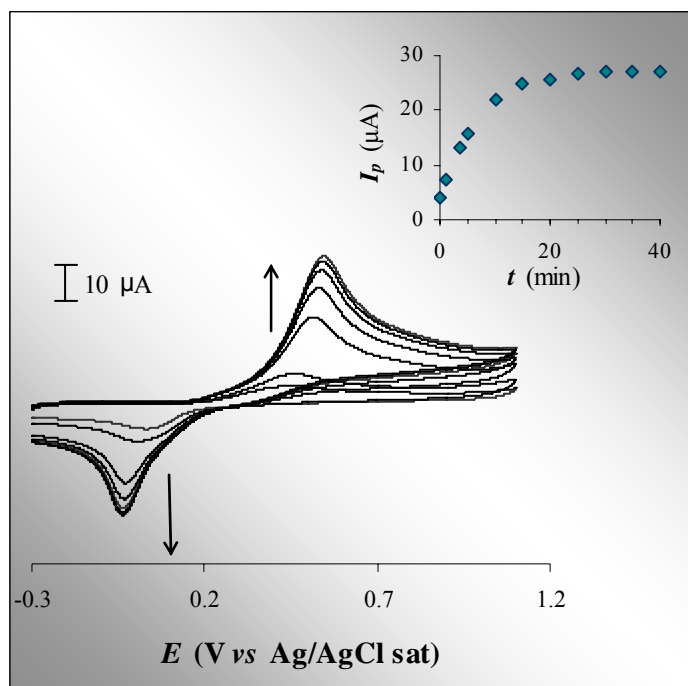
Figure 2.1. Incorporation of DA into the 9.2 μm NA-coated electrode: cyclic voltammograms in 1.00×10^{-4} mol dm^{-3} DA / pH 7.4 phosphate buffer (ionic strength 0.12_4 mol dm^{-3}) recorded in 5 min. time intervals. The first voltammogram was taken immediately after transferring the NA-coated electrode to the DA solution. Scan rate: 0.25 V s^{-1}. Inset: variation of the DA oxidation peak current with time.

At the NA 9.2 μm film (Fig. 2.1), the peak current for the oxidation of DA increased in time, reaching a plateau for times higher than *ca.* 20 minutes, for which the ion exchange equilibrium for DA, given by (Eq. 2.1) was attained. The release of the incorporated DA in the NA film was complete (final peak current < 5 % of the initial value) for 3 h contact the sodium phosphate buffer solution of 0.12_4 mol dm^{-3} ionic strength, showing that trapping of the monocharged cation DA is not very strong. This is the result of the low charge of DA and the effect of the competition of the Na$^+$ ions from the supporting electrolyte, reversing reaction (Eq. 2.1). In addition, there is an effect of the voltammetric cycling regime upon the ejection of the analyte: if the electrode with incorporated DA is cycled repeatedly, DA is completely excluded from the NA coating after *ca.* 30 min. This effect has been observed by others for different systems [10].

For a pure PSS coating (5.4 μm film thickness) the incorporation was very fast, attaining the plateau for $t < 3$ min (Fig. 2.2). The release of DA from the PSS single film was fast as well (*ca.* 3 min after being transferred to pure phosphate electrolyte solution).
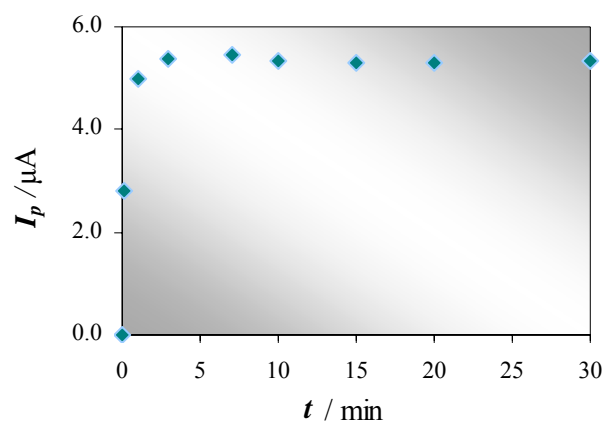
Figure 2.2. Incorporation of DA (1.00×10^{-4} mol dm^{-3} at pH 7.4 phosphate buffer) into the 5.4 μm PSS-coated electrode: variation of the DA oxidation peak current with time. Experimental conditions as in Fig. 2.1.

In the case of the NA/PSS coated electrodes (5.3 and 1.1 NA/PSS mass ratios), the peak current for the oxidation of DA also increased, reaching a plateau at *ca.* 10 min, being an intermediate state between NA and PSS single films. After changing the electrode to a solution of diluted phosphate buffer (0.01 mol dm^{-3}) dopamine was completely released from the film after 30 min.

2.3.2. Distribution coefficients and diffusion features of NA-, PSS- and NA/PSS- films

The amount of DA$^+$ ions incorporated into the NA-, PSS- and NA/PSS films shall be dependent on the charge and size of dopamine cation, on its concentration in the electrolyte solution, on the concentration of competing Na$^+$ ions, as predicted by conventional ion exchange reasoning [1,11]. Also, the DA incorporation will depend on the film thickness, which determines the amount of sulfonate groups in the film, as well as the DA diffusion in the film [1].

In order to evaluate the partition of DA between the electrolyte solution and the NA and NA/PSS (r_m 5.3 and 1.1) coatings, the concentration of DA in the NA film, c_{DA}^{film}, was determined by controlled potential exhaustive electrolysis of DA previously incorporated into the film. The concentration of DA in the NA film (mol dm^{-3}) is given by the following equation [12]:

$$c_{DA}^{film} = \frac{Q}{nFAl}$$

(2.2)

where Q is the electric charge (C), n is the number of transferred electrons ($n = 2$ for DA), F the Faraday constant (96485 C mol^{-1}), A the electrode area (dm^2) and l the NA film thickness (dm).

i) Nafion coatings

The complete electrolysis of the incorporated DA lasted for *ca.* 1 h. No DA was detected in the electrolyte solution, meaning that ejection of the incorporated species did not occur in the present time scale. The results were plotted as a partition isotherm i.e., as c_{DA}^{film} *vs.* $c_{DA}^{so\,ln}$ (Fig. 1) where $c_{DA}^{so\,ln}$ is the concentration of DA in solution (Fig. 2.3).
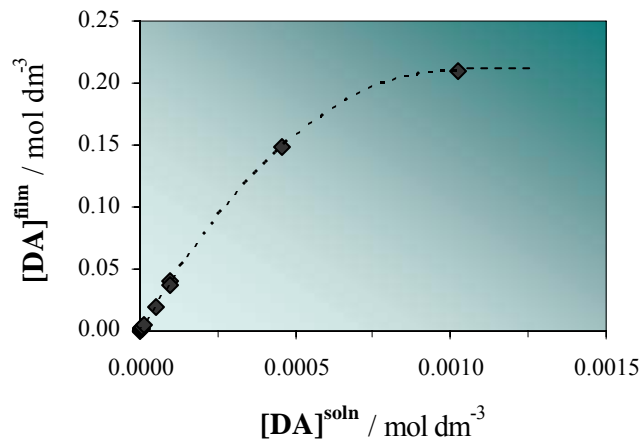
Figure 2.3. Variation of the DA concentration in the 9.2 μm NA-film as a function of the DA concentration in the sodium phosphate electrolyte solution (ionic strength 0.12$_4$ mol dm^{-3}). The concentration of DA in solution used in this experiment range between [0-1.02×10^{-3}] mol dm^{-3}.

The plot clearly shows that saturation of the NA exchange sites will occur for the higher values dopamine solution concentration. The asymptotic value at the plateau corresponds to occupation of all available ion-exchange sites, i.e., can be used to calculate the total concentration of ion-exchange sites. That value i.e., $c_{DA}^{MAX(film)}$ was 0.21 mol dm^{-3}. The slope of the partition isotherm at the lowest concentration values (Fig. 2.4) gives k_D, the distribution coefficient of DA partitioning into the NA film.

Figure 2.4. Calibration plot of DA concentration in NA-film *vs* DA concentration in the electrolyte solution, for a concentration of DA within the interval [0-4.86×10^{-5}] mol dm^{-3}.

When the exchange analyte is a trace species and solution concentration of the exchanged cation, Na$^+$, is relatively high (in the present case $C_{Na^+}^{soln} = 0.090$ mol dm^{-3}) the ion-exchange reaction given by Eq. 2.1, may be regarded as a partition reaction (Eq. 2.3) [1,12]:

$$DA^{+(soln)} \rightleftharpoons DA^{+(film)} \qquad (2.3)$$

and the partition coefficient is given by:

$$k_D = \frac{c_{DA}^{film}}{c_{DA}^{soln}} \qquad (2.4)$$

The meaningful value of k_D is that calculated for $c_{DA}^{soln} < 1 \times 10^{-4}$ mol dm^{-3} (*cf.* Fig. 2.3) as the slope of the isotherm, i.e., $k_D = 401$. This value means that an ion-exchange pre-concentration of DA into the 11 μm NA-coated GC electrode will be effective, i.e., the NA film prefers the DA$^+$ counteraction over Na$^+$. An ion-exchange selectivity coefficient (of DA$^+$ over Na$^+$, corresponding to Eq. 2.1) could be calculated once the film volume is known [5]. However, in the present case the film thickness is merely an estimated value based on a recast density which can hold an error depending on the actual swelling of the NA film.

The maximum concentration of incorporated DA, $c_{DA}^{MAX(film)}$ which was 0.21 mol dm^{-3}, gives also the total concentration of ion-exchange sites, corresponding to the total concentration of Na$^+$ counter-ions initially present at the NA film. Considering the estimated thickness of 11 μm, that value will give 1.38×10^{-8} mol of ion-exchange groups, SO$_3^-$. If nafion would have a degree of sulfonation of 100%, the total number of sulfonate exchange sites for the 11 μm NA film, estimated from the deposited nafion mass, would be 1.19×10^{-7} mol. Therefore, the actual degree of sulfonation for NA may be calculated from the ratio of that value to the real concentration of exchange sites. That ratio is 8.5, giving a degree of sulfonation of 13 % which compares well with that expected for Nafion 1100, 12.5 % [5].

Besides the above mentioned considerations on the ion-exchange features of the present NA films, the overall ion-exchange process depends also on the mass transport of the analyte throughout the coating, expressed by the apparent diffusion coefficient, D_{app}, that in most of the cases is smaller than the diffusion coefficient for the species in solution [1]. The solution value of DA has been determined by flow injection methods in pH 7.4, 0.1 mol dm^{-3} phosphate buffer solution as $(6.0 \pm 0.3) \times 10^{-6}$ cm^2 s^{-1} [13] or $(6.05 \pm 0.25) \times 10^{-6}$ cm^2 s^{-1} [14]. In the present study the diffusion coefficient of DA has been estimated from cyclic voltammetric data obtained with the GCE in *ca.* 9.7×10^{-5} mol dm^{-3} DA / pH 7.4, 0.09 mol dm^{-3} sodium phosphate buffer solutions. For scan rates (*v*) above 0.1 V s^{-1} the DA electrode reaction at the GCE presented an irreversible behaviour (cathodic-to-

anodic peak separations higher than 0.4 V) that could be characterized by the corresponding equation for the oxidation peak current [15]:

$$I_p = 2.99 \times 10^5 n (\alpha_c n_\alpha)^{1/2} c_{DA} D^{1/2} v^{1/2} \tag{2.5}$$

where n_α is the number of electrons transferred up to, and including the rate determining step and α_c is the transfer coefficient for the rate determining step.

In these cases the shape factor $|E_p - E_{p/2}|$ is given by [15]:

$$\left| E_p - E_{p/2} \right| = 47/(\alpha_c n_\alpha) \ \text{ in mV at } 20^\circ\text{C} \tag{2.6}$$

Therefore, combining the above equations, one can calculate the diffusion coefficient. The plot of the oxidation peak current *vs* the square root of the scan rate gave a straight line with a slope 7.012×10^{-6} AV^{-1}s (mean value of two determinations) and the mean $|E_p - E_{p/2}|$ value was 0.102 mV.

From these values the diffusion coefficient of DA in phosphate buffer was 6.1×10^{-6} cm^2 s^{-1}, which is very close to the referenced values. In the case of linear sweep or cyclic voltammetric measurements for an incorporated species at a modified electrode, carried out under diffusion-controlled conditions (which is the case for DA at the present NA electrodes [9] and is evident in the voltammetric peaks presented in Fig. 2.1, that have the typical diffusive tail [1]), the comparison of peak currents for the bare GCE and for the NA-coated electrode (with the same surface area *A*), at the same scan rate and dipped in the same DA solution yield the following relation [1]:

$$\frac{I_p^{film}}{I_p^{so\ln}} = \left(\frac{D_{app}}{D} \right)^{1/2} k_D \tag{2.7}$$

where k_D is given by Eq. 3.4, D_{app} is the apparent diffusion coefficient (cm^2 s^{-1}) in the film and D is the diffusion coefficient of the solution (cm^2 s^{-1}).

In the present case, for $v = 0.2$ V s^{-1}, the ratio of the cyclic voltammetric oxidation peak currents of DA corresponding to the NA-coated electrode and to the GCE immersed in the same solution was 6.34. Substituting this value and that of the partition coefficient in Eq. 2.7, D_{app} is estimated as 1.5×10^{-9} cm^2 s^{-1}, which is, in fact, a much lower value than that in solution. As far as we know there is no referenced value for DA in similar experimental conditions and for NA-coated electrodes. Though, DA diffuses slower than the competing cation Na$^+$ which has an apparent diffusion coefficient of 9.44×10^{-9} cm^2 s^{-1}, in nafion [5]. This fact, associated to the rather high concentration of sodium cation in solution, may give an explanation for the relatively low pre-concentration of DA (limit of detection $ca.$ 1×10^{-6} mol dm^{-3}, for a 3 min. accumulation period). However, in spite of this, the present NA-coated electrodes were selective to ascorbate and urate anions, presented a better sensitivity compared to the bare GCE with a fast response time and, above all can be used physiological like conditions, in the linear sweep mode at scan rates higher than 0.5 V s^{-1}, precluding any interference from the DA regenerative cycle induced by AA.

ii) PSS coatings

For pure PSS coatings no equilibrium partition isotherms could be obtained, since DA was promptly rejected after being transferred to pure phosphate electrolyte solution. This is indicates that the diffusion coefficients within those films shall be identical to the one in solution. This is in accordance with the formation of swollen PSS films with a loose structure [3].

iii) NA/ PSS mixed coatings

The results were plotted as a partition isotherm i.e., as c_{DA}^{film} vs. $c_{DA}^{so\ln}$ (see Fig. 2.5) where c_{DA}^{film} and $c_{DA}^{so\ln}$ are the concentrations of DA in the film and in solution, respectively. The concentration of DA in the films (mol dm^{-3}), was calculated by Eq. 2.2, where the film densities were assumed to be weight mean values for the corresponding PSS/NA mixtures. The plot clearly shows that saturation of the NA exchange sites will occur for the higher values of DA concentration in solution. The asymptotic value at the plateau corresponds to occupation of all available ion-exchange sites, i.e., can be used to estimate the maximum

amount of incorporated dopamine, $c_{DA}^{MAX(film)}$. That value was 0.10 mol dm^{-3} and 0.050 mol dm^{-3} for NA/PSS r_m 5.3 and r_m 1.1, respectively.
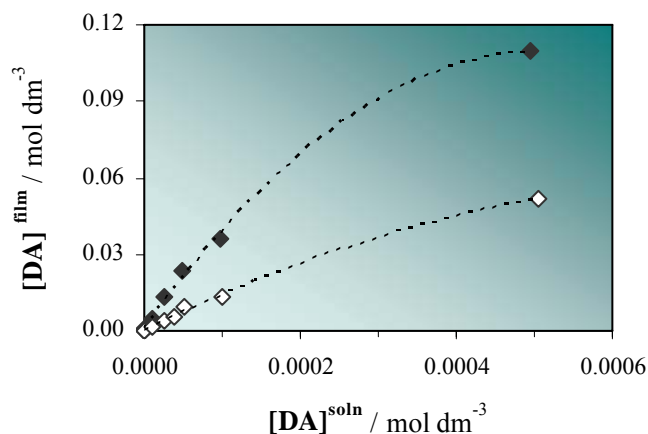
Figure 2.5. Concentration of dopamine in the NA/PSS films, c_{DA}^{film}, as a function of $c_{DA}^{so\ln}$, the DA concentration in the phosphate electrolyte solution (ionic strength 0.12_4 mol dm^{-3}). Black markers: NA/PSS r_m 5.3, white markers: NA/PSS r_m 1.1. The concentration of DA in the solution used range between $[0-5.05 \times 10^{-4}]$ mol dm^{-3}.

The slope of the partition isotherms at the lowest concentration values (Fig. 2.6) gives k_d, the distribution coefficient of DA partitioning into the NA/PSS films.
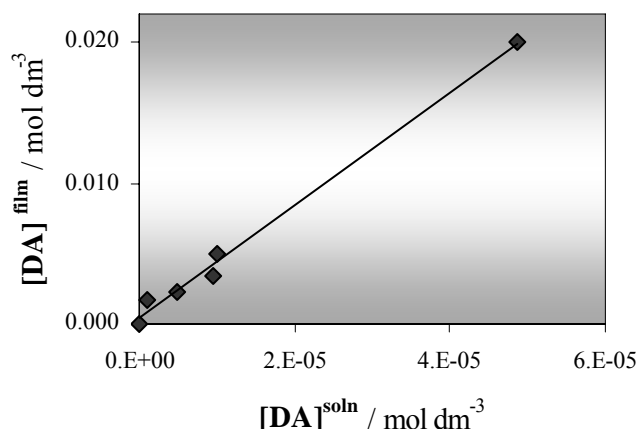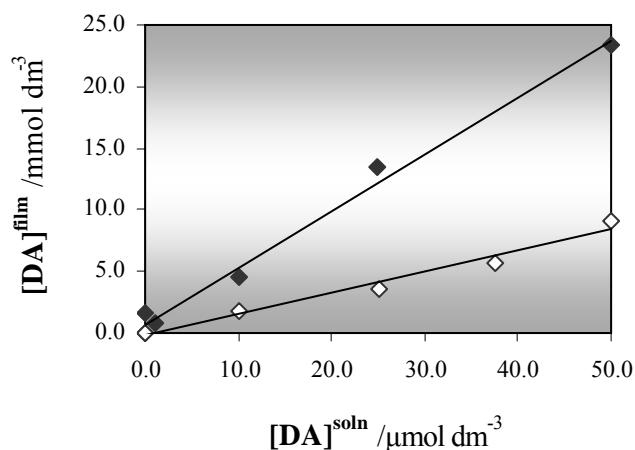

Figure 2.6. Calibration plot of DA concentration in NA-film *vs* DA concentration in the electrolyte solution, for a concentration of DA within the interval $[0-5.00 \times 10^{-5}]$ mol dm^{-3}.

Also in this case, the exchange analyte is a trace species and solution concentration of the exchanged cation, Na^+, is relatively high. Therefore, the ion-exchange reaction may be regarded as a partition reaction [1] and partition coefficient is given by Eq. 2.4. The meaningful value of k_D is that calculated for $c_{DA}^{so\,ln} \leq 1 \times 10^{-5}$ mol dm^{-3} (*cf.* Fig. 6) as the slope of the isotherm, i.e., $k_D = 462$ for NA/PSS r_m 5.3 and $k_D = 173$ for NA/PSS r_m 1.1. This value means that an ion-exchange pre-concentration of DA into the NA/PSS films is effective. These computations assume that the electrochemical reversibility of the reaction is identical in the solution/electrode and in the polymer/electrode interfaces. In the present case, the DA oxidation proceeds in the quasi-reversible region at all electrodes. For example, at the GCE the typical value of $E_{p/2}$ is 0.08 V (at 0.05 Vs^{-1} within the experimental error of $\pm$ 5 mV). Only for NA/PSS r_m 5.3, $E_{p/2}$ increased to 0.1 V.

In the case of linear sweep or cyclic voltammetric measurements for an incorporated species at a modified electrode, carried out under diffusion-controlled conditions the comparison of peak currents for the bare GCE and for the NA/PSS-coated electrodes (with the same surface area A), at the same scan rate and dipped in the same DA solution, yield to Eq. 2.7 [1]. In the present case, for $v = 0.2$ V s^{-1}, the ratio of the cyclic voltammetric oxidation peak currents of DA corresponding to the polymer-coated electrodes and to the bare GCE immersed in the same solution of DA, was 9.72 for the NA/PSS r_m 5.3 and was 6.83 for the NA/PSS r_m 1.1. Substituting these values and those of the partition coefficients in Eq. 2.3, D_{app} is estimated as 2.7×10^{-9} cm^2 s^{-1} for the NA/PSS r_m 5.3 and as 9.6×10^{-9} cm^2 s^{-1} for for the NA/PSS r_m 1.1. These values are, in fact, much lower than D in solution. Further a comparison with D_{app} in pure NA (1.5×10^{-9} cm^2 s^{-1})[1], shows that increasing amounts of PSS in the mixtures NA/PSS lead to an increase of D_{app} for dopamine.

The ion-exchange and mass transport data for single NA- and mixed NA/PSS- (r_m of 5.7 and 1.1) polymeric films are summarized in table 2.2.

Table 2.2. Ion-exchange and mass transport data for single NA- and mixed NA/PSS- coatings.

Polymeric film	k_D	D_{app} (cm^2 s^{-1})	$c_{DA}^{MAX(film)}$ (mol dm^{-3})
NA-	401	1.5×10^{-9}	0.21
NA/PSS- (r_m 5.3)	462	2.7×10^{-9}	0.10
NA/PSS- (r_m 1.1)	173	9.6×10^{-9}	0.05

2.4. Conclusions

In the present chapter the ion-exchange and mass transport features of dopamine in the several polymeric films (NA-, PSS- and NA/PSS-) were evaluated. The results highlighted that:

i)   dopamine is effectively incorporated into NA by ion-exchange (coupled to the effect of hydrophobic interactions, c.f. results in section 3.3.1), as revealed by the k_D values obtained ($k_D > 1$), and its mass transport throughout the ionomer layer, expressed by D_{app}, is much slower than in solution ($D_{app} < D$);

ii)   PSS layers produced from casting solutions of high ionic strength shall be swollen in such a way that the electrostatic effect of sulfonic groups towards monopositively charged dopamine will be diminute and, due to the very loose morphology [3] the mass transport shall be straightforward ($D_{app} \approx D$);

iii)   as the PSS content in the mixtures NA/PSS increases the overall incorporation decreases (lower $c_{DA}^{MAX(film)}$ values) but the apparent diffusion coefficient increases, which is related to the morphological characteristics of these polymeric mixed coatings (*cf.* section 3.3.2).

These assumptions for the ion-exchange and mass transport characteristics are quite important and useful, to explain some of the permeselective properties of these polymeric films (NA-, PSS- and NA/PSS-), evaluated in section 3.3.1 of this thesis.

References

[1] P. Ugo, L. M. Moretto, *Electroanalysis* 7 (1995) 1105.

[2] S. C. C. Monterroso, H. M. Carapuça, A. C. Duarte, *Electroanalysis* 15 (2003) 1878.

[3] S. C. C. Monterroso, H. M. Carapuça, A. C. Duarte, *Talanta* 64 (2005) 644.

[4] C. M. A. Brett, D. A. Fungaro, J. M. Morgado, M. H. Gil, *J. Electroanal. Chem.* 468 (1999) 26.

[5] M. N. Szentirmay, C. R. Martin, *Anal. Chem* 56 (1984) 1898-1902.

[6] A. Zook, J. Leddy, Anal. Chem. 68 (1996) 3793.

[7] P. Ugo, B. Ballarin, S. Daniele, G.A. Mazzocchin, *J. Electroanal. Chem.* 291 (1990) 187.

[8] Sigma–Aldrich Catalogue, Ref. Product Number 24, 305-1.

[9] L. S. Rocha; H. M. Carapuça, *Bioelectrochem* 69 (2006) 258.

[10] J. R. Schneider, R.W. Murray, *Anal. Chem.* 54 (1982) 1508.

[11] K. Doblhofer, in: Lipkowski, J., Ross, P.N, (Eds.), *Thin polymer films on electrodes: a physicochemical approach*, Electrochemistry of Novel Materials, VCH publ. Inc., New York, 1994.

[12] M. Maizels, W. R. Heineman, C. J. Seliskar, *Electroanalysis* 12 (2000) 241.

[13] G. W. Zou, Z. Liu, C. X. Wang, *Anal. Chim. Acta.* 350 (1997) 359.

[14] G. Gerhardt, R. N. Adams, *Anal. Chem.* 54 (1982) 2618.

[15] R. Greef, R. Peat, L. M. Peter, D. Pletcher, J. Robinson, *Instrumental methods in electrochemistry*, Southampton Electrochemistry group, , Ellis Horwood limited, England, 1985.

CHAPTER 3

Ion-exchange voltammetry with

Nafion/Poly(sodium 4-styrenesulfonate)

mixed coatings on mercury film electrodes

CHAPTER 3   Ion-exchange voltammetry with Nafion/ Poly(sodium 4-styrenesulfonate) mixed coatings on mercury film electrodes

3.1. Introduction

3.2. Experimental

    3.2.1. Chemicals

    3.2.2. Instrumentation

    3.2.3. Preparation of the chemically modified electrode

    3.2.4. Voltammetric Procedures

3.3. Results and Discussion

    3.3.1. Ion-exchange features of NA- PSS- and NA/PSS- mixed films coated on GCE

    3.3.2. Morphologic features of the mixed NA/PSS coatings

    3.3.3. Formation of thin mercury film at NA/PSS modified GC electrodes

    3.3.4. Reproducibility of the NA/PSS mixed coatings and incorporation of lead(II)

    3.3.5. Application of the NA/PSS (r_m 5.3)-TMFE in the ASV determination of lead(II)

3.4. Conclusions

3.1. Introduction

The use of cation-exchange polymers for modification of mercury film electrodes consists in an established and reliable methodology that allies the minimisation of electrode fouling effects, by precluding the income of interfering species towards the electrode surface, with the selective determination of cations [1,2,3,4,5].

Nafion (NA), the most commonly employed ionomer in speciation studies of heavy metals [1,2,3,6,7,8,9,10,11]. This cation-exchange polymer presents almost ideal properties (inert, nonelectroactive, hydrophilic and insoluble in water) for the modification of electrode surfaces [6,12], however, the easier coating procedure (recasting from a solution without adding any casting solvents), often presents lack of reproducibility [7,13].

Recently, poly(sodium 4-styrenesulfonate), PSS, was used for coating thin mercury film electrodes (TMFEs) and applied to the direct determination of trace metals in estuarine waters by anodic stripping voltammetry (ASV) [4,5]. PSS coatings (recasting from a solution of high ionic strength) proved to be mechanically stable and very reproducible and with satisfactory exclusion properties. Also, there was an enhancement in the sensitivity of the voltammetric signal of lead(II) compared not only with that of the bare TMFE, but also with that of NA modified TMFE for similar film thicknesses [4,5]. This can be related to the electrostatic effect created by the considerable film charge density leading to an effective accumulation of metal ions in polyelectrolyte films [14].

To the best of our knowledge, only two systems using mixed polymeric coatings on glassy carbon/MFE have been reported in the literature: Nafion/poly(vinylsulfonic acid) [3,15] and Nafion/poly(vinylsulfonic acid-co-maleic anhydride) [3]. The objective of those studies was to improve the cation-exchange ability of NA films by combination with a polymer with higher degree of sulfonation, but no significant improvements were obtained. Trial tests using a mixed Nafion/poly(styrenesulfonic acid) films were reported, but no detailed experiments/characterization of that modified electrode were reported [3].

In the present chapter the morphology, reproducibility and perm-selectivity (inclusion and exclusion) properties of NA/PSS mixed coatings with different mass were

evaluated. Afterwards, the analytical performance, based on the reproducibility, the sensitivity and the anti-fouling features towards surfactants, in the square-wave anodic stripping voltammetric determination of trace lead at the several mass ratio NA/PSS modified thin mercury film electrode (TMFE), was assessed. Finally, the best coating was applied to untreated polluted estuarine waters.

3.2. Experimental

3.2.1. Chemicals

Poly(sodium 4-styrenesulfonate), PSS (M_w 70,000; degree of sulfonation 1.0) and Nafion, NA (5 wt. % solution in a mixture of lower aliphatic alcohols and water) were purchased from Sigma-Aldrich and used as received. All chemicals were of analytical reagent grade and solutions were prepared with ultra-pure water (18.2 MΩcm, Milli-Q systems, Millipore-waters). Sodium chloride, potassium chloride (Merck, suprapur) and 1000 ppm AA-Spectrosol metal ion (Pb, Hg, Cu) standards (BDH) were used. Stock solutions of PSS (120 mM in monomer units) and of NA (25×10^{-3} mol dm^{-3} in monomer units) were prepared in phosphate buffer solution (0.022 mol dm^{-3} KH$_2$PO$_4$/0.041 mol dm^{-3} Na$_2$HPO$_4$, pH 7.4, ionic strength 0.14$_9$ mol dm^{-3}) and in methanol, respectively, and stored at 4 ºC. Stock surfactant solutions of Triton X-100, sodium dodecyl sulphate (SDS), hyamine (HYA) and bovine serum albumine (BSA) (all 0.1%) were all stored at 4 ºC. All measurements were carried out at room temperature (18-20 ºC).

3.2.2. Instrumentation

Voltammetric measurements were performed with a BAS 100B/W electrochemical analyser (Bioanalytical Systems) connected to a Cell Stand BAS-C2. The working electrode was a glassy carbon disc (BAS, MF-2012, 3 mm diameter), the auxiliary electrode was a Pt wire and the reference electrode was Ag/AgCl (sat. KCl). A combined glass electrode (Orion 9104SC) connected to a pH meter (Cole Parmer, Model 05669-20)

was used for pH measurements. Dissolved organic carbon (DOC) determinations were made by an automated procedure [16] using a 4-channel Alliance segmented flow analyser; model Evolution II. Scanning electron microscopy coupled to electron dispersive spectroscopy (EDS) was conducted at a S-4100 HITACHI system.

3.2.3. Preparation of the chemically modified electrode

Prior to coating, the glassy carbon electrode (GCE) was conditioned by polishing with alumina slurry (0.3 μm), sonicated in pure water and activated by multicycle scanning in acetate buffer, pH 4 (25 cycles) [5]. The different polymer coatings on the GCE were obtained by the droplet evaporation method [5] where the PSS and NA single coatings were produced by application of 5 and 3 μL, correspondingly, of the polymeric solution (10×10^{-3}, 30×10^{-3} or 60×10^{-3} mol dm^{-3} in monomeric units for PSS and 4.5×10^{-3}, 11×10^{-3} or 15×10^{-3} mol dm^{-3} in monomeric units for NA) directly on the electrode surface. Then, the solvent was evaporated under a low flux warm air stream (*ca.* 60ºC).

For assembling the NA-PSS mixed coatings, a 25×10^{-3} mol dm^{-3} NA ethanolic solution was mixed with suitable amounts of 120×10^{-3} mol dm^{-3} PSS solution in order to obtain different NA/PSS mass ratios, r_m (27, 5.3 and 1.1), maintaining the NA volume constant. A 3 μL microdroplet was then applied on the electrode surface and the solvents were evaporated as mentioned above.

The electrochemically active surface area of the glassy carbon electrode measured by chronoamperometry (in 9.854×10^{-4} mol dm^{-3} ferricyanide/1.0 mol dm^{-3} KCl solution) was (7.192 ± 0.065) mm^2.

Thin mercury films were *ex-situ* plated from a 1.2×10^{-4} mol dm^{-3} Hg(NO$_3$)$_2$ in 7.25×10^{-3} mol dm^{-3} nitric acid solution (pH *ca.* 1.9) by electrodeposition through the polymer coatings at -1.3 V for 20 s, stirring the solution with a magnetic stirrer (BAS-C2 stand, position 3). The un-coated mercury film electrode was obtained in a similar fashion except for the polymer coating step. When required, the utilized polymer layer was wiped off with a wet tissue and the GC surface was re-conditioned as mentioned above.

3.2.4. Voltammetric Procedures

Cyclic voltammetry and linear sweep voltammetry of organic species were conducted in 10 mL phosphate buffer solution, pH 7.4. Square-wave anodic stripping voltammetric (SWASV) experiments at the NA/PSS-TMFEs were carried out in 10 mL NaCl 0.5 mol dm^{-3} solutions spiked with lead(II) as a reference metal cation (concentration of lead(II) 6.00×10^{-8} mol dm^{-3}). The deposition step lasted 20 s (t_d) at -0.8 V whilst the solution was stirred (BAS-C2, position 3). Equilibration time was 5 s. The stripping step was initiated at -0.8 V and ended at -0.1 V. The SW parameters were: amplitude 25 mV, frequency 50 Hz and step potential 0.005 V. Between each scan, a cleaning step was performed (E_{clean} = -0.2V for 5 s).

For the SWASV determinations in estuarine water, 10 mL of the fresh sample, filtered through a 0.45 μm membrane (Millipore), was pipetted into the voltammetric cell and the measurement was carried out promptly (accumulation time 180 s). Both the un-coated TMFE and the NA/PSS-TMFEs were used. The quantification of the total concentrations of lead and copper was performed by SWASV following a published procedure [17]. Deposited mercury charges were calculated by electronic integration of the linear sweep stripping peak of mercury, at v = 0.005 Vs^{-1}. The electrolyte solution was ammonium thiocyanate 5×10^{-3} mol dm^{-3} (pH 3.5) [17]. The stripping step runned from -0.15 V to +0.6 V.

All peak currents and charges quoted are mean values of 4 replicate measurements. All solutions were purged with nitrogen for 5 min. prior to the voltammetric experiments.

3.3. Results and Discussion

3.3.1. Ion-exchange features of NA-, PSS- and NA/PSS- mixed films coated on GCE

The inclusion of PSS into Nafion based films aims at improving both the reproducibility of the NA coatings and the incorporation features towards positively charged species. The key question is to know whether the enclosure of the PSS polyelectrolyte in the highly hydrophobic NA framework may result in stable and functional coatings on glassy carbon surfaces. Preliminary experiments were done with GC electrodes coated with the single polymers, NA (mass loadings of 2.1, 5.5 and 6.9 μgmm^{-2} corresponding to estimated thicknesses in the range 1 to 4 μm; d = 1.58 g/cm^3 [3,18,19, 20], and PSS (mass loadings of 1.4, 4.3 and 8.6 μg mm^{-2} corresponding to estimated thicknesses between 2 and 11 μm; d = 0.801 g/cm^3 [3,5,21].

The ion-exchange properties of the NA and PSS single coatings, towards target organic species were evaluated. The selected electroactive species were: uric acid (UA) (M_w 168), cathecol (C) (M_w 110) and dopamine (DA) (M_w 192). Under the working conditions (pH of 7.4, ionic strength 0.14_9 mol dm^{-3}) uric acid is anionic (charge -1), cathecol is neutral and dopamine is cationic (charge +1). Table 3.1 shows the variation of the oxidation peak currents obtained with NA- and PSS-coated GCEs with different loadings, relative to the bare GCE.

Table 3.1. Variation of linear sweep voltammetric oxidation peak currents, relative to the bare GC electrode (in percentage values) of cathecol, urate and dopamine cation at NA and PSS coated GCEs of different loadings. Scan rate 0.05 V s^{-1}.

	Mass loading (μg mm^{-2})	Peak current variation (%)		
		Cathecol	Urate	Dopamine
NA/GCE	2.1	-43	-92	+114
	5.0	-47	-100	+178
	6.9	-54	-100	+156
PSS/GCE	1.4	-9	0	+27
	4.3	-5	-7	+33
	8.6	-6	-14	+33

For cathecol, only partial exclusion was observed for the NA films. Being neutral specie, the exclusion shall result simply from the size-exclusion features of the polymeric coatings, without contribution from electrostatic interactions. For the thicker NA electrode, the exclusion was only approximately 50%. Probably, molecular interactions (due to the high hydrophobicity of NA) are occurring, allowing some incorporation of cathecol, as was reported for dopamine (see bellow) or other organic species [12,22]. On the other hand, restriction to cathecol by PSS films was lower than 10%. This dissimilarity is related to the morphologic features of the polymeric films, i.e., the rigid and compact structure presented by NA [5,9] versus the spongy and loose surface of PSS films [5]. Thus, for PSS films, the rather small neutral cathecol species freely breaks into the coating and is oxidized at the glassy carbon surface.

The exclusion properties towards urate are based, not only on the semi-permeability to molecular size, but also on the electrostatic repulsions between this anion and the sulfonate groups of both NA and PSS. This explains the total exclusion of urate in NA compared with the neutral and smaller cathecol molecule. Though, PSS presented a low efficiency in preventing the diffusion of urate, due to specific morphologic features of these films.

For the positively charged dopamine, enhanced peak currents were observed, indicating the incorporation of this cationic species into both films. For NA, it has been already established that the incorporation of dopamine is determined not only by ion-exchange but also by hydrophobic interactions between dopamine and the hydrofluorcarbon backbone of NA [12,18,22]. This aspect is confirmed by the results in Table 3.1, where higher dopamine oxidation peak currents were observed for NA coatings compared to those for PSS (e.g., +178 % for NA with mass loading 5.0 μg mm^{-2} *vs.* +33 % for PSS at 4.3 μg mm^{-2}), despite of the higher content of sulfonate groups in PSS (20 nmol mm^{-2} *vs.* 4.4 nmol mm^{-2} for NA; values based on the monomer concentrations and assuming 100% sulfonation for NA).

For thicker NA films, the dopamine oxidation signal decreased pointing to the probable occurrence of mass transport limitations. In fact, apart from ion-exchange reasoning and from the occurrence of short range molecular interactions between the

polymer matrix and the target species, the actual mass transport features of the species in the polymer layer, expressed by the apparent diffusion coefficient, D_{app}, play an important role [2]. The apparent diffusion coefficient may differ from that in the bulk solution, thus influencing the magnitude of the electrochemical signal. Accordingly to data presented in chapter 2, section 2.3.2., a D_{app} for dopamine of 1.5×10^{-9} cm^2 s^{-1} and a maximum amount of incorporated dopamine, c_{DA}^{film}, of 0.21 mol dm^{-3} were obtained for the NA coatings in contact with phosphate buffer solutions. The diffusion coefficient for soluble dopamine in the same electrolyte was 6.1×10^{-6} cm^2 s^{-1}.

Different NA:PSS mass ratios (r_m) were tested for improving reproducibility of the NA films, keeping appropriate size/charge exclusion properties. Two aspects were considered in the preparation of mixed NA/PSS coatings: i) the NA mass loading was kept constant at 4.9 µg mm^{-2}, a value that ensures desirable exclusion/incorporation of organics without evidence of mass transport limitations, and ii) the loading of PSS was changed in the range 0.18 to 4.6 µg mm^{-2}. Figure 3.1 presents the loading characteristics of the tested mixed coatings.
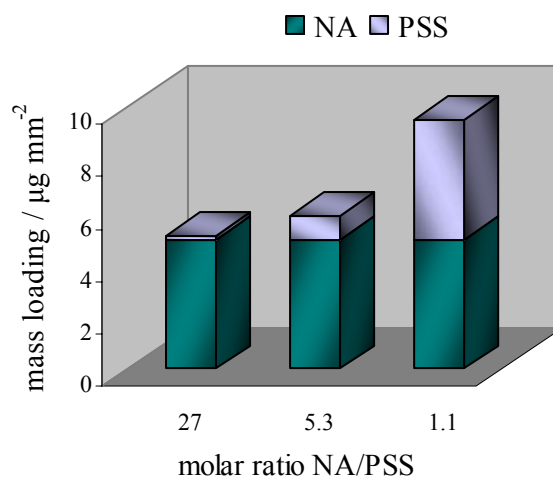
Figure 3.1. Mass loading characteristics of the ion-exchange NA/PSS films. The NA/PSS mixed coatings presents the following values for total mass loading: 5.1, 5.8 and 9.5 µg mm^{-2} for a mass ratio (r_m) of 27, 5.3 and 1.1, respectively.

The variation of the oxidation peak currents at the NA/PSS electrodes was evaluated and compared to the bare GCE (Table 3.2).

Table 3.2. Variation of linear sweep voltammetric oxidation peak currents, relative to the bare GC electrode (in percentage values) of cathecol, urate and dopamine cation ($\sim 1 \times 10^{-3}$ mol dm^{-3} solutions) at mixed NA/PSS coated GCE with different mass loading ratios. Scan rate 0.05 V s^{-1}.

NA:PSS ratio (r_m)	Peak current variation (%)		
	Cathecol	Urate	Dopamine
27	-33	-100	+166
5.3	-12	-70	+131
1.1	-4	-22	+58

Similarly to NA and PSS single films, cathecol was only partially excluded by the NA/PSS mixed coatings confirming that exclusion of the neutral species is simply due to the semi-permeability to molecular size. Higher restriction was achieved for the NA/PSS coating with the highest NA content (r_m=27) and all NA/PSS films were less efficient than single NA-coated electrodes (*cf.* Table 3.1). This means that the inclusion of PSS into NA increases the permeability to molecular size of the final mixed films. The same general conclusion can be draw for the exclusion of urate: despite the overall increase of the content of sulfonate groups due to PSS in the mixed NA/PSS coating, the selectivity towards anions was not improved.

For dopamine, increased peak currents were observed, indicating the incorporation of this cationic species into all NA/PSS coatings. The incorporation capability of these mixed coatings was more effective for lower PSS contents, which induces the incorporation of dopamine via the hydrophobic interactions, as demonstrated for single coated electrodes. The decrease in the peak currents with the increase in the PSS content is smaller than expected due to variation in the mass transport features of dopamine in the mixed films. Effectively, compared with the D_{app} of pure dopamine, 1.5×10^{-9} cm^2 s^{-1}, the introduction of increasing amounts of PSS in the mixed coatings led to an increase in D_{app} to 2.7×10^{-9} cm^2 s^{-1} for the NA/PSS with r_m=5.3 and to 9.6×10^{-9} cm^2 s^{-1} for r_m=1.1. For PSS single coatings the diffusion coefficients within the films are identical to the ones in solution, which is related to the swollen and loose structure of the PSS films (provides an easy to move). In addition, the maximum amount of incorporated dopamine, decrease from 0.21 mol dm^{-3} for the pure NA, to 0.10 mol dm^{-3} and to 0.050 mol dm^{-3} for NA/PSS r_m=5.3 and r_m=1.1, respectively. These data are presented in chapter 2, section 2.3.2.

The typical linear scan voltammograms (normalized for concentration) of the target species are presented in Fig. 3.2.
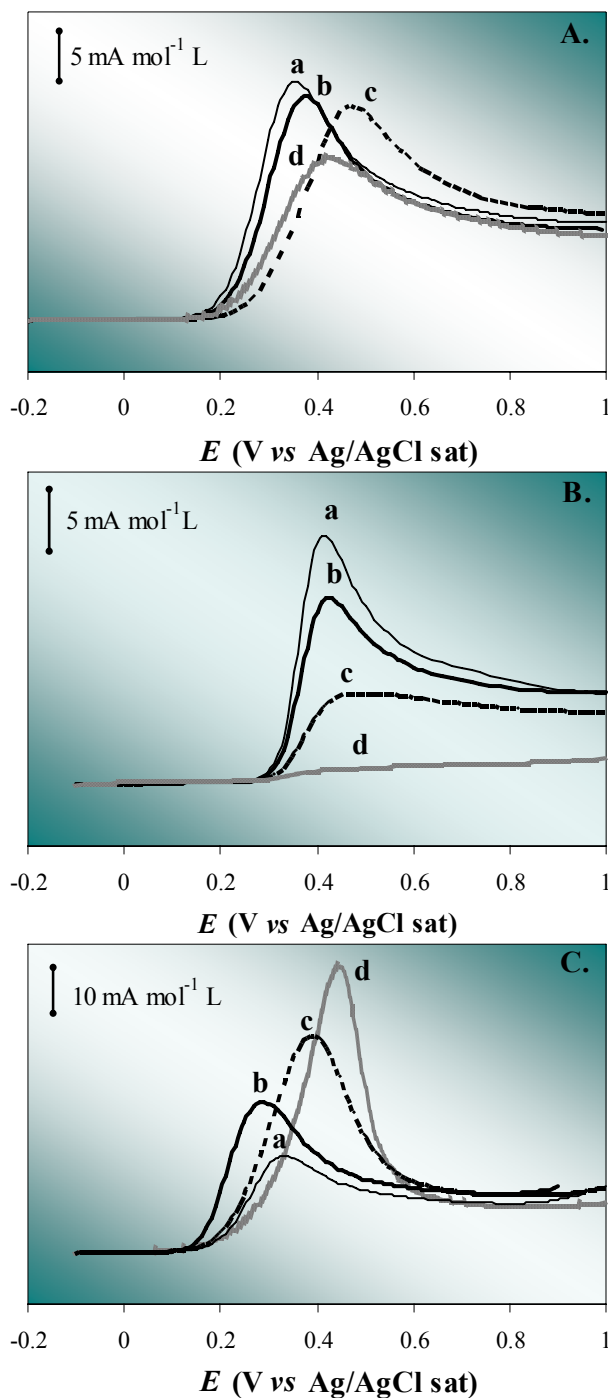
Figure 3.2. Linear sweep voltammograms, normalized for concentration, for the oxidation of (A) cathecol, (B) uric acid (~1×10^{-3} mol dm^{-3} solutions in pH 7.4 phosphate buffer), (C) dopamine (5 mmol dm^{-3} solution in pH 7.4 phosphate buffer): GCE (a), NA/PSS; r_m 1.1 (b), NA/PSS; r_m 5.3 (c) and NA/PSS; r_m 27 (d). Scan rate 0.050 V s^{-1}.

3.3.2. Morphologic features of the mixed NA/PSS coatings

The incorporation/exclusion of target species at the NA/PSS films, besides being closely related to the ion-exchange features of the mixed coatings, may depend also on the film morphological characteristics. Also, the structural properties of the individual polymers may have to be taken into account. Recasted Nafion is constituted by randomly dispersed hydrophobic domains of the fluorinated backbone which contact through water channels with the ionic parts, the sulfonate groups and their counter-ions, Na^+ (including, eventually, added electrolyte) [23]. There are evidences that the sulfonate groups are organized in nanoclusters of hydrophilic nature scattered into the fluorinated backbone hydrophobic domains [23,24]. On the other hand, in single PSS films, the PSS polyelectrolyte presents a coiled structure that will build up in a non-organized fashion for these types of high mass loading films [5]. In this case, no hydrophobic/hydrophilic clusters are expected to occur.

Therefore, the morphologic/structural properties of the mixed NA/PSS coatings shall be dependent not only on the mentioned properties of the individual polymers but also on the specific interactions between these two polymers with such different structural characteristics.

Scanning electron micrographs highlight the morphological differences for NA/PSS coatings of different composition (*cf.* Figure 3.3). In all cases, the surface reveals the appearance of bead-shaped domains with different dimensions (hardly seen in the case of NA/PSS (r_m 27) at the present magnification, probable dimensions in the nanometer scale), dispersed in a compact matrix that might be constituted mainly by NA. Increasing the PSS content in the NA/PSS mixed coatings led to an evident increase of the coverage by the bead-shaped domains, as well as to an increase of the size of those domains (*cf.,* Figure 3.3 for r_m 5.3 (A) and r_m 1.1 (A)). For NA/PSS (r_m 5.3), the bead-shaped domains assumed dimensions within the low micrometer range (diameter *ca.* 0.1 – 0.5 μm). For the coatings NA/PSS (r_m 1.1) those domains attained dimensions in the micrometer range (diameter *ca.* 0.3 to 1 μm).
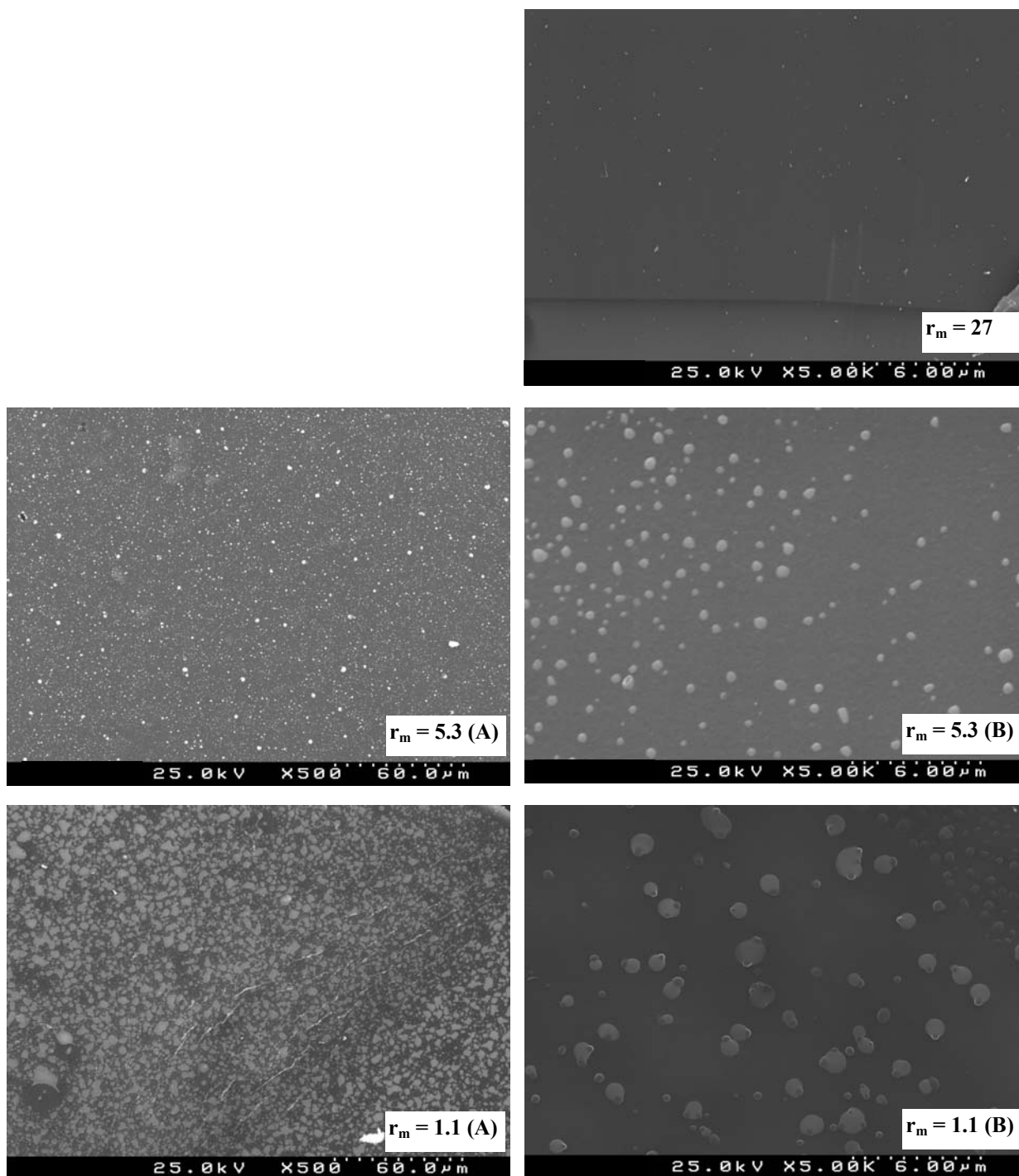
Figure 3.3. Scanning electron micrographs (×500 or ×5000) of different NA/PSS coatings on GGE: NA:PSS, molar ratios 27, 5.3 and 1.1. For r_m 5.3 and r_m 1.1 two micrographs are displayed (A and B) corresponding to different magnifications.

A semi-quantitative in situ elemental analysis by EDS indicated a very high predominance of fluorine in the compact matrix, while in the spherical clusters only a

residual amount could be detected. Additionally, sulphur was detected in both regions, as expected because of the sulfonate groups. Further, in the compact matrix, phosphorous, potassium and an excess of sodium (relative to sulphur) were detected, indicating that, during the formation of the mixed film, some phosphate buffer (from the PSS casting solution) was included into the NA matrix. So, the compact matrix must be constituted by a NA region of low permeability and high hydrophobic nature scattered by a population of bead shaped clusters constituted by the hydrophilic PSS polyelectrolyte. In these clusters EDS indicates the presence of Na, K, P and S, draw from PSS and from the phosphate buffer in the casting solution. These coatings are clear examples of phase separation in polymeric matrices.

Interestingly, the NA/PSS film (r_m 1.1) presents a non-homogeneous surface where distinct structural features could be observed, as depicted from the micrographs in Figure 3.3 (r_m 1.1, B) and in Figure 3.4.
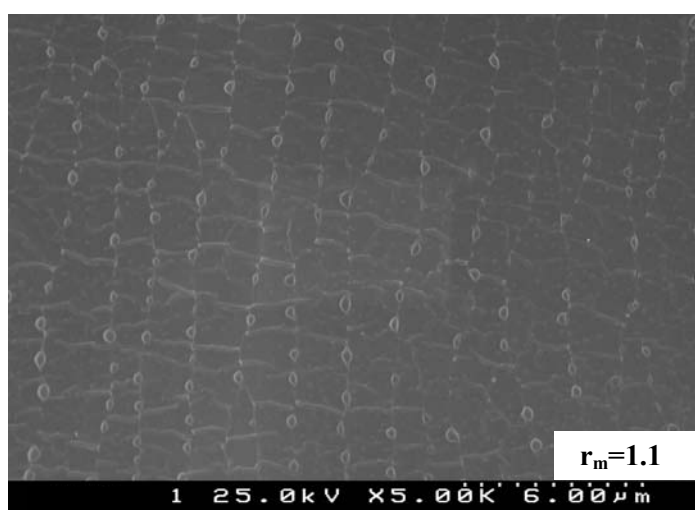
Figure 3.4. Scanning electron micrograph (×5000) of the NA/PSS coating (r_m 1.1) of Figure 3.3 at a highly structured site on the surface.

Besides the randomly dispersed PSS beads (micrograph in Figure 3.3 (B), r_m 1.1), there are regions presenting highly structured arrangements, resembling a symmetrical network (Figure 3.4). The occurrence of such a degree of organization may be induced by the process of solvent evaporation. In fact, local processes of swelling shrinkage during the film formation may lead to pattern arrangements occurring as a consequence of mechanical instability induced by temperature and/or concentration gradients. This effect is known as

the Rayleigh-Bénard instability [25], leading then to the formation of organized structures in polymer coatings produced by solvent evaporation.

Additionally, surface-tension-driven flows can result in increased surface instability, producing regular structures (i.e., the Marangoni effect [26]). This effect is predominant for high concentrations of polymer or high surface tension. In the present mixed films, for $r_m = 1.1$, the higher content of PSS may produce significant alterations in the film surface tension. Hence, the present mixed films appear to be build up in a semi-self-organized fashion induced by the effect of the solvent evaporation (conducted at *ca.* 60ºC) coupled to the occurrence of phase separation. Additional effects of film surface tension may also occur.

Therefore, for a high relative amount of NA (r_m 27), the morphology of the NA/PSS coating is close to that observed for a single Nafion electrode [10], and this fact sustains the observations described in previous sections regarding the good molecular exclusion of urate and high incorporation of dopamine. For the coatings with higher contents of PSS, this polyelectrolyte phase is confined to the bead domains of micrometer dimension and no spongy structure [5] was formed. However, these domains shall constitute well defined hydrophilic phases, bringing about some of the characteristic properties of PSS.

3.3.3. Formation of thin mercury film at NA/PSS modified GC electrodes

The mixed NA/PSS ion-exchange coatings may be applied as an upgrading arrangement for mercury film electrodes for determination of metal cations in natural waters. Thus, it is important to assess the features of mercury films plated throughout the polymer mixed coatings. The characteristic electric charges for thin mercury films, *ex-situ* deposited on glassy carbon coated with NA, different NA/PSS and PSS (162 ± 15 µC, 2σ) agree within the experimental error with those for the bare GCE (173 ± 11 µC, 2σ). These data suggests that the formation of the mercury film on the various electrodes is not significantly altered by the presence of the coating barrier.

It is rather unlikely that a perfect thin layer of Hg microdroplets, plated onto the glassy carbon surface, is produced under the present conditions [5,9,15]. Considering the deposited charges, the present mercury films might correspond to thin films [27,28] with an estimated thickness of approximately 2 nm. The reproducibility of the film formation for each coating was fair (relative standard deviation (RSD) values between 5 and 15%), being the best results obtained for the single PSS-coated electrode, as was expected according to reported data [4].

3.3.4. Reproducibility of the NA/PSS mixed coatings and incorporation of lead(II)

The reproducibility of the NA/PSS coatings as well as the performance of TMFE modified with NA/PSS for anodic stripping voltammetry (ASV) was evaluated by examining the square-wave (SW) stripping data for a selected metal cation, lead(II). The analytical characteristics of the NA/PSS-TMFE mixed coatings were compared with those of NA- and PSS- coated TMFEs. Figure 3.5 displays the SW peak currents of lead, $I_{p(Pb)}$, for six different coated electrodes of each type (n'). For each experiment four repeated measurements of I_p were done.
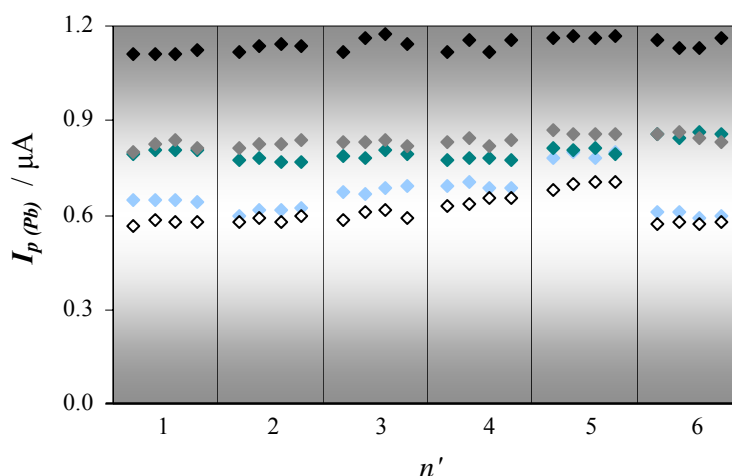
Figure 3.5. SWASV peak current values for repeated measurements (N'=4) in a test solution 6.0 $\times 10^{-8}$ mol dm^{-3} Pb^{2+} in 0.5 M NaCl, at different electrodes: PSS-TMFE 2.1 µg mm^{-2} (♦); NA-TMFE 4.9 µg mm^{-2} (♦); and NA/PSS-TMFE with different NA/PSS mass ratios, 27 (♦), 5 (♦) and 1 (◊). For each type of electrode six (n') replicate coatings were tested. E_{dep}= −0.8 V, t_{dep} = 20 s. SW parameters: a = 0.025 V, f = 50 Hz and v = 0.25 V s^{-1}.

The results reveal three groups of data:

i)   PSS-TMFE, where the peak current values were clearly higher and more consistent;

ii) NA/PSS-TMFE with mass ratios 1.1 and 5.3, where the peak current values were *ca.* 30% lower than those for the PSS electrode and the overall consistency of the data was fair;

iii) NA-TMFE and NA/PSS-TMFE with ratio 27, where the peak currents were *ca.* 40 - 45% lower than those for the PSS electrode and the data were very inconsistent.

Assuming that NA is 100 % sulfonated (which is an overestimated assumption), the sulfonate molar content (based in monomeric units) due to NA in the mixed coatings and in the single NA electrode would be 4.5 nmol mm^{-2}. To the PSS-TMFE 2.1 µg mm^{-2} electrode corresponds a SO_3^- content of 10 nmol mm^{-2}, a higher value than for the NA electrode. The higher content of ion-exchange sulfonate groups in PSS gives an explanation to the higher $I_{p(Pb)}$ values, meaning that improved accumulation of lead within the PSS film occurred.

Table 3.3 presents the median, the range and the variance between samples for the $I_{p(Pb)}$ values for the different polymer coated electrodes.

Table 3.3. Statistical characterization of the results obtained with the NA-TMFE, the PSS-TMFE and with the different NA/PSS-TMFE (NA:PSS mass ratios, r_m, of 27, 5.3 and 1.1). Experimental details as in Fig. 3.5.

Electrode	Median (µA)	Range (µA)	Reproducibility based on σ_b^2
NA-TMFE	0.657	0.210	0.019
NA/PSS-TMFE (r_m 27)	0.590	0.143	0.010
NA/PSS-TMFE (r_m 5.3)	0.796	0.097	0.004
NA/PSS-TMFE (r_m 1.1)	0.835	0.068	0.001
PSS-TMFE	1.14	0.061	0.001

These data put in evidence the improvement of the analytical performance of the mixed modified electrodes with the increase of the PSS content. Accordingly to all the statistical parameters, the mixed NA/PSS modified electrode presenting the best performance is the NA/PSS-TMFE (r_m 1.1). However, the differences from NA/PSS-TMFE (r_m 5.3) were not very significant ($I_{p(Pb)}$ differs by only 5%).

The reproducibility of the coatings, expressed as the variance between n samples, was substantially improved as the PSS content in the mixed film increased. The NA/PSS-TMFE (r_m =1.1) presented an identical reproducibility to that of the single PSS coated electrode. Several studies pointed out the poor reproducibility associated with NA coatings produced by the solvent evaporation method (without the addition of any recasting solvent) [5,7,13], and the present data emphasize the reported information.

Lead(II) incorporation experiments were performed for NA, NA/PSS r_m 5.3, and PSS films equilibrated with 6.00×10^{-8} mol dm^{-3} Pb(II) in solution. The charge values resulting from incorporated lead cations were 6.42×10^{-8} C (corresponding to 3.33×10^{-13} mol) for NA, 6.36×10^{-8} C (corresponding to 3.30×10^{-13} mol) for NA/PSS r_m=5.3, and 8.51×10^{-8} C (corresponding to 4.41×10^{-13} mol) for PSS. For pure PSS film, the incorporation of lead was 34% higher than that of the other films, supporting the larger SWASV signals observed for these electrodes. This increase renders unlikely any decrease in the apparent diffusion coefficient of lead in PSS.

3.3.5. Application of the NA/PSS (r_m 5.3)-TMFE in the ASV determination of lead(II)

The mixed coating NA/PSS (r_m 5.3) was selected for further application, taking into account the good analytical performance towards the SWASV of lead(II), the good reproducibility of the recasted coatings, as well as the incorporation/exclusion features towards small cationic, anionic and neutral species.

Calibration curves were obtained for lead in the range 2.00 to 10.0 $\times 10^{-8}$ mol dm^{-3} (t_{ac}= 20 s at -0.8 V), for the mixed NA/PSS electrode and with a single NA-TMFE. The calibration slopes were 16.9 ± 0.4 A mol^{-1}dm^3 (r = 0.999, N = 5) and 13.6 ± 0.3 Amol^{-1}dm^3 (r = 0.999, N = 5) for NA/PSS-TMFE and for NA-TMFE, respectively. Hence, the sensitivity of NA/PSS-TMFE increased 23% comparing to the NA-TMFE (in accordance with the increase of 21% obtained for the average $I_{p(Pb)}$ values in Figure 3.5). The limits of detection (LOD) were identical for both electrodes, 3.6-5.5$\times 10^{-9}$ mol dm^{-3} (3σ). The overall RSD values were between 0.3 % and 2.7 % for the NA/PSS-TMFE and 0.7 % and 4.4 % for NA-TMFE showing that the repeatability of the ASV signals was enhanced for the electrode modified with the mixed polymeric coating.

The mechanical stability of the NA/PSS-TMFE was also evaluated. The modified MFE can be used for at least 60 consecutive stripping experiments (a set of five data points were taken at half hour intervals, with a total experimental time of six hours) without any significant change of the analytical signal. A 6% decrease occurred in the last measurement set, being the RSD values of the SWASV determinations always less than 3%. Therefore, the NA/PSS-TMFE may be used consecutively, without any apparent degradation of the integrity of the mercury film and/or of the polymeric coating.

The anti-fouling ability of the NA/PSS-TMFE was evaluated and compared with that of the TMFE, assessing the SWASV signal of lead in the presence of several surfactants (Fig. 3.6). At the present experimental conditions Triton X-100 is non-ionic (average M_w 625), hyamine, HYA, is a cationic surfactant (M_w 448), sodium dodecyl sulphate, SDS, is anionic (M_w 288.4), whereas bovine serum albumin, BSA, is an anionic globular protein of high molecular weight (M_w 68,000).
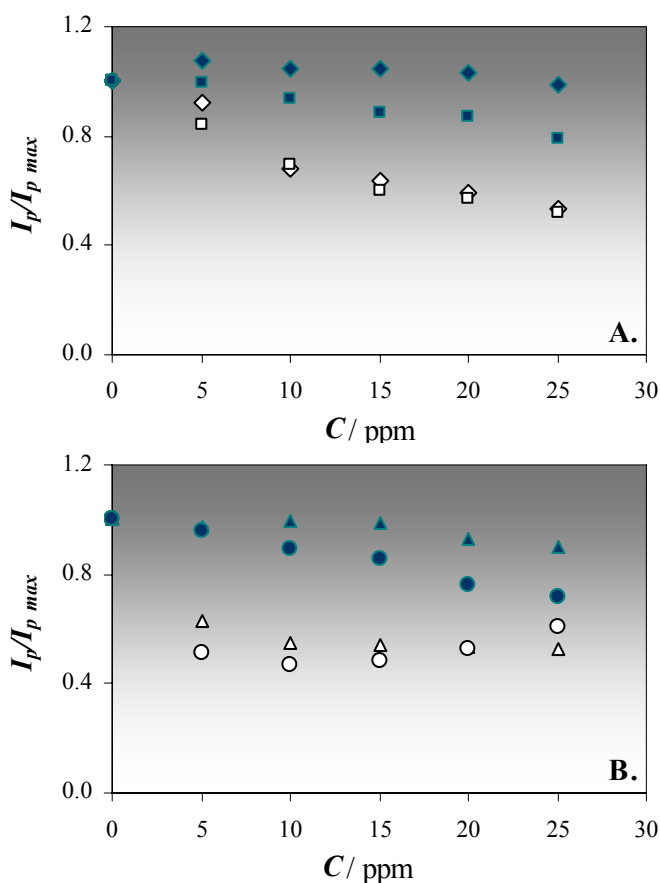
Figure 3.6. Effect of surfactants on the stripping peak current of lead, I_p, expressed as a normalized current relative to the value obtained in the absence of the surfactant, $I_{p\ max}$, at the TMFE (white markers) and at the NA/PSS-TMFE (r_m 5.3) (black markers). **A**: Triton X-100, squares and SDS, diamonds; **B**: HYA, circles and BSA, triangles. Experimental conditions as in Fig. 3.5.

At the bare TMFE, all surfactants produced significant current decreases reaching approximately half the initial value for surfactant concentrations greater 10 ppm. For the NA/PSS-TMFE the overall resistance to fouling was significantly improved. The worse results were obtained for HYA and Triton-X100 at the 25 ppm level, where signal hindering attained round 20%. Nevertheless, the NA/PSS modified electrode presented a much higher protection against HYA than single PSS-TMFEs, where total fouling occurred for HYA concentrations greater than 3 ppm [5], and single NA-TMFEs, where, in 5 ppm HYA solutions the ASV signal of lead decreased about 30% [8]. This improvement may be related to the morphology features of the NA/PSS mixed coating with a rather compact structure, despite the presence of the PSS bead shaped clusters, allied to high sulfonate content.

For Triton X-100, there are several reports showing its severe interference in ASV signals on polymer-modified MFEs [3,4,7]. For example, at a PSS-TMFE [4], lead(II) peak current decayed 60% for 25 ppm Triton X-100. Triton X-100 is inconsistent: there are situations where the lead stripping current increases for small concentrations of Triton X-100 and then levels off, suggesting a specific interaction between the lead(II) cation and TritonX-100 [3,7]. In other cases the opposite occurs and current decreases occur [29]. Therefore, it may be considered that the anti-fouling characteristics of the mixed coating NA/PSS modified TMFE are improved compared to other known electrodes modified with cation-exchange polymers, and are promising for applications in complex matrices.

The NA-PSS coated TMFE was tested in the SWASV determination of trace metals in estuarine water containing moderate levels of dissolved organic matter (DOC 8.4 ppm; salinity 17‰) and trace amounts of lead and copper (total concentrations $[Pb] = 2.4 \times 10^{-9}$ mol dm^{-3} and $[Cu] = 5.6 \times 10^{-9}$ mol dm^{-3}). Figure 3.7 clearly shows the improved ability of this electrode compared to the bare TMFE in the detection of ASV-labile lead and copper in this complex medium. The baseline turned out cleaner and the peak resolution and height were significantly improved.
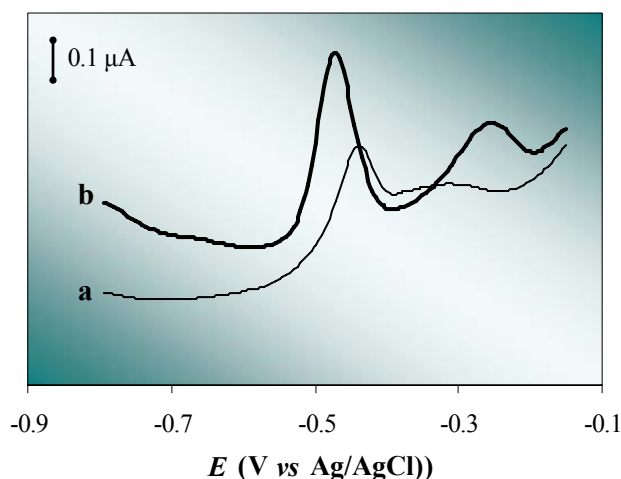
Figure 3.7. SWASV of an estuarine water sample (DOC 8.4 ppm) with the bare TMFE (a) and with the NA/PSS-TMFE (r_m 5.3) (b). t_{ac} =180 s at −0.8V; other experimental conditions as in Figure 3.5.

3.4. Conclusions

The present study shows that mechanically stable mixed films of two dissimilar sulfonated polymers can be easily prepared by solvent evaporation on a glassy carbon substrate. These coatings present a heterogeneous structured surface morphology, where phase separation is clearly observed between the hydrophobic nafion ionomer, which constitutes the film matrix, and the hydrophilic PSS polyelectrolyte. Randomly distributed PSS bead-shaped domains, associated with self-organized PSS structures are observed for electrodes with higher amounts of PSS. The present mixed polymer films represent an example of a rather complex system presenting appealing morphological features due to a combination of different physical processes occurring during the solvent evaporation step. Though, the film casting process was reproducible and allowed the preparation of reliable modified electrodes.

The use of mixed NA/PSS coated TMFE allows the formation of stable thin mercury films for ASV determinations, ensuring a suitable sensitivity, charge selectivity and interesting anti-fouling features. However, as the PSS content increases, the perm-selective properties are less suitable and the general behaviour approaches that of single coated PSS electrodes. Though, the reproducibility of the coatings, the incorporation of metal cations and the repeatability of the SWASV signals are improved, resembling the features of single coatings of PSS.

The film NA/PSS (r_m 5.3) was considered to present the right combination of characteristics for application in the direct SWASV determination of trace heavy metals. Calibration in the lead concentration range (2.00 to 10.0 $\times$ 10^{-8} mol dm^{-3}) for an accumulation time of 20 s at -0.8 V showed a 23% increment in sensitivity, compared to the NA-TMFE. This electrode was tested in the SWASV analysis of ASV-labile lead and copper at the low nanomolar level, in estuarine waters containing moderate amounts of dissolved organic matter, where the uncoated TMFE had a reduced performance due to partial fouling.

References

[1] P. Ugo, L.M. Moreto, F. Vezzá, *Chem.Phys.Chem* 3 (2002) 917.

[2] P. Ugo, L. M. Moretto, *Electroanalysis* 7 (1995) 917.

[3] C. M. A. Brett, D. A. Fungaro, J. M. Morgado, M.H. Gil, *J. Electroanal. Chem*. 468 (1999) 26.

[4] S. C. C. Monterroso, H. M. Carapuça, A. C. Duarte, *Electroanalysis* 15 (2003) 1878.

[5] S. C. C. Monterroso, H. M. Carapuça, A. C. Duarte, *Talanta* 64 (2005) 644.

[6] B. Hoyer, T. M. Florence, G. E. Batley, *Anal. Chem.*, 59 (1987) 1608.

[7] M. E. R. Dam, K. N. Thomsen, P. G. Pickup, K. H. Schroder, *Electroanalysis*, 7 (1995) 70.

[8] M. Buckova, M.Vanickova, J. Labuda, *Chem. Papers*, 50 (1996) 279.

[9] F-M. Matysik, S. Matysik, A. M. O. Brett, C. M. A. Brett, *Anal. Chem*. 69 (1997) 1651.

[10] J. Murimboh, T. M. Lam, M. N. Hassan, C. L. Chakrabarti, *Anal. Chim. Acta* 423 (2000) 205.

[11] H. –J. Kim, K. –S. Yun, E. Yoon, J. Kwak, *Electrochim. Acta* 50 (2000) 4471.

[12] M. W. Espenscheid, A. R. Ghatak-Roy, R. B. Moore, R. M. Penner, M. N. Szentirmay, C. R. Martin, *J. Chem Soc., Faraday Trans. 1*, 82 (1986) 1051.

[13] M. Tecier, J. Buffle, *Anal.Chem*. 68 (1996) 3670.

[14] G. S. Manning, *J.Chem.Phys*. 51 (1969) 924.

[15] C. M. A. Brett, V. A. Alves, D. A. Fungaro, *Electroanalysis*, 13 (2001) 212.

[16] C. B. Lopes, S. Abreu, M. Válega, R. M. B. O. Duarte, M. E. Pereira, A. C. Duarte *Anal. Lett.* 39 (2006) 1979.

[17] S. C. C. Monterroso, H. M. Carapuça, J. E. J. Simão, A. C. Duarte, *Anal. Chim. Acta* 503 (2004) 203.

[18] M. N. Szentirmay, C. R. Martin, *Anal. Chem* 56 (1984) 1898.

[19] A. Zook, J. Leddy, *Anal. Chem*. 68 (1996) 3793.

[20] P. Ugo, B. Ballarin, S. Daniele, G.A. Mazzocchin, *J. Electroanal. Chem*. 291 (1990) 187.

[21] J. Ruths, F. Essler, G. Decher, H. Riegler, *Langmuir* 16 (2000) 8871.

[22] C. R. Martin, H. Freiser, *Anal. Chem*. 53(1981) 902.

[23] A. Vishnyakov, A.V. Neimark, *J. Phys. Chem. B* 104 (2000) 4471.

[24] P.J. James, J.A. Elliot, T.J. Mc Master, J.M. Newton, A.M.S. Elliot, D. Hanna, M.J. Miles, *J. Mater. Sci*. 35 (2000) 5111.

[25] L. Weh, A. Venthur, *J. Colloid Interface Sci*. 271 (2004) 407.

[26] L. Weh, A. Venthur, *Macromol. Mater. Eng*. 289 (2004) 227.

[27] T. M. Florence, *J. Electroanal. Chem*. 27 (1970) 273.

[28] H. P. Wu, *Anal. Chem*. 66 (1994) 3151.

[29] M. Vaníckova, J. Labuda, E. Paulovicova, M. Vanicková, M. Fisera, *Chem. Anal. (Warsaw)* 39 (1994) 615.

CHAPTER 4

Evaluation of Poly(sodium 4-styrenesulfonate) film coating in thin mercury film electrodes for lead(II) determination

CHAPTER 4   Evaluation of Poly(sodium 4-styrenesulfonate) film coating in thin mercury film electrodes for lead(II) determination

4.1. Introduction

The use of ion-exchange polymers for modification of electrodes and for developing electrochemical sensing devices is still an area of continuous interest, where the study of the adsorption features, structural architectures and molecular/ionic incorporation properties is of crucial importance [1,2,3,4,5].

In chapter 3, the application of novel nafion (NA) and poly(sodium 4-styrenesulfonate) (PSS) mixed coatings in ASV studies of trace metals was evaluated . The main goal was to combine the excellent exclusion properties and the inherent insolubility in the aqueous media of NA ionomer, with the electrostatic accumulation of cationic species within the PSS polyelectrolyte films, which was achieved with the NA/PSS (r_m 5.3) modified thin mercury film electrode (TMFE).

The present study extends the idea of using single PSS coatings as a way to enhance the electrostatic accumulation of cations within the films, thus enlarging the voltammetric signal. If a significant amount of charge is present in the film at a not too high ionic strength the electrostatic effect will be large and the concentration of the metal cation within the film might become orders of magnitude larger than the metal in the solution. This constitutes effectively a pre-concentration step in the PSS film, as long as the thickness of the diffusion layer associated with the time scale of the technique does not exceed the film thickness, and would be then followed by a direct voltammetric measurement. In chapter 3, the thickness of the PSS film of 11 μm was obtained for a loading of 8.6 μg mm^{-2} which is of the same order of magnitude of the thickness of the diffusion layer for a square wave voltammetry of lead(II) performed at 25Hz, assuming that the diffusion coefficient of lead ions in the film is the same as in solution.

The main objective in this chapter is the evaluation of the incorporation features of such adsorbed PSS coatings towards lead(II). The ideal PSS coated electrode would be that with the highest density of –SO$_3^-$ groups and the lowest leakage to the test solution, in order to obtain the maximum loading of divalent cations in the film, previously to the voltammetric determination. Therefore the effects of the PSS mass loading, PSS molecular weight and concentration of the casting solution were analysed, as well as the effect of the ionic strength of the supporting electrolyte for ion-exchange voltammetry.

4.2. Experimental

4.2.1. Chemicals

Poly(sodium 4-styrenesulfonate), PSS, monomer mass: 206.20, pKa = 1 [6] (M_w = 150,000; 70,000; 32,000), was purchased from Aldrich and used as received. All chemicals were of analytical reagent grade and all solutions were prepared with ultra-pure water (Direct-Q3 UV system, Millipore). Sodium chloride (Merck, Suprapur), phosphate buffer solution (0.026 mol dm^{-3} KH$_2$PO$_4$/0.041 mol dm^{-3} Na$_2$HPO$_4$, pH 7.4, ionic strength 0.14$_9$ mol dm^{-3}, Merck, Suprapur) and 1000 ppm AA-Spectrosol metal ion (Hg, Pb) standards (BDH) were also used. Stock solutions of PSS (7.0, 15, 34, 60 e 119 mmol dm^{-3} in monomer units) were prepared in pure water (absence of added electrolyte) or in phosphate buffer of different ionic strengths.

4.2.2. Instrumentation

Voltammetric measurements were performed with a BAS 100B/W electrochemical analyser connected to a Cell Stand BAS-C2 (Bioanalytical Systems). The PSS coatings were prepared onto a glassy carbon disc (3 mm diameter, BAS, MF-2012). The auxiliary and reference electrodes were a Pt wire and a Ag/AgCl (sat. KCl), respectively.

Scanning electron microscopy (SEM) was conducted on an Analytical FE-SEM SU-70 Hitachi, UHR 1.0nm/15kV (1.6nm/1kV).

4.2.3. Preparation of the PSS modified electrodes

Prior to coating, the GCE was pre-conditioned as described before [7]. The coatings were prepared by solvent evaporation placing a 5 µL microdroplet of the selected PSS solution directly on the glassy carbon surface. Then, the solvent was evaporated under a low flux air stream (*ca.* 60ºC for ~10 min). When required, the utilized polymer layer was wiped off with a wet tissue and the GC surface was re-conditioned.

For ion-exchange voltammetry, thin mercury films electrodes (TMFE) were *ex-situ* plated through the PSS coating at −1.3 V for 20 s with stirring (BAS-C2 stand, position 3) in 1.2×10^{-4} mol dm^{-3} Hg(NO$_3$)$_2$ in 7.25×10^{-3} mol dm^{-3} nitric acid (pH *ca.* 1.9). Conventional TMFE were prepared using the same experimental conditions. The thickness of the *ex-situ* plated mercury film was calculated from the charge corresponding to the deposited mercury using the Faraday law [23] and the Hg atomic radius (1.44 Å) [8]. The average charge was 219 µC (RSD 3.2%; *N'* = 12), resulting in an estimated thickness of 1.3 nm, corresponding to a very thin mercury film [9,10].

Unless otherwise stated, all peak currents quoted are mean values of three replicate measurements at each of two different TMFE or PSS-coated electrodes.

4.2.4. Voltammetric procedures

Ion-exchange voltammetry (SWASV mode) were carried out in 10 mL NaCl electrolyte solutions of different ionic strength (0.50 and 0.0032 mol dm^{-3}), spiked with lead(II) as reference metal ion (concentration 6.00×10^{-8} mol dm^{-3}). The deposition step lasted 20 s at −0.8 V with stirring (BAS-C2, position 3). The SW stripping step was from −0.8 to −0.15 V (equilibration period 5 s). The SW parameters were: amplitude 25 mV, frequency 50 Hz and step potential 5 mV. Except otherwise stated, a 10 s cleaning step (E_{clean} = −0.2 V) between scans was used. All solutions were purged with nitrogen for 5 min prior to the voltammetric experiments and blanked although. Measurements were carried out at room temperature (18–20 ºC).

4.3. Results and Discussion

4.3.1. Behaviour of PSS modified electrodes in lead(II) determinations

The mechanical stability and the repeatability of the TMFE modified with adsorbed PSS polyelectrolytes films and its anti-fouling properties were evaluated in this section.

i) Mechanical stability of SWASV measurements

An important issue to be evaluated for modified electrodes is the integrity of the mercury film and the mechanical and physical stability of the polyelectrolyte coatings itself, when immersed in the working solution.

Previous work [11] has shown that PSS coatings (M_w 70,000; mass loading 4.8 µg mm^{-2}) prepared from 0.14$_9$ mol dm^{-3} phosphate buffer and used in 0.50 mol dm^{-3} NaCl medium were mechanically stable. As a first test, forty consecutive determinations of the lead SW peak current ($I_{p(Pb)}$) were done for similar electrodes and the results confirm those from Monterroso *et al.* [11]. The performance of the modified TMFE using a PSS polymeric coating prepared from water was also evaluated. Figure 4.1 represents the signals for the PSS modified TMFE, $I_{p(Pb)}$.
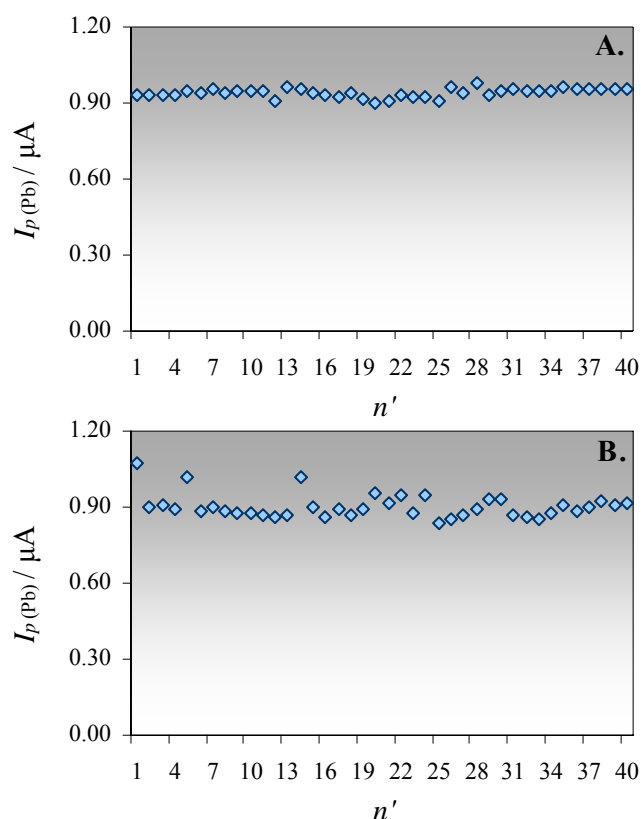
Figure 4.1. Variation of the $I_{p(Pb)}$ values for two PSS coated electrodes (M_w 70,000; mass loading 4.8 µg mm^{-2}) prepared from (A) water and (B) 0.14$_9$ mol dm^{-3} phosphate buffer. Electrolyte solution: 0.50 mol dm^{-3} NaCl. Concentration of lead: 6.00×10^{-8} mol dm^{-3}. Experimental SW parameters conditions: t_{dep} 20 s at -0.8 V, $a = 25$ mV and $f = 50$ Hz.

In what concerns the stability of these modified electrodes, there was no significant change of the Pb analytical signal over the 40 consecutive measurements. In fact, there was an improvement in the mechanical stability of the PSS-TMFE prepared from water, since there was a decrease in the RSD values from 5.3%, for those recasted from 0.14_9 mol dm^{-3} phosphate buffer, to 1.9%. Additionally, these experiments also prove the great mechanical and physical integrity of the PSS film itself, adsorbed at the glassy carbon surface, in neutral medium. Therefore, the same PSS-TMFE (prepared from water and 0.14_9 mol dm^{-3} phosphate buffer) can be used for at least 40 consecutive stripping experiments with no significant variation of the lead(II) analytical signal.

The typical SWASV voltammograms are presented in Fig. 4.2. For both types of PSS coated electrodes, the peaks were symmetric with E_p = - 480 ($\pm$ 5) mV and with a width-at-half-height ($W_{1/2}$) of 59 mV.   These values were very close to those for the unmodified TMFE (E_p = - 490 mV; $W_{1/2}$ = 59 mV).
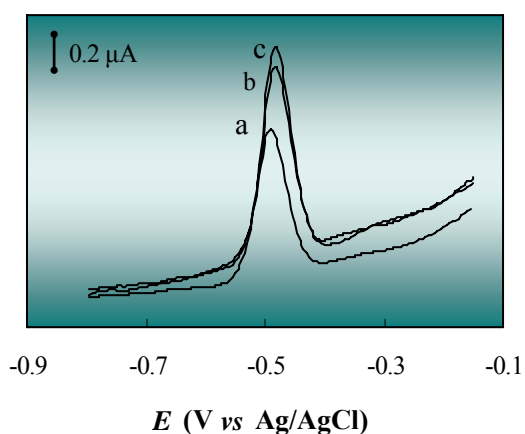
Figure 4.2. Typical SW voltammograms for the (a) bare TMFE and for PSS-coated electrodes prepared from (b) 0.14_9 mol dm^{-3} phosphate buffer and (c) water. Other experimental conditions as indicated in Fig. 4.1.

The SW signal could eventually be altered by setting an insufficient time for total reestablishment of the initial conditions at the interface PSS/electrolyte, therefore an adequate cleaning period must be applied. As described in the experimental section, before each scan a 10 s cleaning period was performed. No statistically defined variations were seen increasing that period: for 10 s, the $I_{p(Pb)}$ was 0.910 (RSD 5.9%, N' = 30) and for 60 s,

the $I_{p(Pb)}$ was 0.962 (RSD 5.9%, $N' = 30$) and the peak current were randomly distributed for consecutive measurements. So, the cleaning time of 10 s before each scan was enough to assure the equilibrium of the metal cation at the interfaces mercury/PSS/electrolyte, i.e., the metal cations had time to diffuse back to the electrolyte phase before the next accumulation step takes place.

ii)   Anti-fouling properties

The anti-fouling ability of the PSS-TMFE, prepared in both water and 0.14_9 mol dm^{-3} phosphate buffer, was evaluated and compared with that of the TMFE, assessing the SWASV signal of lead in the presence of two surfactants (Fig. 4.3). At the present experimental conditions Triton X-100 is non-ionic detergent (average M_w 625), whereas bovine serum albumin, BSA, is an anionic globular protein of high molecular weight (M_w 68,000).
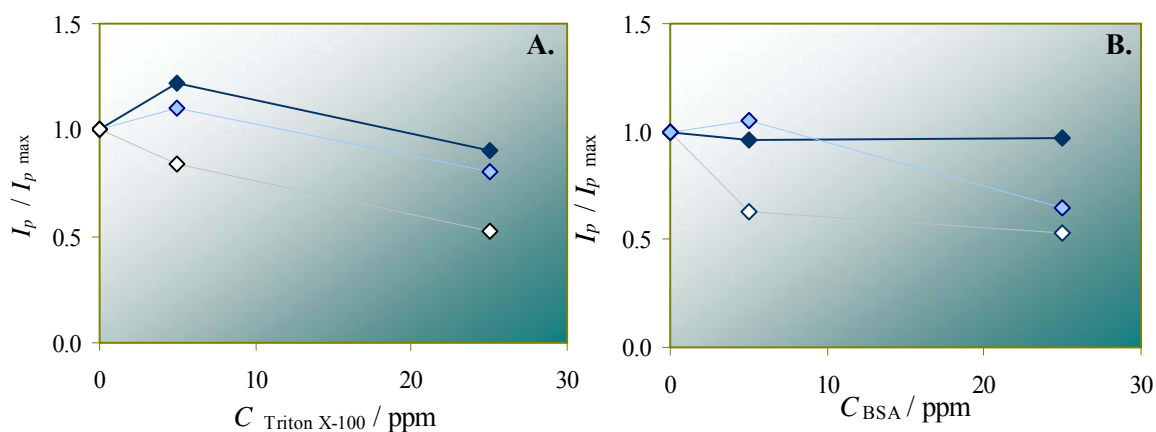
Figure 4.3. Effect of surfactants: Triton X-100 (A.) and BSA (B.) on the I_p of lead(II), expressed as a normalized current relative to the value obtained in the absence of the surfactant, $I_{p\,max}$, at the TMFE (white markers), at the PSS-TMFE recasted from phosphate buffer 0.14_9 mol dm^{-3} solution (blue) and from water (dark blue). Other experimental conditions as in Figure 4.1.

At the bare TMFE, both surfactants produced significant current decreases reaching approximately half the initial value for a surfactant concentration of 25 ppm. For the PSS-

TMFE the overall resistance to fouling was significantly improved, especially when PSS coatings prepared from water were used.

For Triton X-100 at the 25 ppm level, the signal hindering attained round 20% at the PSS recasted from 0.14_9 mol dm^{-3} phosphate buffer solution and in the case of the PSS prepared from water much higher protection was attained (the decrease in the SWASV signal of lead was *ca.* 9%). The results obtained for BSA were identical. This protein was totally excluded, even at the 25 ppm concentration level, at the modified PSS-TMFE recasted from water, and a decreased of 35% occurred at the PSS-TMFE prepared from a 0.14_9 mol dm^{-3} phosphate buffer solution. These differences are related to the morphology features of the PSS coatings prepared from different casting solutions (*cf.* section 4.3.2.2). For both Triton X-100 and BSA surfactants the decrease obtained at the TMFE was *ca.* 47%.

4.3.2. Effect of PSS casting solution characteristics

The influence of the composition of the PSS casting solution, the amount of deposited PSS and the molecular weight on the features of the PSS coatings for ion-exchange voltammetry was evaluated. Also the morphology of these polymeric films was assessed by SEM.

4.3.2.1. *Effect of the PSS mass loading*

The mass loading was changed by varying the concentration of the PSS solution, to give loadings in the range 1.0 – 17 μg mm^{-2}. The PSS (M_w 70,000) coatings were recasted from water and from a 0.14_9 mol dm^{-3} ionic strength phosphate buffer solution by solvent evaporation. Figure 4.4 displays SWASV peak currents of lead for PSS coated electrodes of different loadings, in 0.50 mol dm^{-3} NaCl electrolyte.
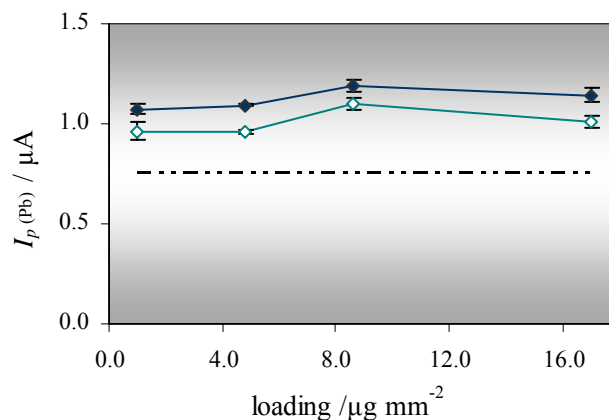
Figure 4.4. Effect of the PSS mass loading on the $I_{p(Pb)}$ values prepared from 0.14_9 mol dm^{-3} phosphate buffer (white marks) and water (blue marks) solutions. PSS M_w 70,000. The experiment was performed in 0.5 mol dm^{-3} NaCl electrolyte solution. Other parameters as in Fig. 4.1.

The data shows no statistically defined tendency irrespectively of the PSS casting solution (0.14_9 mol dm^{-3} phosphate buffer or water) in NaCl 0.50 mol dm^{-3} medium. A plateau was defined, with an average value of 1.12 (RSD 4.4%) for PSS coated electrodes prepared from phosphate buffer and an average value of 1.01 (RSD 5.5%) for those prepared from PSS water solutions. The RSD values for the un-coated TMFE were similar. So, for the considered loading range there was no effect of the PSS loading on $I_{p(Pb)}$.

At this relatively high ionic strength of the external medium, the PSS coatings tend to be pressed over the electrode surface. In spite of the increase in the amount of PSS, lead(II) was accumulated at the same extent as loading increased, pointing to the maintenance of a rather constant charge density of sulfonic groups. The total charge of $-$ SO$_3^-$ groups within the coating does not contribute to lead accumulation. Therefore, more PSS also mean more volume leading to a constant charge density in the film and, consequently, to a constant lead pre-concentration. So, in the present experimental conditions, the voltammetric behaviour, illustrated in Fig.4.4, turns out similar for both PSS casting solutions (water and 0.14_9 mol dm^{-3} phosphate buffer).

The effect of the mass loading was extended for the case of a very low ionic strength of the electrolyte, 0.0032 mol dm^{-3}. Fig 4.5 shows the results.
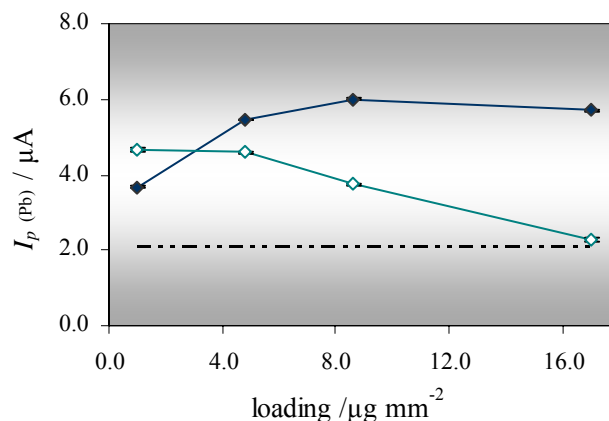
Figure 4.5. Effect of the PSS mass loading on the $I_{p(Pb)}$ values prepared from 0.14_9 mol dm^{-3} phosphate buffer (white marks) and water (blue marks) solutions. PSS M_w 70,000. The experiment was performed in 0.0032 mol dm^{-3} NaCl electrolyte solution. Other parameters as in Fig. 4.1.

Under these conditions, the curves diverge: for the PSS electrodes prepared from 0.14_9 mol dm^{-3} phosphate buffer, the $I_{p(Pb)}$ values decay systematically, while for the PSS-coated electrodes prepared from water, a plateau was defined for loadings above 4.8 µg mm^{-2}. The lead(II) peak currents were higher compared to those obtained for the 0.50 mol dm^{-3} electrolyte solution (*cf.* Fig. 4.4) and the other SWASV parameters were similar (E_p and $W_{1/2}$).

In a low ionic strength medium there are two points to be highlighted. First, for the PSS electrodes prepared from phosphate buffer, the peak current decay, pointing to a systematic destabilisation of the film with increasing loading, indicates leaching of PSS into the voltammetric solution. For the highest loading tested, the peak currents were close to the value obtained for the uncoated TMFE. Second, for the PSS electrodes prepared from water that effect was not observed. Considering that this type of coating is supposed to be denser and present a polymer backbone chain conformation that allows the intensification of hydrophobic forces with the carbon surface, one may expect a better mechanical stability.

Accordingly to the results obtained in a previous work, the 4.8 µg mm^{-2} PSS-TMFE (M_w 70,000) prepared from phosphate buffer and tested in 0.50 mol dm^{-3} NaCl, proved to have good reproducibility and repeatability [5,7,11]. These features were also evaluated in the present work for the same type of electrode in 0.0032 mol dm^{-3} electrolyte medium. The SW peak currents of lead(II) for six repeated measurements at four different coated

electrodes (*n'*) of each type (prepared from phosphate buffer 0.14_9 mol dm^{-3} and from water) were recorded (Fig. 4.6).
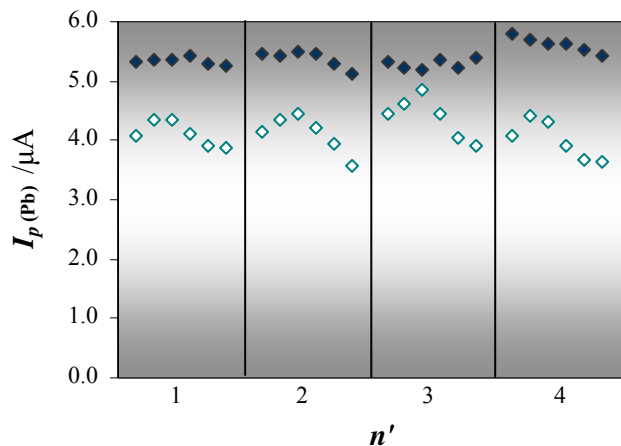
Figure 4.6. SWASV peak current values for six repeated measurements (*N'*=6) at four different PSS-modified electrodes: PSS prepared from water (black marks) and from 0.14_9 mol dm^{-3} phosphate buffer solution (white marks). PSS: M_w 70,000, mass loading 4.8 µg mm^{-2}. Electrolyte solution: 0.0032 mol dm^{-3} NaCl. Other parameters as in Fig. 4.1.

The median $I_{p(Pb)}$ value achieved with the PSS-coated electrode prepared from water was higher compared to that for the PSS electrode prepared from phosphate buffer (5.38 *vs.* 4.14 µA). On the other hand, the range for the $I_{p(Pb)}$ values for those electrodes was about 50% lower than for the electrodes prepared from phosphate buffer. Moreover, the analysis of the parameter σ_b^2 (that estimates the reproducibility of the measurements [12]) shows that the variance between samples of the PSS electrode prepared from water was slightly improved compared to that for the electrode prepared from phosphate buffer (0.12 *vs.* 0.16). The parameter σ_W^2 (that estimates the repeatability of the measurements [12]) shows a major difference between the two types of electrodes: the variance within samples for the PSS electrodes prepared from water was about nine times lower than for the ones prepared from phosphate buffer (0.01 *vs.* 0.09). In conclusion, the performance of the PSS electrodes prepared from water was improved meaning that this type of coatings allowed the formation of a stable electrode for ion-exchange voltammetry of lead in a supporting electrolyte of very low ionic strength.

4.3.2.2. *Effect of the ionic strength of the PSS casting solution*

Other parameter that influences the final properties of deposited polyelectrolytes is the ionic strength of the casting solution. The ionic strength of the PSS phosphate buffer casting solution was changed in the range 0-0.25 mol dm^{-3}, for a PSS mass loading of 4.8 μg mm^{-2} and M_w 70,000. The experiments were performed in NaCl 0.0032 mol dm^{-3} electrolyte medium and the results are displayed in Fig. 4.7.
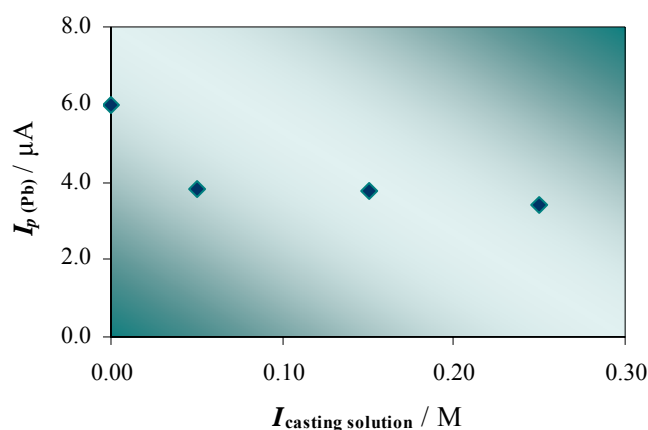
Figure 4.7. Variation of $I_{p(Pb)}$ values for PSS coated electrodes (mass loading 8.6 μg mm^{-2}; M_w 70,000) as a function of the ionic strength of the PSS phosphate buffer casting solution. Electrolyte solution: 0.0032 mol dm^{-3} NaCl. Other parameters as in Fig. 4.1.

A progressive decrease of *ca.* 40% of the analytical SWASV signals of lead was seen in the ionic strength interval under study. Considering the method of preparation of the PSS coatings by the single drop solvent evaporation, the observed behaviour may be correlated to volume changes of the PSS solutions for different ionic strengths. As the phosphate concentration (ionic strength) of the PSS casting solution increases, the polyelectrolyte chains will be more coiled in solution and the overall film shall be more expanded, while in pure water they will be essentially linear, due to the electrostatic repulsion. During the casting process performed by solvent evaporation, the PSS layer prepared from phosphate solution will have a globular conformation, whereas the one casted from water will present a layered conformation, which corresponds to a thinner and more compact coating. From the thickness estimates, the concentration of the sulfonic exchange groups in PSS coatings, as well as of the sodium counter-anions, can be

calculated as 3.9 mol dm^{-3}, revealing a large charge density inside the polyelectrolyte layer. This value is the same for the other film loadings because the polymer density was assumed constant.

A detailed SEM examination of the PSS coatings (M_w 70,000) prepared from water and from phosphate buffer 0.14$_9$ mol dm^{-3} was done (Fig. 4.8), in order to evaluate the effect of the ionic strength of the PSS casting solution influences in the morphology of these films and, consequently, its analytical performance.

SU70-72 15.0kV 16.0mm x2.00k SE(M)   20.0um SU70 15.0kV 18.0mm x10.0k SE(M)   5.00um
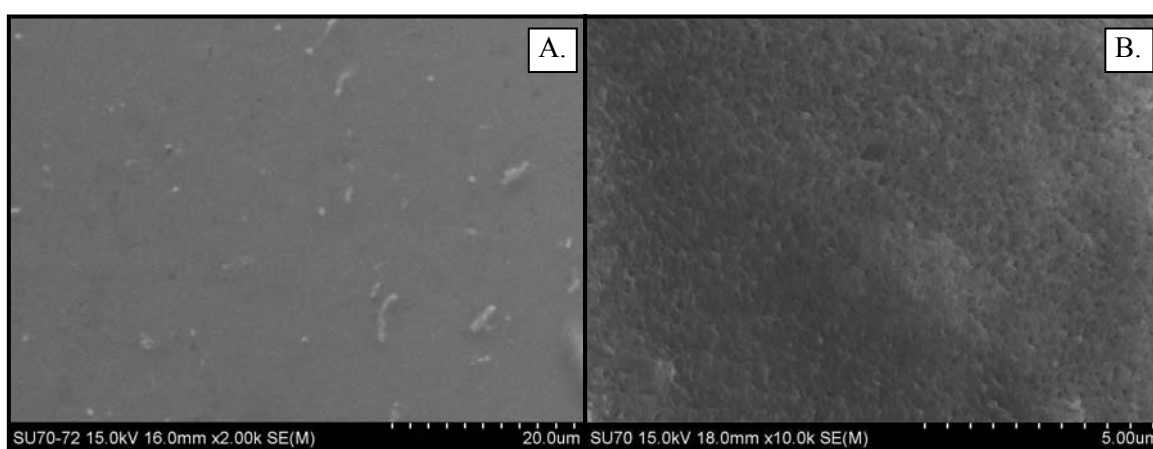
Figure 4.8. Typical scanning electron micrographs of PSS coatings (M_w 70,000) on a PSS coated GC electrode. PSS mass loading 8.6 μg mm^{-2} prepared from water (A × 2000) and from 0.14$_9$ mol dm^{-3} phosphate buffer solution (B × 10000).

Figure 4.8A shows that coatings prepared without adding electrolyte are very compact and even with higher magnification no further details were revealed. On the other hand, PSS coatings prepared from phosphate buffer (Fig. 4.8B) presented a spongy structure suggesting the formation of a tri-dimensional layer of higher thickness that may be more loosely bounded to the electrode surface. The schematic representation presented in Fig. 4.9 describes the mentioned above.
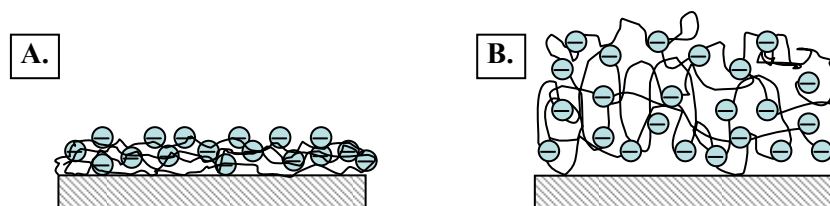
Figure 4.9. Schematic representation of the PSS film deposited on the GC electrode: prepared from water (A) and from 0.14_9 mol dm^{-3} phosphate buffer solution (B).

The comparative intensity of forces (electrostatic, hydrophobic or others) between PSS and the surface of the glassy carbon as well as forces within the PSS polyelectrolyte itself certainly play their part in the adhesion and morphology of the PSS films. The compactness of the coating deposited from water solution could be a consequence of the linear conformation of the polymeric chains formed in this medium, i.e. the polyelectrolyte molecules may be stretched due to charge repulsion (sulfonate groups and their counter-ions, Na$^+$). The PSS coating would be more stacked, with a denser structure where hydrophobic/dipolar interactions with the glassy carbon surface might prevail over electrostatic ones, leading to a higher stability. For a high ionic strength of the PSS deposition solution charge shielding increases and polyelectrolyte molecules change from a stretched to a coiled conformation [13,14]. Hence, the PSS film is thicker.

In order to a polyelectrolyte accumulate from a solution with added salt onto carbon, an additional chemical interaction must be operative, e.g., hydrophobicity or dipolar interactions. If the polyelectrolyte has a hydrophobic backbone, as is the case of PSS, it may adsorb also partly in a coiled or globule conformation [15]. However, if the electrostatics is too high the polyelectrolyte may even desorb [16]. High salt concentration can lead to irreversible swelling and overall material loss and the hydrophobic forces cannot hold on the PSS coating on the glassy carbon surface. Data reported in the previous sections support these considerations.

4.3.2.3. Effect of the PSS molecular weight (M_w)

PSS-coated electrodes were also prepared from PSS with different molecular weights of 32,000 and 150,000 and tested in 0.0032 mol dm^{-3} NaCl electrolyte solution. A mass loading of 8.6 µg mm^{-2} was selected. The results are presented in Fig. 4.10.
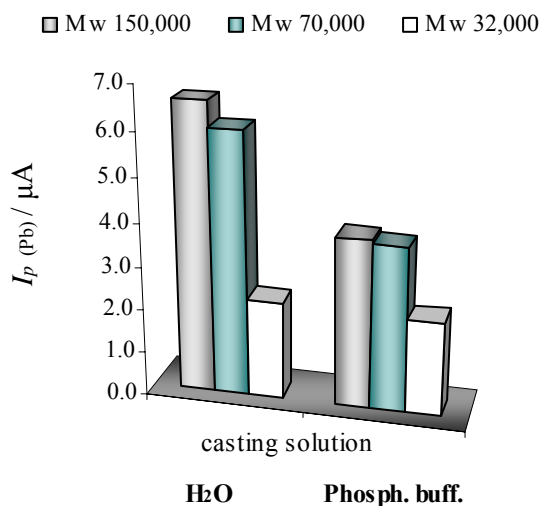
Figure 4.10. Variation of $I_{p(Pb)}$ values for PSS coated electrodes (mass loading 8.6 µg mm^{-2}) of different molecular mass, M_w: 150,000 (grey bars), 70,000 (blue bars) and 32,000 (white bars), prepared from water and 0.14$_9$ mol dm^{-3} phosphate buffer solutions. The dash black line corresponds to the signal obtained at the uncounted TMFE. Electrolyte solution: 0.0032 mol dm^{-3} NaCl. Other parameters as in Fig. 4.1.

The $I_{p(Pb)}$ for M_w 32,000, independently of the PSS casting solution used, decreased to values close to the ones for the TMFE itself. Hence, lowering M_w lead to a reduction of the stabilisation of the PSS coatings, even for those prepared from water. One might advance that for shorter chains lower hydrophobic interactions exist at the coating/glassy carbon interface. Also, the irregularity of the deposits might get higher as the molecular mass decreased, favouring the solubilisation of the PSS coatings.

On the other hand, for electrodes prepared from PSS with M_w 150,000, the $I_{p(Pb)}$ increased slightly compared to the values for electrodes prepared from PSS with M_w 70,000 (12% for water PSS casting solutions and 6% for phosphate buffer casting solutions). In spite of this slight increase, the cleaning time required to assure the equilibrium of the metal cation at the interfaces mercury/PSS/electrolyte had to be

extended (90 s instead of the usually applied time of 10 s), given that the peak current intensities were systematically increasing (*ca.* 35%; *N'*=5), as a result of the consecutive accumulation of lead inside the PSS layer.

So, the best performance is achieved for the TMFE coated with PSS with a M_w 70,000, since it provides a significant increase in the SWASV signal of lead(II) and the total time of the analytical measurement, that includes the time needed for the cleaning procedure, is short.

4.3.3. Effect of the ionic strength of the electrolyte medium solution

Accordingly to previous works, the permeability and structure of the polyelectrolyte layer were found to depend strongly on the ionic strength of the electrolyte solution [17], thus affecting the analytical response of metal cations. This was briefly demonstrated in section 4.3.1.

The variation of the $I_{p(Pb)}$ as a function of the ionic strength of the supporting electrolyte NaCl was studied for PSS coating 8.6 µg mm^{-2} recasted from water and phosphate buffer (0.14_9 mol dm^{-3}) solution. The results obtained were compared with those for the unmodified TMFE (Fig. 4.11).
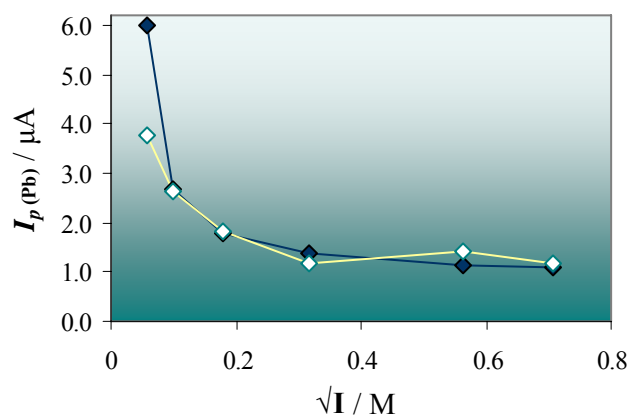
Figure 4.11. Variation of $I_{p(Pb)}$ for different values of ionic strength of the NaCl electrolyte solution: PSS coated electrodes prepared from 0.14_9 mol dm^{-3} phosphate buffer (white line) and water (dark blue line) solutions. PSS mass loading: 8.6 µg mm^{-2}. Other parameters as in figure 4.1.

The general shape of the curves, i.e. a decrease in the $I_{p(Pb)}$ values increasing the ionic strength of the electrolyte solution, was identical for both electrodes. There was always incorporation of lead(II) into the PSS coatings due to ion-exchange with the cations in the film: for ionic strength 0.50 mol dm^{-3} the peak current of lead was *ca.* 1.5 that for the bare TMFE, whereas for the ionic strength 0.0032 mol dm^{-3} the incorporation was improved, especially for the PSS coating prepared from a pure water solution. In fact, at low ionic strengths the electrostatic effect will be large and the concentration of the metal cation within the film becomes larger than the metal in the solution (preconcentration), resulting in the enhancement in the SWASV analytical signal of lead(II). This reveals that there is a compromise between the variation of the sulfonic charge density and the electrostatic repulsion forces as the film volume changes with ionic strength of the external medium.

4.4. Conclusions

In the present work PSS coated electrodes were prepared by solvent evaporation on glassy carbon in diverse experimental conditions. The results highlighted that to obtain PSS coatings mechanically stable, a compromise between the physical adsorption forces at the interface electrode/PSS and the additional swelling of the PSS layer with the external electrolyte should exist. Also the morphologic features must be considered. For PSS electrodes prepared from water a compact coating, that will be more resistant to solubilisation, is formed; otherwise, coatings prepared from 0.14$_9$ mol dm^{-3} phosphate buffer presented a spongy and fragile structure and are liable to solubilisation.

The accumulation of lead cation was higher for a very low ionic strength of the electrolyte where swelling is favoured. This is due to the effective charge density of sulfonic groups inside the PSS layer that depends not only on the charge shielding (higher for 0.5 mol dm^{-3}), but also on the PSS coating volume (higher for 0.0032 mol dm^{-3}). As a consequence, an increase in $I_{p(Pb)}$ of *ca.* 1.5 fold in 0.50 mol dm^{-3} NaCl external medium and of *ca.* 3 fold in NaCl 0.0032 mol dm^{-3}, relative to the unmodified TMFE were

obtained. However, there is always the possibility of PSS film solubilisation in lower ionic strength media, as a result of a significant leakage of PSS at this ionic strength and/or to a film expansion related to the lower screening of the charges.

The main goal of the present work was to obtain the best conditions for the preparation of a PSS coated glassy carbon electrode with a high negative charge density within a low volume film, allowing a fast and significant accumulation of divalent cations in the film that could be analysed by direct voltammetry. For the present electrodes, although reproducible and repeatable measurements were obtained, the lead cation pre-concentrations were not as high as we expected to be (at least 100 times). In the near future we will be interested in the development of different charged polymer films with high charge density and sufficiently rigid and stable to resist to the expansion at low ionic strengths.

References

[1] A. J. Bard, L.R. Faulkner, *Electrochemical Methods: Fundamentals and Applications* (2nd ed.), John Wiley & Sons, Inc., New York, 2001, chap. 14.

[2] K. Doblhofer, in J. Lipkowski, P.K. Ross (Eds.) *Electrochemistry of Novel Material, Frontiers of Electrochemistry*, VCH Publ., Inc., USA, 1994, chap. 4

[3] P. Ugo, L.M. Moretto, F. Vezzà, *ChemPhysChem* 3 (2002) 917.

[4] C.M.A. Brett, D.A. Fungaro, J.M. Morgado, M.H. Gil*, J. Electroanal. Chem.* 468 (1999) 26.

[5] S.C.C. Monterroso, H.M. Carapuça, A.C. Duarte, *Talanta* 65 (2005) 644.

[6] Y. Lvov, K. Ariga, M. Onda, I. Ichinose, T. Kunitake, *Colloids and Surfaces A: Physicochem. Engineer. Aspect*s 146 (1999) 337.

[7] L.S. Rocha, J.P. Pinheiro, H.M. Carapuça, *Langmuir* 22 (2006) 8241.

[8] H-J. Diederich, S. Meyer, F. Scholz, *Fresenius J. Anal. Chem.* 349 (1994) 670-675.

[9] S.C.C. Monterroso, H.M. Carapuça, J.E.J. Simão, A.C. Duarte, *Anal. Chim. Acta* 503 (2004) 203.

[10] H.P. Wu, Anal. Chem*.*, 68, (1996) 1639.

[11] S.C.C. Monterroso, H.M. Carapuça, A.C. Duarte, *Electroanalysis* 15 (2003) 1878.

[12] J.C. Miller, J.N. Miller, *Statistics for Analytical Chemistry*, 3rd ed., Ellis Horwood PTR/Prentice Hall, Great Britain, 1993.

[13] A. Fery, B. Schöler, T. Cassagneau, F. Caruso, *Langmuir* 17 (2001) 3779.

[14] K. Ren, Y. Wang, J. Ji, Q. Lin, J. Shen, *Colloids and Surfaces B: Biointerfaces* 46 (2005) 63.

[15] M. Gopinadhan, H. Ahrens, J.-U. Günther, R. Steitz, C.A. Helm, *Macromolecules* 38 (2005) 5228.

[16] S.T. Dubas, J.B. Schlenoff, *Macromolecules* 32 (1999) 8153.

[17] A.A. Antipov, G.B. Sukhorukov, H. Möhwald, *Langmuir*, 19 (2003) 2444

CHAPTER 5

Evaluation of nanometer thick mercury film electrodes for stripping chronopotentiometry

CHAPTER 5   Evaluation of nanometer thick mercury film electrodes for stripping chronopotentiometry

5.1. Introduction

5.2. Theory

    5.2.1. Depletive Stripping Chronopotentiometry (SCP) at the rotating TMFE

    5.2.2. Scanned Stripping Chronopotentiometry at the TMFE

5.3. Experimental

    5.3.1. Chemicals

    5.3.2. Instrumentation

    5.3.3. Preparation of the thin mercury film electrode

    5.3.4. Optimisation of the thin mercury film electrode

    5.3.5. Chronopotentiometric procedures

5.4. Results and Discussion

    5.4.1. Evaluation of the stability and durability of thin mercury film electrodes with different thickness

    5.4.2. Stripping regime in constant-current SCP using the TMFE

    5.4.3. Determination of the detection limits for SCP at the 7.6 nm thickness TMFE

    5.4.4. SSCP studies

        5.5.4.1. Experimental verification of the SSCP equation at the TMFE

        5.4.4.2. SSCP for metal ion speciation studies: Simple labile systems

5.5. Conclusions

5.1. Introduction

There is an increasing interest in, and demand for, the development of methods capable to perform trace metal speciation in environmental and biological matrices [1]. Electrochemical methods, in particular stripping techniques, like stripping chronopotentiometry (SCP) and anodic stripping voltammetry (ASV), are of particular utility for studies on metal ion speciation [2].

SCP represents a valuable alternative to ASV [3], allowing the elimination of adsorption complications, that hinder data interpretation in the case of ASV measurements [4,5,6]. When operated in the scan deposition potential mode, i.e., scanning stripping chronopotentiometry (SSCP) a full theoretical supported way to interpret metal complexation parameters is provided [2,7,8,9].

SCP and SSCP are typically performed on mercury electrodes, being the hanging mercury drop electrode (HMDE) and the mercury microelectrode over a supporting iridium micro-disk, currently used in speciation studies. So far, the application of the mercury film electrode (MFE), of micrometer thickness, was been extended only to SCP experiments of trace metals [10]. Despite of the well defined hydrodynamic conditions during the deposition step and a wide range of oxidation currents that could be applied in full depletion conditions, there were some disadvantages associated with the MFE, namely lack of reproducibility and a complex preparation procedure [10,11].

In this chapter the potentialities of homogeneous, stable and highly reproducibility thin mercury film electrodes (TMFE) of nanometer thickness (prepared by simple and reliably methodology [12]), were evaluated in the SCP/SSCP measurements of trace metals. The applicability of the TMFE was extended to the determination of metal speciation parameters, like the stability constant (K), where two metal-complex systems were used: Pb(II)-carboxylated latex nanospheres and Pb(II)-pyridine-2,6-dicarboxylic acid.

5.2. Theory

5.2.1. Depletive Stripping Chronopotentiometry (SCP) at the rotating TMFE

In the depletive regime the number of moles deposited equals:

$$N_{deposited} = \frac{I_d^* t_d}{nF} \qquad (5.1)$$

and the number of moles reoxidised is given by:

$$N_{oxidised} = \frac{I_S \tau^*}{nF} \qquad (5.2)$$

where I_s is the stripping current (A), and τ^* is the limiting value for the transition time (s) obtained for deposition potentials much larger than the standard potential, $E_d << E^0$. In the depletion mode the number of deposited moles equals the number of moles reoxidised and the limiting transition time is given by:

$$\tau^* = I_d^* t_d / I_s \qquad (5.3)$$

representing the charge balance for complete depletion [8].

5.2.2. Scanned Stripping Chronopotentiometry at the TMFE

The SSCP curves are plotted from a series of measurements made over a range of deposition potentials, E_d (V). The potential is held at E_d during the deposition time, t_d (s), after which the oxidizing current is applied until all the metal is reoxidised.

i) Metal-only case SSCP [2,10,13]

For a given potential, the deposition current, I_d (A), at a rotating TMFE is given by:

$$I_d = \frac{nFAD_M(C^*_M - C^0_M)}{\delta_M} \tag{5.4}$$

where c^*_M is the metal concentration in the bulk solution (mol m^{-3}), c^0_M is the metal surface concentration (mol m^{-3}) and δ_M is the Nernst diffusion layer thickness (m). For the rotating disk electrode (RDE) the last parameter is expressed by:

$$\delta_M = 1.61 D_M^{1/3} \omega^{-1/2} \upsilon^{1/6} \tag{5.5}$$

being ω (rad s^{-1}) and the angular speed rotation for the RDE ($\omega = 2\pi v_{rot}$, where v_{rot} is the speed of rotation), υ the kinematic viscosity (m^2 s^{-1}), which is defined as the viscosity divided by the density of the test solution, and D_M is the diffusion coefficient of the metal M (m^2 s^{-1}). The other symbols in equation (5.5) have their usual meaning. The limiting value of the deposition current, I^*_d, obtained at large negative potentials at which the concentration of metal ion at the electrode surface is essentially equals to zero ($c^0_M \rightarrow 0$), is given by:

$$I^*_d = \frac{nFAD_M C^*_M}{\delta_M} \tag{5.6}$$

Using equations (5.3) and (5.6) it is possible to determine the equivalent surface area of the TMFE, A (m^2).

The equation that fully describes the relation between τ and E_d (SSCP curve) for the rotating TMFE in the full depletion regime, is equal to that of the conventional HMDE, is given by:

$$\tau = \frac{I^*_d \tau_d}{I_s}\left[1 - \exp\left(\frac{t_d}{\tau_d}\right)\right] \tag{5.7}$$

in which the characteristic time constant of the deposition process, τ_d (s), is defined by:

$$\tau_d = \frac{V_{Hg\,dep}\,\delta}{AD_M\theta} \tag{5.8}$$

where θ the free metal surface concentration ratio ($\theta = c_M^0 / c_{M^0}^0$). For a reversible electron transfer reaction, M+ne$^-$↔M^0, and a given deposition potential, E_d:

$$\theta = \exp\left(\frac{nF(E_d - E^0)}{RT}\right)$$
(5.9)

Assuming a thin-film condition, the volume of the mercury electrode, $V_{Hg,dep}$ (m^3), can be estimated from the amount of charge of mercury using the Faraday law and assuming the Hg atomic radius (r_{Hg}) as 1.44×10^{-10} m [12]:

$$V_{Hg,dep} = \frac{(4/3)\pi r_{Hg}^3 N_a Q_{Hg}}{2F}$$
(5.10)

ii) SSCP in Labile Systems with $D_{ML} < D_M$ [2,7]

Considering the formation of a labile 1:1 metal complex, ML, between the electroactive metal ion M and the ligand L:

$$\text{M+L} \underset{K_d}{\overset{K_a}{\rightleftarrows}} \text{ML}$$
$$\downarrow\uparrow_{n\bar{e}}$$
$$\text{M}^0$$
(5.11)

the stability constant, K (m^3 mol^{-1}), is defined by $K = c_{ML}^* / (c_M^* c_L^*)$. For labile complexes, the rates of dissociation/association are sufficiently high relative to the experimental timescale, in order to maintain full equilibrium between complexed and free metal. Under conditions of sufficiently excess of ligand (as typically used in stripping experiments) we can define $K' = K c_{L,t}^*$ (where $c_{L,t}^*$ is the total concentration of L in the bulk solution (mol m^{-3})). Thus we can write:

$$\theta = \frac{C_{M,t}^0 / C_{M^0}^0}{1 + K'}$$
(5.12)

where $c_{M,t}$ is the total metal concentration (mol m^{-3}).

If the diffusion coefficient of the metal complex species, D_{ML} ($m^2\ s^{-1}$), is lower than that of the free metal ion (D_M), i.e. $D_{ML}<D_M$ (the general case), the deposition current and τ_d, are modified since D_M is replaced by:

$$\overline{D} = \frac{D_M c_M^* + D_{ML} c_{ML}^*}{c_{M,t}^*} \tag{5.13}$$

and the corresponding diffusion layer thickness, $\overline{\delta}$ (m), is modified accordingly for the given hydrodynamic conditions:

$$\overline{\delta} = 1.61 \overline{D}^{1/3} \omega^{-1/2} \upsilon^{1/6} \tag{5.14}$$

The expression for τ_d (former Eq. 5.8) thus becomes:

$$\tau_d = \frac{V_{Hg\,dep}\ \overline{\delta}}{A\overline{D}(1+K')\theta} \tag{5.13}$$

The equation for the SSCP wave for a labile complex ML, τ, is given from equation (7), though substituting I_d^* by $I_{d,M+L}^*$, that is expressed by $I_{d,M+L}^* = \tau_{M+L}^* I_s/t_d$ (τ_{M+L}^* is the limiting SCP transition time obtained from of the SSCP curve in the presence of a ligand). The coefficient in equation (5.7), $I_d^* \tau_d / I_s$, is a factor that does not affect the position of the wave on the E_d axis [2]. Therefore, an explicit expression for the shift of the half-wave potential due to the formation of a complex, $\Delta E_{d,1/2}$ (equivalent to the DeFord-Hume expression) can be obtained considering only the exponential term. In the case of a kinetic current, the shape of the SSCP wave remains unchanged and the same approach can be used, yielding [9]:

$$\ln(1+K') = -(nF/RT)\Delta E_{d,1/2} - \ln(\tau^*_{M+L}/\tau^*_M)] \tag{5.16}$$

5.3. Experimental

5.3.1. Chemicals

All chemicals were of analytical reagent grade and all solutions were prepared with ultra-pure water (18.3 MΩ cm, Milli-Q systems, Millipore-waters). Sodium nitrate, potassium chloride, nitric acid 65% (Merck, suprapur), hydrochloric acid 37% (trace select, Fluka) and 1000 ppm Hg and Pb AA-Spectrosol metal ion standards (BDH) were also used. Ferricyanide standard solution (1.929×10^{-3} mol dm^{-3}) in 1.0 mol dm^{-3} KCl was used for chronoamperometry. Nitric acid (0.1 M) and sodium hydroxide solutions (0.1 mol dm^{-3}) were used for pH adjustments. Stock solution of MES 2-(N-morpholino-ethanesulfonic acid) buffer was prepared from the solid (Merck). Solutions of ammonium acetate (NH$_4$Ac 1.0 mol dm^{-3} /0.5 mol dm^{-3} HCl) pH buffer and ammonium thiocyanate 1.0 mol dm^{-3} were prepared monthly and used without further purification. Monodisperse carboxylated latex nanospheres were obtained from Ikerlat Polymers (Spain): a=40.0 nm, $C_{L,t}$=5.2$\times 10^{-5}$ mol COOH per gram. These nanospheres were cleaned by the manufacturer, who provided a conductimetric and potentiometric characterization of each sample. Pyridine-2,6-dicarboxilic acid (PDCA) was from Fluka (purum).

Biohit Proline pipettes equipped with disposable tips were used for appropriate dilutions. All measurements were carried out at room temperature (18-20 ºC).

5.3.2. Instrumentation

An Ecochemie Autolab PGSTAT10 potentiostat (controlled by GPES 4.9 software from EcoChemie, the Netherlands) was used in conjunction with a Methrohm 663 VA stand (Methrohm, Switzerland). The three electrode configuration was used comprising a TMFE plated onto a rotating glassy carbon (GC) disc (1.9 mm diameter, Methrom) as the working electrode, a GC rod counter electrode and a double junction Hg│Hg$_2$Cl$_2$│KCl(3 mol dm^{-3}) encased in a 0.01 mol dm^{-3} NaNO$_3$ solution. The electrochemically active surface area of the glassy carbon electrode, (3.098 $\pm$ 0.015) mm^2, was measured by

chronoamperometry (in 1.929×10^{-3} mol dm^{-3} ferricyanide/1.0 mol dm^{-3} KCl solution; two polishing experiments, each with four replicate determinations).

A combined glass electrode (Radiometer Analytical pHC3006-9) connected to a pH meter (Thermo Electron Corporation, Model Orion 3-Start) was used for pH measurements.

5.3.3. Preparation of the thin mercury film electrode

Prior to coating, the glassy carbon electrode (GCE) was conditioned following a reported polishing/cleaning procedure [14], described in chapter 2.2.3. These polishing and electrochemical pre-treatments were repeated daily.

The thin mercury film was than *ex-situ* prepared in 0.03 to 1.2×10^{-4} mol dm^{-3} mercury(II) nitrate in thiocyanate media (5.0×10^{-3} mol dm^{-3}, pH 3.4) by electrodeposition at -1.3 V for different deposition times (180, 240 or 360 s) and a rotation rate of 1000 rpm [12,14]. The charge associated to the deposited mercury (Q_{Hg}) was calculated by electronic integration of the linear sweep stripping peak of mercury, for $v = 0.005$ V s^{-1}. The electrolyte solution was ammonium thiocyanate 5 mM (pH 3.4) [12]. The stripping step began at -0.15 V and ended at +0.6 V [15]. All charges quoted were mean values of 3 replicate measurements (RDS<3%). The thickness and repeatability of the TMFEs were estimated using this mean value of $Q_{Hg.}$

When not in use the GCE was stored dry in a clean atmosphere [12].

5.3.4. Optimisation of the thin mercury film electrode

The stability of the pre-plated TMFE of different thicknesses (1.9, 2.4, 3.6 and 7.6 nm) was evaluated following the variation of the square-wave anodic stripping voltammetric (SWASV) signal of Pb(II) in a set of 60 consecutive stripping measurements. In addition, the charge associated to the deposited mercury (Q_{Hg}) was determined for two replicate films prior to the set of ASV experiments. The mean value of Q_{Hg} was compared

to the final mercury charge of each film of different thickness, used in the set of ASV determinations.

For the SWASV experiments the electrolyte used was a 20 mL $NaNO_3$ 0.01 mol dm^{-3} solution spiked with 6.00×10^{-8} mol dm^{-3} Pb(II). The deposition and equilibrium time were 20 and 5 s, respectively, for a deposition potential of -0.8 V and a rotation rate of 1000 rpm. The stripping step was initiated at -0.8 V and ended at -0.15 V. The instrumental parameters in SWASV were: amplitude 0.025 V, frequency 25 Hz and step potential 0.005 V. All solutions were purged with nitrogen for 5 min, prior to the voltammetric experiments and blanked during data acquisition.

5.3.5. Chronopotentiometric procedures

Stripping chronopotentiometric measurements were carried out in 20 mL 0.01 mol dm^{-3} $NaNO_3$ solutions spiked with lead(II) as a reference metal ion (concentration of Pb(II) 1.19×10^{-7} mol dm^{-3}). The following conditions were used: deposition potential, -0.65 V; deposition time ranging from 0 to 300 s; rest time of 10 s for a deposition potential of -0.65 V; oxidising current, 2×10^{-9} A to 500×10^{-9} A, applied in a stripping range from -0.65 V to -0.37 V. All solutions were purged for 60 minutes in the beginning of every SCP experiment and 60 s (assisted by mechanical stirring of the rotating GCE) after each measurement.

The SSCP waves were constructed from a series of individual SCP measurements, by plotting the peak area as a function of the deposition potential, i.e. [-0.65, 0.48] V. For each point the potential was held at E_d for a deposition period of 40 s, followed by the application of a oxidising current of 75×10^{-9} A (complete depletion), until the potential reached a value that is well passed the transition plateau (-0.37 for Pb at the TMFE).

The stability constant, K, of the Pb(II)-carboxylated latex nanospheres (40 nm radius) system was determined by SSCP at the TMFE and HMDE. Two SSCP waves were obtained for Pb(II) (2.42×10^{-7} mol dm^{-3} in NaNO3 0.01 mol dm^{-3}), in the absence and in the presence of an excess of carboxylated latex nanospheres (0.1% w/w). Previous to the addition of the ligand, the solution was set at pH 5.5 using MES 2-(N-morpholino-ethanesulfonic acid) buffer.

5.4. Results and Discussion

5.4.1. Evaluation of the stability and durability of thin mercury film electrodes with different thickness

Electrodeposition of mercury onto glassy carbon in acidic solutions of thiocyanate, provides highly homogeneous and reproducible mercury films of nanometer thickness [12]. In the present work, the performance of this type of TMFE, ex-situ prepared in thiocyanate media, was evaluated in order to assess their potential application for SCP/SSCP experiments. A good mechanical stability of the thin mercury films represents a major improvement for the in field application of SCP/SSCP.

The variation of the stripping peak current of lead(II) was evaluated for TMFEs of thickness of 1.9, 2.4, 3.6 and 7.6 nm during 60 consecutive stripping experiments. The amount of deposited mercury (measured as Q_{Hg}) was determined before and after the consecutive stripping measurements, in order to assess the durability of the several TMFEs. Table 5.1 presents these data.

Table 5.1. Variation of $I_{p(Pb)}$ (in percentage values) during 60 consecutive SWASV experiments (lead(II) concentration of 1.19×10^{-7} mol dm^{-3} in 0.01 mol dm^{-3} NaNO$_3$) at TMFEs of different thickness ; SW parameters: $E_d= -0.8$ V, $t_d = 20$ s, $a = 0.025$ V, $f = 25$ Hz and $v = 0.125$ V s^{-1}. Charge determination (LSV): $E_i= -0.15$ V, $E_f= 0.6$ V and $v = 0.005$ V s^{-1}.

TMFE thickness (nm)	$I_{p(Pb)}$ variation (%)	Q_{Hg} variation [a] (%)
1.9	-25.2	-17.3
2.4	-17.4	-21.2
3.6	-15.8	-7.2
7.6	-9.0	-1.2

[a] Variation of the charge values, Q_{Hg}, relative to fresh mercury films (*cf.* section 5.3.4.).

The decrease in $I_{p(Pb)}$ during the consecutive experiments was smaller for the thicker TMFE. Similarly, the decrease of the Q_{Hg} followed the same trend. These features suggest that the degradation of the thinner mercury films was faster than for the thicker, i.e. the loss of small mercury droplets from the GC surface or their coalescence may have occured.

It must be noted that, the variation in the Q_{Hg} values only assess qualitatively the mechanical stability of the TMFE, since the mercury charge measured before and after the sixty SWASV consecutive experiments, was measured on different mercury films. However, it has been already shown that the mercury film deposits are very reproducible when prepared in thiocyanate media (RSD less than 3%) [12]. In conclusion, by selecting a 7.6 nm thickness mercury film electrode, it was possible to perform daily SSCP experiments with a single mercury deposit. In these conditions, the variation in the I_{pPb} ASV signal for 60 consecutive stripping experiments, was less than 10% and the deviations of the Q_{Hg} values, were smaller than 2% . For that reason, the mechanical stability and durability of the TMFE was considered suitable for the present experimental demands.

5.4.2. Stripping regime in constant-current SCP using the TMFE

The use of a thin mercury film for SCP shall provide a rapid metal transport during the stripping step and, as a result, the measurements are performed frequently under conditions of complete depletion [13]. In the present study, the influence of the SCP oxidative current (I_s) in the lead(II) signal using a thin mercury film electrode (thickness of 7.6 nm) was evaluated. Depending on the magnitude of I_s, the prevailing conditions during the stripping step could range from linear diffusion, for high I_s values ($I_s\tau^{1/2}$ constant), to the complete depletion limit for low I_s values ($I_s\tau$ constant) [3,6]. The first step was to establish the oxidation current range, under which the depletion of the metal was complete and where the influence of the dissolved oxygen in solution is minimized.

The SCP signals obtained at the TMFE for the current range $[5\text{-}500]\times10^{-9}$ A, were well defined and resolved ($w_{1/2}$ varied between 0.033 and 0.034). The results revealed that the depletion of lead(II) during the stripping step from the thin mercury film was essentially complete, in the oxidation current range $[5\text{-}500]\times10^{-9}$ A (Fig. 5.1). Although, for lower stripping currents, the $I_s\tau$ parameter was not held constant due to the interferences caused by the dissolved oxygen in the test solution.
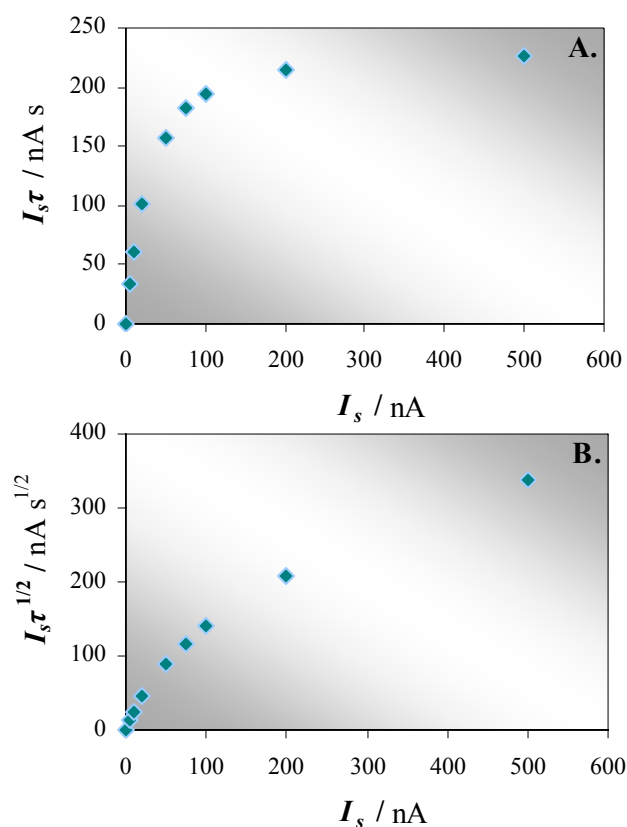
Figure 5.1. Evaluation of the SCP stripping regime for a TMFE (thickness 7.6 nm) by plotting: (A.) $I_s\tau$ vs. I_s (conditions of complete depletion), and (B.) $I_s\tau^{1/2}$ vs. I_s (conditions of semi-infinite linear diffusion) within the I_s interval of $[0\text{-}500]\times10^{-9}$ A. The transition times (τ) were measured in a solution of lead(II) (1.19×10^{-7} mol dm^{-3} in 0.01 mol dm^{-3} NaNO$_3$) and for a deposition time of 40 s.

The interval of operational I_s values can be precisely defined, evaluating the linearity of the $1/I_s$ vs τ plots (Fig. 5.2).
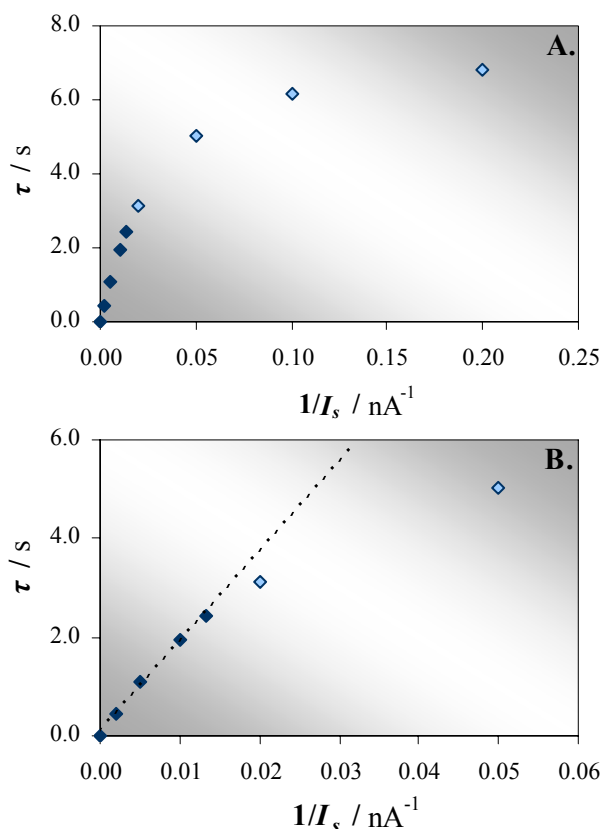
Figure 5.2. Effect of the oxidizing current (I_s) in the SCP signal of Pb(II) 1.19×10^{-7} mol dm^{-3} in 0.01 mol dm^{-3} NaNO$_3$) for a TMFE (thickness 7.6 nm). Deposition time: 40 s. The data are plotted as: τ *vs* $1/I_s$ for I_s values ranging: (A.) $[5-500]\times10^{-9}$ A and (B.) $[20-500]\times10^{-9}$ A.

Figure 5.2B shows that for $1/I_s$ higher than 0.013×10^{-9} A^{-1}, corresponding to a stripping current of 75×10^{-9} A, a deviation to linearity of the τ *vs.* $1/I_s$ plot occurred. In fact, a decrease in the SCP signal of lead (τ) occurred and by interpolation of the linear section of the τ *vs.* $1/I_s$ plot ($\tau = 1.825\times10^{-7}$ $1/I_s + 7.602\times10^{-2}$) it was possible to predict this variation. The reduction of the SCP signal tend to be progressively higher for lower I_s values, reaching 81% for a stripping current of 2×10^{-9} A.

The influence of dissolved O$_2$ in the test solution only became negligible for stripping currents higher than 75×10^{-9} A, since the chemical oxidation component was insignificant relative to the imposed oxidising current. Accordingly to this results the interval of operational I_s values was set as $[75-500]\times10^{-9}$ A. The stripping current selected for the following studies was 75×10^{-9} A (lowest working I_s value under the present conditions), given that a higher sensitivity was obtain.

5.4.3. Determination of the detection limits for SCP at the 7.6 nm thickness TMFE

Compared to the HMDE, a substantial increase of sensitivity in the stripping measurements was achieved, due to the higher area to volume ratio of the TMFE [13]. However, due to its small volume saturation may occur, for higher metal concentrations or longer deposition times.

To assess these features for the present TMFE (thickness 7.6 nm), the influence of the deposition time (t_d) and the concentration of lead (C_{Pb}) in the SCP signal was studied. Fig. 5.3 presents the variation of τ with the deposition time, in the interval of [0-300] s for a lead concentration of 1.19×10^{-7} mol dm^{-3}. All τ values had RSD ranging between 0.1 and 1.6%, evidencing no differences of the repeatability of the SCP signals.
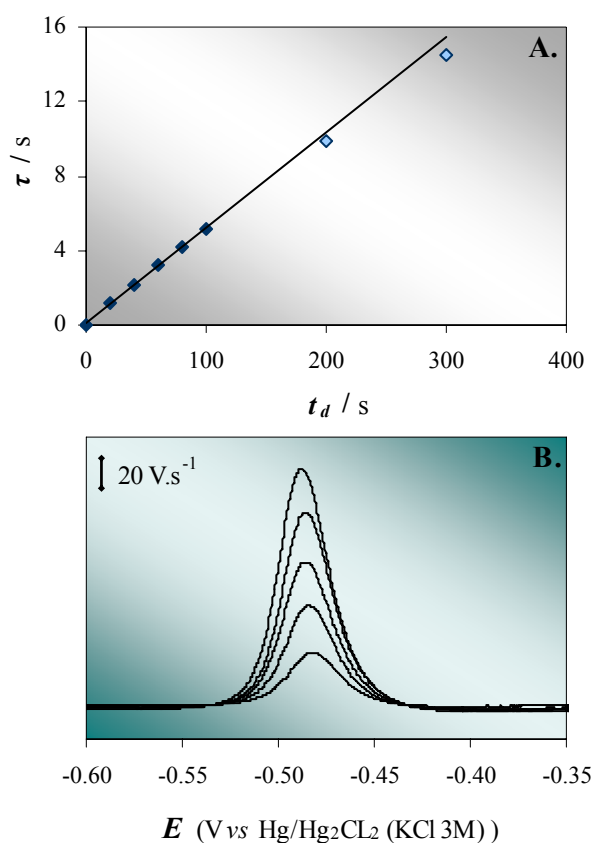
Figure 5.3. Effect of the deposition time (t_d) in the SCP signal of lead (τ) at the TMFE (7.6 nm thickness) and for t_d values of: 20, 40, 60, 80, 100, 200 and 300 s at a deposition potential of -0.65 V. Calibration plot (A.) and SCP signals for t_d within the interval of [20-100] s (B.). Experiments performed in 0.01 mol dm^{-3} NaNO$_3$ using a Pb(II) concentration of 1.19×10^{-7} mol dm^{-3} and a I_s of 75×10^{-9} A.

The results showed a linear variation of τ with the deposition time within the interval of [0-100] s, with a good definition of the SCP signals, even for lower t_d values (Fig. 5.3B). Though, a negative deviation to linearity was observed for $t_d \geq 200$ s (Fig. 5.3A), due to a decrease and distortion of the SCP signal, as the thin mercury film began to saturate.

The working concentration range of lead(II) was also evaluated for a deposition time of 40 s. The calibration curve is displayed in Fig. 5.4A and Fig. 5.4B shows the typical signals for the addition of lead in the range [15-240]$\times 10^{-9}$ mol dm^{-3}.
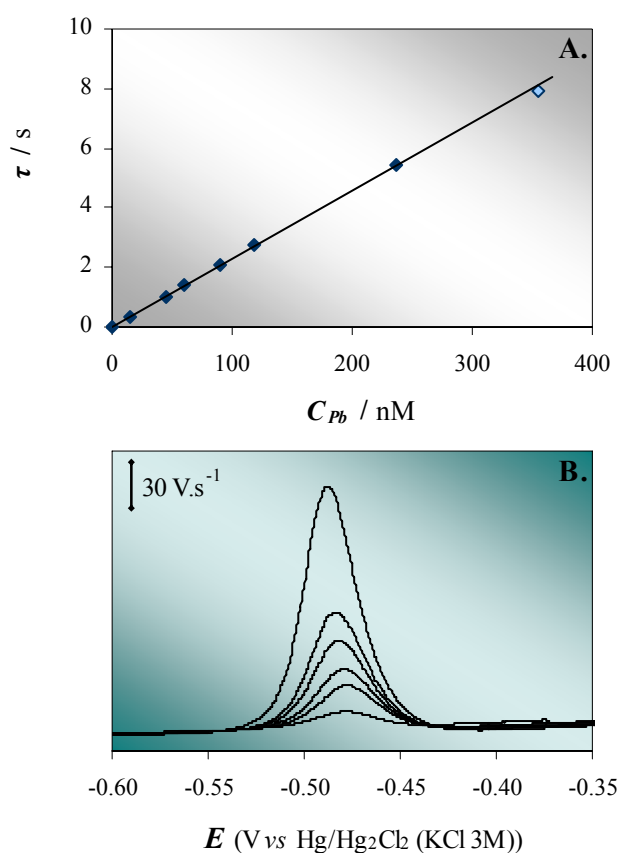
Figure 5.4. Variation of the SCP signal (τ) as a function of the concentration of Pb(II) at the TMFE (7.6 nm thickness), for a Pb(II) concentration (x10^{-9} M): 15, 45, 60, 89, 120, 240, 360. Calibration plot (A.) and respective SCP signals (B.) for a concentration range [0-240]$\times 10^{-9}$ mol dm^{-3}. The experiments were performed in 0.01 mol dm^{-3} NaNO$_3$ using t_d of 40 s and a I_s of 75$\times 10^{-9}$ A.

The linearity was maintained in the concentration interval of [0-240]$\times 10^{-9}$ mol dm^{-3}. The calibration data were: slope=2.28$\times 10^{-2}\pm 1 \times 10^{-4}$ s nmol dm^{-3} and correlation coefficient =9.99$\times 10^{-1}$ (N=7; t_d =40 s and a I_s=75$\times 10^{-9}$ A). For a lead concentrations above 240$\times 10^{-9}$

mol dm^{-3} a negative variation of τ was observed (Fig. 5.4). This deviation to the linearity, suggests the beginning of the TMFE saturation.

The saturation occurs at this electrode (TMFE: thickness 7.6 nm; equivalent area 9.38×10^{-6} m^2) for a lead(II) concentration of 1.19×10^{-7} mol dm^{-3} and within the time deposition interval of [200-300] s or the equivalent combination of this parameters (*cf.* Eq.7). The limit of detection (LOD) for a 40 s deposition time was 2.4×10^{-9} mol dm^{-3} (3σ) ($N=7$), however lower values can be achieved by increasing the deposition time (e.g. 1.6×10^{-9} mol dm^{-3} for 60 s).

The repeatability of the SCP signal of lead(II) at the optimized conditions for a single *ex situ* formed TMFE, was evaluated for 60 successive measurements (Fig. 5.5).
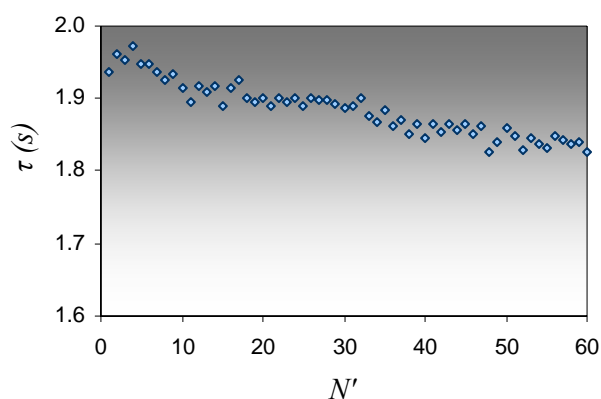
Figure 5.5. SCP signal (τ) for repeated measurements ($N'=60$) in a test solution of 1.19×10^{-7} mol dm^{-3} of lead(II) in 0.01 mol dm^{-3} NaNO$_3$, at the TMFE (7.6 nm thickness). The other experimental conditions used were: $I_s = 75 \times 10^{-9}$ A and t_d of 40 s.

A decrease in the transition time of 7.5% occurred during the repeated SCP measurements of lead(II), being the overall RSD less than 2.0%. The stability/durability of the *ex-situ* TMFE used in this set of experiments was also evaluated. The charge associated with this mercury deposit (Q_{Hg}) was compared with a mean value (2 replicates) of other preplated TMFEs (see section 5.3.4). The results pointed out a decrease of 8.5% in the Q_{Hg}. However and according to section 5.4.1, this parameter only provides qualitatively information on the conditions of the TMFE. As a result, this nanometer tick MFE is recommended to be used for a maximum of 60 consecutive stripping experiments, revealing no significant alteration in the analytical signal.

5.4.4. SSCP studies

5.5.4.1. Experimental verification of the SSCP equation at the TMFE

As far as we know the application of a nanometer tick mercury film as the working electrode for the build up of SSCP curves has never been exploited. The SSCP theoretical curve was calculated using expression (5.7) (valid for the RDE) for: $E^0 = -0.380$ V, n=2, $D_{Pb}=9.85\times10^{-10}$ m^2 s^{-1}, $\delta_{Pb}=4.93\times10^{-5}$ m, $v=9.78\times10^{-4}$ m^2 s^{-1} and $V_{Hg} =2.35\times10^{-15}$ m^3 (deposited Q_{Hg} for 4 replicates measurements was 6.02×10^{-4} C) for the TMFE. The SCP experimental parameters used were: t_d=40 s, I_s=7.5$\times10^{-8}$ and the Pb(II) concentration was of 1.19×10^{-7} mol dm^{-3}. The depletive SSCP curve for Pb(II) (calibration) using the TMFE (thickness 7.6 nm) was measured and the experimental results were compared with those calculated from equation (5.7). Fig. 5.6 shows these results.
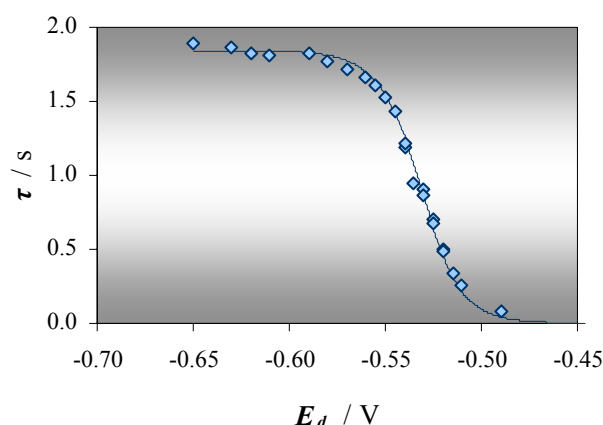
Figure 5.6. Experimental (diamonds) and fitted (full line) SSCP waves for a Pb(II) concentration of 1.19×10^{-7} mol dm^{-3} at the TMFE (thickness of 7.6 nm). Experimental data was obtained in 0.01 mol dm^{-3} NaNO$_3$ media at a pH 3.4, using the following SCP experimental parameters: t_d=40 s and I_s=7.5$\times10^{-8}$ A.

The fitting of the SSCP experimental wave using the TMFE was done also, through the analysis of the variation log[($\tau^*-\tau$)/τ] *vs.* E_d in the rising portion at the foot of the wave (Fig. 5.7).
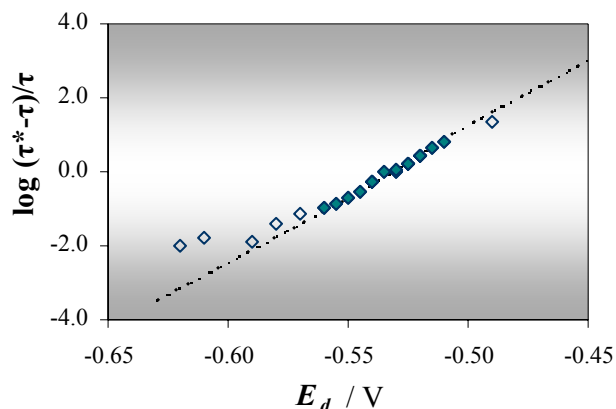
Figure 5.7. Log analysis of the experimental SSCP wave (♦ and ◊) for Pb(II) at the TMFE (data presented in figure 5.6). The slope for experimental SSCP curve was determined in the steepest region (♦). Dashed line on the SSCP wave indicates the region of the steepest slope at the foot of the wave.

The slope obtained for the $\log[(\tau^*-\tau)/\tau]$ *vs* E_d plot was of 36.1 ± 0.8 V^{-1} for the experimental SSCP wave. This value compares very well with the slope obtained for the theoretical SSCP wave, i.e. 36.7 V^{-1}. In conclusion the experimental SSCP curve was in perfect agreement to that predicted by the theory for the TMFE.

Within the framework of this study one of the most important features to be evaluated was the repeatability of the SSCP curves using the same TMFE. Three experimental SSCP waves were obtained (Fig. 5.8).
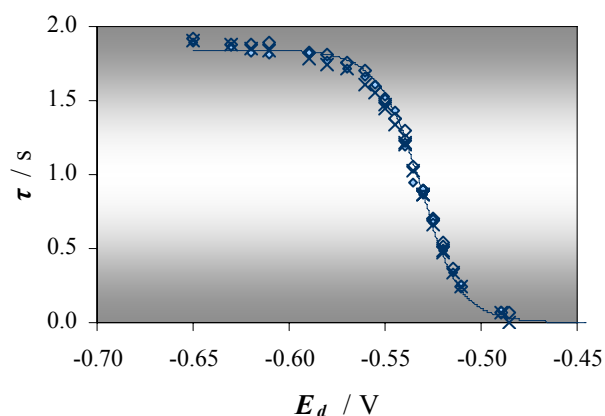
Figure 5.8. Fitted (full line) and experimental (♦, ◊ and ×) SSCP waves for a Pb(II) concentration of 1.9×10^{-7} M at the TMFE (thickness of 7.6 nm); the symbols correspond to different SSCP curves performed using the same TMFE: (♦) calibration 1, (◊) calibration 2 and (×) calibration 3. Other conditions as indicated in figure 5.6.

The present results reveal that the SSCP experimental curves were identical within the experimental error, with the limiting transition times, τ^*, of 1.842, 1.865 and 1.851 s and the half-wave deposition potentials, $E_{d,1/2}$, of -0.5300, 0.5295 and -0.5305 V, for wave 1, 2 and 3, respectively. However, the SCCP waves present a slight deviation in the steepest region towards negative potentials. That reflects a decrease in the slope of the $\log[(\tau^*-\tau)/\tau]$ vs E_d plot (36.1±0.8, 35.2±0.5 and 33.5±0.7 V^{-1} for wave 1, 2 and 3, correspondingly). This suggests the beginning of the TMFE degradation which, accordingly to section 5.4.3, can be used for a maximum of 60 consecutive experiments. In this study each SSCP wave was obtained using 28 experimental points and thus, the set of three correspond to 84 measurements. Considering that well defined SSCP waves can be achieved with a set of 15 experiments, four SSCP curves can be obtained per TMFE.

5.4.4.2. SSCP for metal ion speciation studies: Simple labile systems

The applicability of the TMFE in SSCP experiments for the determination of complexation parameters was evaluated. Two labile ML systems were used in this study, one with $D_{ML}<D_M$ and the other with $D_{ML}=D_M$.

i) Labile system with $D_{ML}=D_M$

The interaction of lead(II) with 2,6-pyridinedicarboxylicacid (PDCA) was studied with SSCP at the TMFE. The SSCP curves for lead(II) with and without an excess of carboxylated PDCA at pH 5.5, are presented in Fig. 5.9. The experimental log K value at the TMF-RDE was compared with that of the HMDE and also, with the theoretical value predicted by the speciation program MEDUSA [16].
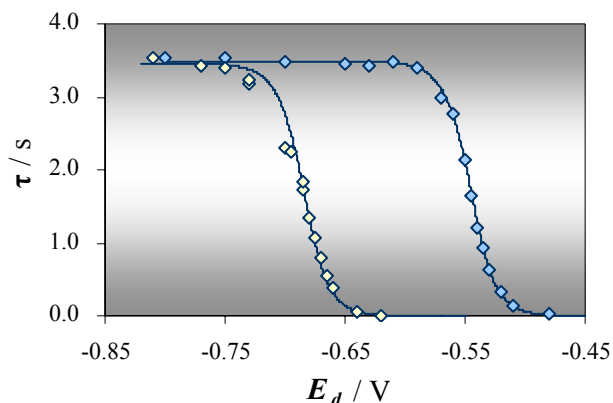
Figure 5.9. Experimental (♦, ◊) and fitted (full line) SSCP waves for Pb(II) and Pb(II)-PDCA system at pH 5.5 at the TMFE (thickness of 7.6 nm). Experimental curves were measured for a Pb(II) concentration of 1.19×10^{-7} mol dm^{-3} in the absence (♦) and presence of 2.19×10^{-5} mol dm^{-3} PDCA (◊) in 0.01 mol dm^{-3} NaNO$_3$. Other parameters: $E^0 = -0.384$ V, n=2, $D_{ML}=9.85 \times 10^{-10}$ m^2 s^{-1}, $\delta_M=4.93 \times 10^{-5}$ m and $V_{Hg}=2.35 \times 10^{-15}$ m^3. Other SCP experimental parameters: t_d=80 s and I_s=7.5$\times 10^{-8}$ A.

The theoretical and experimental log K values are presented in table 5.2.

Table 5.2. Stability constants for the Pb-PDCA system obtained at the TMF-RDE for 5 measurements (experimental conditions as in Fig. 5.9), at the HMDE and the theoretical value predicted by the speciation program MEDUSA.

	TMF-RDE	HMDE	MEDUSA
$log\ K$ / dm^3 mol^{-1}	9.58 9.54 9.51 9.53 9.57	9.4	9.3

The log K for the Pb(II)-PDCA system, computed from the shift in the half wave position (by means of Eq. 5.16) was 9.55±0.03 dm^3 mol^{-1} (N'=5) at the TMFE. This value is in satisfactory agreement with the value of 9.4 dm^3 mol^{-1} obtained at the HMDE in similar experimental conditions (ionic strength and pH) and with the theoretical value of 9.3 dm^3 mol^{-1} obtained with the code MEDUSA [16].

ii) Labile system with $D_{ML} < D_M$

The Pb(II)-carboxylated latex nanospheres complex was used as a model for the labile metal-ligand system for the determination of the stability constant, K, where $D_{ML} < D_M$. Figure 5.10, shows the SSCP waves for lead(II) in the absence and the presence of an excess of carboxylated latex nanospheres (colloidal particle radius of 40 nm), at pH 5.5.
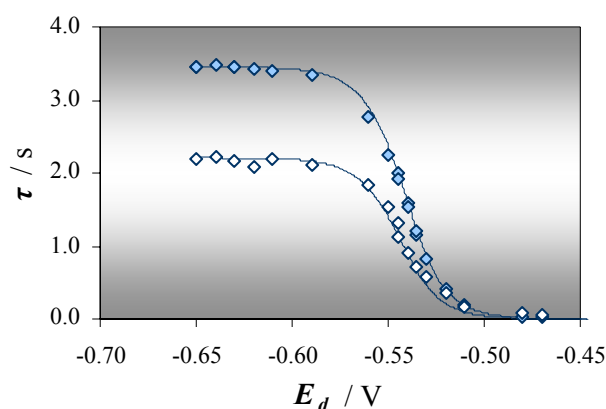
Figure 5.10. Experimental ($\blacklozenge$, $\lozenge$) and fitted (full line) SSCP waves for Pb(II) and Pb(II)-carboxylated latex nanospheres system at pH 5.5 at the TMFE (thickness of 7.6 nm). Experimental curves were measured for a Pb(II) concentration of 1.19×10^{-7} mol dm^{-3} in the absence ($\blacklozenge$) and presence of the latex nanospheres ($\lozenge$) at 0.1% (w/w) in 0.01 mol dm^{-3} NaNO$_3$. Other parameters: $E^0 = -0.374$ V, $n=2$, $D_{ML}=1.26 \times 10^{-10}$ m^2 s^{-1}, $\delta_M=2.48 \times 10^{-5}$ m and $V_{Hg} = 2.35 \times 10^{-15}$ m^3. Other experimental conditions as indicated in figure 5.9.

The fitted wave for the labile Pb(II)-carboxylated latex nanospheres system, was calculated by means of Eq (5.7). Table 5.3 presents the log K obtained using Eq. (16) for the TMF-RDE and the value calculated at the HMDE [16].

Table 5.3. Stability constants for the Pb-latex system obtained at the TMF-RDE (4 measurements), in 0.01 M $NaNO_3$ media at pH 5.5 (other experimental conditions as in Fig. 5.10), and the value obtained at the HMDE [16].

	TMF-RDE	HMDE
$log\ K$ / dm³ mol⁻¹	4.91 4.78 4.78 4.87	[4.8-4.9]

The mean log K value (four measurements, $N'=4$) was 4.84 ± 0.07 dm³ mol⁻¹, which is in agreement with the value of [4.8-4.9] dm³ mol⁻¹ attained at the HMDE, in identical experimental conditions (ionic strength 0.01 dm³ mol⁻¹ and pH 5.6).

A detailed examination of the electrode surface by means of the optical microscopy was done after the use of the carboxylated latex nanospheres in the set of experiments. Fig. 5.11 presents the respective photographs of the mercury film surface. Based on this optical microscopic study, it is obvious that the electrode surface is being blocked and damaged, by the adsorption of carboxylated latex nanospheres, which appears in Fig. 5.11 as small portions in white. Despite of this phenomenon, there are no significant differences in the log K values obtained at this electrode and at the HMDE.

Figure 5.11. Optical micrographs: × 50 (A.) and × 100 (B.) of a thin mercury film electrode (7.6 nm of thickness) plated on a glassy carbon electrode, after being used in SSCP experiments with carboxylated latex nanospheres.

A promising approach to avoid these problems, guarantying the feasibility of the results obtained, is the use of a cation-exchange polymer for the modification of the mercury film coating. This polymeric coating might not only stabilized the electrode surface but also minimized the electrode fouling effects, precluding the adsorption of the anionic carboxylated latex nanospheres.

In fact, an attentive was made to modify the TMFE with PSS polyelectrolyte coatings recasted from water. Accordingly to the results presented in chapter 4, the PSS-TMFE (M_w 70,000 and mass loading 4.8 μg mm^{-2}) presents satisfactory and efficient exclusion properties towards tensioactive species (BSA and triton X-100) and significant enhancements in the ASV signal of lead(II), in a electrolyte medium with lower ionic strength. Although, these polyelectrolyte coatings proved to be very unstable, when applied to the thin mercury film deposited on a rotating disk electrode. The high rotations speeds applied to the electrode induced the leakage of the PSS film to the solution and, as a result, no increments in the ASV signals of lead(II) were obtained, when compared with the non modified TMFE.

In the future, it would be interesting to apply different charged polymer films with a high charge density, however, sufficiently rigid and stable in order to resist to the expansion at low ionic strengths and to the rotation of the disk electrode.

5.5. Conclusions

The present work reveals that a thin mercury film electrode can be successfully applied in SCP/SSCP studies of heavy metals. The high sensitivity and resolution obtained at the TMFE and also the low deposition times which in turn are used, made this electrode an excellent complement to the conventional mercury electrodes.

The optimized TMFE (film thickness of 7.6nm) can be use for 1 day-term (60 SCP consecutive measurements) with no significant variation in the analytical signal (RSD less than 2%) and no apparent degradation of electrode surface (RSD less than 3% for the Q_{Hg}). Due to the low thickness and volume of this electrode (7.6 nm and 2.4×10^{-14} m^3,

correspondingly), the stripping step follows a thin-layer behaviour and, as a result, the depletion effects predominate ($I_s\tau$ regime). Therefore, high stripping currents can be used (I_s values higher than 75×10^{-9} A) preventing dissolved oxygen interference. The SCP signals obtained at the TMFE are narrow and well defined, even when low concentrations of Pb(II) and short deposition times are used, which in turn shorten the analysis times. The limit of detection (3σ) for Pb(II) was 2.4×10^{-9} dm^3 mol^{-1} using a stripping current of 75×10^{-8} A and a deposition time of 40 s.

The calculated SSCP curves are in excellent agreement with experimental data for Pb(II) at the TMFE. A single TMFE can be used to obtain four identical and well defined SSCP curves, each one with 15 experimental points (15 individual SCP measurements). When applied to the determination of complexation parameters, the log K of the labile system Pb(II)-carboxylated latex nanospheres system, calculated from the shift in the SSCP half-wave potential ($\Delta E_{d,1/2}$) at the TMFE, is in accordance with the value obtained at the HMDE, in identical experimental conditions, despite of adsorption of carboxylated latex nanospheres onto the mercury coating. Also the log K values obtained for the Pb(II)-PDCA, are quite similar with the ones obtained at the HMDE and with the theoretical values predicted by MEDUSA.

References

[1] M.-L. Tercier-Waeber, J. Buffle, F. Confalonieri, G. Riccardi, A. Sina, F. Graziottin, G. C. Fiaccabrino, M. Koudelka-Hep, *Meas. Sci. Technol.* 10 (1999) 1202.

[2] H. P. van Leeuwen, R. M. Town, *J. Electroanal. Chem.* 536 (2002) 129.

[3] R. M. Town, H. P. van Leeuwen, *J. Electroanal. Chem.* 509 (2001) 58.

[4] M. L. Tercier, J. Buffle, *Anal. Chem.* 68 (1996) 3670.

[5] G. E. Batley, T. M. Florence, *Electroanal. Chem. and Interf. Electrochem.* 55 (1974) 23.

[6] H. P. van Leeuwen, R. M. Town, *J. Electroanal. Chem.* 523 (2002) 16.

[7] R. M. Town, H. P. van Leeuwen, *J. Electroanal. Chem.* 541 (2003) 51.

[8] H. P. van Leeuwen, R. M. Town, *Environ. Sci. Technol.* 37 (2003) 3945.

[9] J.P. Pinheiro, H.P. Van Leeuwen, *J. Electroanal. Chem.*, 570 (2004) 69.

[10] N. Serrano, J. M. Díaz-Cruz, C. Ariño, M. Esteban, *J. Electroanal. Chem.* 560 (2003) 105.

[11] D. Jagner, M. Josefson, S. Westerlund, *Anal. Chem.* 53 (1981) 1406.

[12] S.C.C. Monterroso, H. M. Carapuça, J. E. J. Simão, A. C. Duarte, *Anal. Chim. Acta* 503 (2004) 203.

[13] A. J. Bard, L.R. Faulkner, *Electrochemical Methods: Fundamentals and Applications* (2nd ed.), John Wiley & Sons, Inc., New York, 2001, chap. 11-12.

[14] S. C. C. Monterroso, H. M. Carapuça, A. C. Duarte, *Electroanalysis* 15 (2003) 1878.

[15] L. S. Rocha, H. M. Carapuça, J. P. Pinheiro, *Langmuir* 22 (2006) 8241.

[16] R. F. Domingos, C. Huidobro, E. Companys, J. Galceran, J. Puy, J. P. Pinheiro, *J. Electroanal. Chem.* 617 (2008) 141

CHAPTER 6

Evaluation of trace metal dynamic parameters determined by Scanned Stripping Chronopotentiometry (SSCP) at a Thin Mercury Film Rotating Electrode (TMF-RDE)

CHAPTER 6 Evaluation of trace metal dynamic parameters determined by Scanned Stripping Chronopotentiometry (SSCP) at a thin mercury film rotating electrode (TMF-RDE)

6.1. Introduction

6.2. Theory

6.3. Experimental

    6.3.1. Chemicals

    6.3.2. Instrumentation

    6.3.3. Preparation of the thin mercury film electrode

    6.3.4. Chronopotentiometric procedures

6.4. Results and Discussion

    6.4.1. Stability of the TMFE prepared in acidic media

    6.4.2. Experimental lability diagnosis and degree of lability

    6.4.3. Determination of stability constants K in the kinetic current regime

    6.4.4. Determination of kinetic parameters k_a

6.5. Conclusions

6.1. Introduction

Knowledge of dynamics factors, i.e., kinetic features of the interconversion of metal complex species, is fundamental for establishing a rigorous quantitative basis for the relationship between metal ion speciation, bioavailability and biouptake, and thus for establishing the foundations for dynamic risk assessment [1,2,3]. Dynamic metal speciation analysis remains a challenging problem since very few techniques combine the potential to perform dynamic speciation and high sensitivity. Scanning stripping chronopotentiometry (SSCP), fulfil these requirements [1,4,5,6,7], where a rigorous expression was obtained for the SSCP wave for metal complex systems with limited association/dissociation kinetics, based in the Koutecký-Korita approximation, together with steady-state nature of the SSCP experiment [8].

So far, the features of SSCP in dynamic situations (labile, quasi-labile and non-labile) were exploited in the hanging mercury drop electrode (HMDE) and the Hg-Ir microelectrode [1,3]. In chapter 5 of this thesis, the nanometer thin mercury film rotating disk electrode (TMF-RDE) proved to be an excellent complement to the HMDE and microelectrodes in SCP/SSCP studies of metal cations, due to their high sensitivity and good resolution attained [9]. The RDE presents a good potential in dynamic studies, due to the well defined hydrodynamic conditions during the deposition step (Levich equation) [10,11,12] and a range of rotation speeds easily attainable.

In this chapter the features of the rotating TMF-RDE coupled with SSCP in trace metal dynamic speciation were investigated. To accomplish this, the lability diagnosis was validated at the TMFE and the kinetic parameters, i.e., the association rate constants were calculated.

6.2. Theory

Considering the formation of a labile 1:1 metal complex, ML, between the electroactive metal ion M and the ligand L:

$$M+L \underset{k_d}{\overset{k_a}{\rightleftarrows}} ML \qquad (6.1)$$

$$\updownarrow n\bar{e}$$

$$M^0$$

The system is dynamic if the rates for the volume reactions are fast on the experimental timescale, t:

$$k_d t, \; k'_a t \gg 1 \qquad (6.2)$$

i.e., conversion of M into ML, and vice versa, is fast on the timescale considered. Under conditions of ligand excess (section 1.2) we can define:

$$k'_a = k_a c^*_{L,t} \text{ and } K' = k'_a / k_d = K c^*_{L,t} \qquad (6.3)$$

where K is the stability constant ($m^3 \, mol^{-1}$) of ML [1,3].

The rate constant of complex formation, k_a ($m^3 \, mol^{-1} \, s^{-1}$), is generally consistent with a mechanism in which the formation of an outer-sphere complex between the metal and the ligand, with an electrostatically determined stability constant, K_{os} ($m^3 \, mol^{-1}$), is followed by a rate-limiting removal of water from the inner coordination sphere of the metal, k_{-w} (s^{-1}), commonly known as the Eigen mechanism. For a given complex system, the value of K_{os} is usually estimated on the basis of the Debye-Hückel electrostatic for the charge interaction metal-ligand [3,13].

i) SSCP curves in the kinetic current regime

A general expression for the steady-state SSCP curve for the dynamic complexes influenced by homogeneous kinetics, for any D_{ML}/D_M, is based on the Koutecký-Koryta approximation. The equation for the SSCP wave for a labile complex ML, τ (s), can be summarized as [3]:

$$\tau = \frac{I^*_{d(M+L)}\tau_d}{I_s}\left[1 - \exp\left(\frac{t_d}{\tau_d}\right)\right] \qquad (6.4)$$

being $I_d^*{}_{(M+L)}$ the limiting deposition current (A) and τ_d the characteristic time constant (s) of the deposition process, for arbitrary D_{ML} values. These two parameters are defined by [1,3]:

$$I_d^*{}_{(M+L)} = nFAc_M^* \left(\frac{\overline{\delta} - \mu}{\overline{D}(1 + K')} + \frac{\mu}{D_M} \right)^{-1} \tag{6.5}$$

$$\tau_d = \frac{V_{dep\,Hg}}{A\theta} \left(\frac{\overline{\delta} - \mu}{\overline{D}(1 + K')} + \frac{\mu}{D_M} \right) \tag{6.6}$$

where θ is the free metal surface concentration ratio ($\theta = c^0{}_M / c^0{}_M{}^0$), $V_{dep\,Hg}$ is the volume of the electrode that can be estimated assuming a thin-film condition (chapter 5.2.2, Eq. 6.10) [9] and $\overline{D}$ is the average of the diffusion coefficient (m^2 s^{-1}). Considering that the diffusion coefficient of the metal complex species (D_{ML}) is lower than that of the free metal ion (D_M), $\overline{D}$ is expressed by [5]:

$$\overline{D} = \frac{D_M C^*{}_M + D_{ML} C^*{}_{ML}}{C^*{}_{ML}} \tag{6.7}$$

where $\overline{\delta}$ is the thickness of the diffusion layer (m), that for a rotating disk electrode and is given by [10]:

$$\overline{\delta} = 1.61 \overline{D}^{1/3} \omega^{-1/2} \upsilon^{1/6} \tag{6.8}$$

being ω the angular speed rotation for the RDE ($\omega = 2\pi\nu_{rot}$), where ν_{rot} is the speed of rotation) and υ the kinematic viscosity (m^2 s^{-1}) [11]. To describe the effect of ML on the reduction of M to M^0 at the mercury film surface, the well-known concept of a reaction layer, with thickness μ (m) is used. This parameter represents the mobility and mean lifetime of a given free metal, according to:

$$\mu = \left(\frac{D_M}{k_a'} \right)^{1/2} \tag{6.9}$$

In the simplifying Koutecký-Koryta approach for planar diffusion, μ is the basis for the spatial division of the concentration profiles for M and ML into a nonlabile and labile region, separated by a boundary of the reaction layer with thickness μ [3,8,14].

The coefficient in equation (5.4), $I_d^*{}_{(M+L)}\,\tau_d\,/\,I_s$, is a factor that does not affect the position of the wave on the E_d axis [5]. Therefore, an explicit expression for the shift of the half-wave potential due to the formation of a complex, $\Delta E_{d,1/2}$ (equivalent to the DeFord-Hume expression) can be obtained considering only the exponential term. In the case of a kinetic current, the shape of the SSCP wave remains unchanged, accordingly to equations (6.4) and (6.7), and the same approach can be used, yielding [1,3]:

$$\ln(1 + K') = \left(\frac{nF}{RT} \Delta E_{d,1/2} - \ln\left(\frac{\tau^*{}_{M+L}}{\tau^*{}_M} \right) \right) \tag{6.10}$$

being $\tau^*{}_M$ and $\tau^*{}_{M+L}$ the limiting wave heights (s) in the presence and in the absence of ligands, correspondingly. Thus, even in the kinetic current regime, the complex stability constant K' is simply obtained from the SSCP wave parameters.

In the labile limit the stability constant can also be computed from the decrease in the limiting transition time, using the following equation:

$$\frac{\tau^*{}_{M+L}}{\tau^*{}_M} = \left(\frac{\overline{D}}{D_M} \right)^{2/3} = \left(\frac{1 + \varepsilon K'}{1 + K'} \right)^{2/3} \tag{6.11}$$

where $\varepsilon = D_{ML}/D_M$ and p is the hydrodynamic parameter [1,10].

ii) Lability diagnosis and degree of lability (ξ)

SSCP incorporates an experimental lability diagnostic through the comparison between the K values, $K(\Delta E_{d,1/2})$ and $K(\tau^*)$, the first calculated from the shift in the SSCP half-wave deposition potential (Eq. 6.10) and the second from the decrease in the limiting transition time (Eq. 6.11). For labile systems, $K(\Delta E_{d,1/2})$ and $K(\tau^*)$ are equal. As the lability

decreases, the value of $K(\tau^*)$ becomes significantly larger than $K(\Delta E_{d,1/2})$, since the decrease of τ^*_{M+L} provoked by the non-labile complexes being assigned to a lower $\overline{D}$. Eventually when the estimated $\overline{D}$ becomes smaller than D_{ML}, the calculation of K from τ^* becomes impossible, leading to negative values.

The experimental lability diagnosis represents a significant advantage as compared with the traditional use of theoretical lability criteria. In fact, the experimental evidence appears even for small losses of lability, while the theoretical criteria are inequalities thus much less sensitive [1].

A quantitative assessment of lability can be achieved through the lability degree, ξ, that describes the percentage of the kinetic contribution with respect to the maximum kinetic contribution of the complex to the metal flux, once the concentrations, kinetic constants, diffusion coefficients and spatial dimensions of the sensor are known. The ξ parameter is defined by [15]:

$$\xi = \frac{J_{kin} - J_{free}}{J_{lab} - J_{free}} \tag{6.12}$$

where J_{kin}, J_{lab} and J_{free} corresponds to the fluxes (mol m^{-2} s^{-1}) for the ML system kinetically controlled, labile and inert (due to the free metal), respectively and are given by:

$$J_{kin} = k_d \mu c^*_{ML} \tag{6.13}$$

$$J_{lab} = \frac{\overline{D} c^*_{M,T}}{\overline{\delta}} \tag{6.14}$$

$$J_{free} = \frac{D_M c^*_M}{\delta} \tag{6.15}$$

Experimentally the degree of lability can be obtained by subtracting the contribution of the term corresponding to the diffusional transport of free metal in the system:

$$\xi = \frac{\tau^*_{ML,kin} - \tau^*_{freeM}}{\tau^*_{ML,lab} - \tau^*_{freeM}} \tag{6.16}$$

being $\tau^*_{ML,kin}$ the analytical signal for the kinetically controlled ML system(s), $\tau^*_{ML,lab}$ the equivalent signal labile ML case (s) and τ^*_{freeM} the signal for the amount of free metal in the system (s). The τ^*_{freeM} (s) is determined for a given free metal concentration by:

$$I^*_d = \frac{nFAD_M C^*_M}{\delta_M}$$ (6.17)

The degree of lability ranges from 0 to 1. The maximum contribution of the complex arises when the system is labile (ξ=1) and progressively decreases as the ML complex became less labile (ξ=0 when the complex is inert) [15].

By combination of Eq. 6.9 and 6.13 and assuming that $C^*_{ML}=C^*_{M,t}$ - C^*_M, the dissociation rate constant, k_d (s^{-1}), and therefore, the association rate constant,(k_a=k_d K) can be calculated according to:

$$k_a = \left(\frac{J_{Kin}}{C^*_{M,t} - C^*_M}\right)^2 \left(\frac{K'}{D_M}\right) K$$ (6.18)

6.3. Experimental

6.3.1. Chemicals

All chemicals were of analytical reagent grade and all solutions were prepared with ultra-pure water (18.3 MΩ cm, Milli-Q systems, Millipore-waters). Sodium nitrate, potassium chloride, nitric acid 65% (Merck, suprapur), hydrochloric acid 37% (trace select, Fluka) and 1000 ppm Hg and Pb AA-Spectrosol metal ion standards (BDH) were also used. Ferricyanide standard solution (1.929×10^{-3} mol dm^{-3}) in 1.0 mol dm^{-3} KCl was used for chronoamperometry. Nitric acid (1 mol dm^{-3}) and sodium hydroxide solutions (1 mol dm^{-3}) were used for pH adjustments. Stock solution of MES 2-(N-morpholino-ethanesulfonic acid) and MOPS (3-(N-morpholino-propanesulfonic acid) buffers were prepared from the solids (Merck and Fluka, respectively). Nitriloacetic acid (NTA) was from Sigma-Aldrich (99% grade) and iminodiacetic acid (IDA) was from Sigma-Aldrich

(p.a). Solutions of ammonium acetate (NH$_4$Ac 1.0 mol dm^{-3}/0.5 mol dm^{-3} HCl) pH buffer and ammonium thiocyanate 1.0 mol dm^{-3} were prepared monthly and used without further purification. Biohit Proline pipettes equipped with disposable tips were used for appropriate dilutions. All measurements were carried out at room temperature (18-20 ºC).

6.3.2. Instrumentation

An Ecochemie Autolab PGSTAT10 potentiostat (controlled by GPES 4.9 software from EcoChemie, the Netherlands) was used in conjunction with a Methrohm 663 VA stand (Methrohm, Switzerland). The three electrode configuration was used comprising a TMFE plated onto a rotating glassy carbon (GC) disc (1.9 mm diameter, Methrom) as the working electrode, a GC rod counter electrode and a double junction Hg│Hg$_2$Cl$_2$│KCl(3 mol dm^{-3}) encased in a 1 or 0.1 mol dm^{-3} NaNO$_3$ solution, depending on the ionic strength of the test solution, 0.1 or 0.01 mol dm^{-3} of NaNO$_3$, respectively. The electrochemically active surface area of the glassy carbon electrode, (3.098 ± 0.015) mm^2, was measured by chronoamperometry (in 1.929×10^{-3} mol dm^{-3} ferricyanide/1.0 mol dm^{-3} KCl solution; two polishinging experiments, each with four replicate determinations).

A combined glass electrode (Radiometer Analytical pHC3006-9) connected to a pH meter (Thermo Electron Corporation, Model Orion 3-Start) was used for pH measurements.

6.3.3. Preparation of the thin mercury film electrode

Prior to coating, the GCE was conditioned following a reported polishing/cleaning procedure [16], described in chapter 2.2.3. These polishing and electrochemical pre-treatments were repeated daily.

The thin mercury film was then *ex-situ* prepared in 1.2×10^{-4} mol dm^{-3} mercury(II) nitrate in acidic media (pH *ca.* 1.9) by electrodeposition at -1.3 V [17], using a deposition time of 240 s and a rotation speed of the rotating disk of 1000 rpm. The charge associated to the deposited mercury (Q_{Hg}) was calculated by electronic integration of the linear sweep

stripping peak of mercury, for v = 0.005 V s^{-1}. The electrolyte solution was ammonium thiocyanate 5×10^{-4} mol dm^{-3} (pH 3.4) [16]. The stripping step began at -0.15 V and ended at +0.6 V [18]. The charge quoted was a mean value of 15 replicate measurements (RDS<3%). The thickness of the TMFE was estimated using this mean value of $Q_{Hg.}$

  When not in use the GCE was stored dry in a clean atmosphere [16].

6.3.4. Chronopotentiometric procedures

  Stripping chronopotentiometric individual measurements were carried out in 20 mL 0.01 or 0.1 mol dm^{-3} NaNO$_3$ solutions, depending on the reference metal ion used in the set of experiments, lead(II) or cadmium(II), correspondingly. All solutions were purged for 60 minutes in the beginning of every SCP experiment and 80 s (assisted by mechanical stirring of the rotating GCE) after each measurement.

  The SSCP waves were constructed from a series of individual SCP measurements, by plotting the peak area as a function of the range of deposition potential applied, i.e., [-0.70, -0.48] V and [-0.84, -0.65] V for the cationic species lead(II) and cadmium(II), correspondingly. For each point the potential was held at E_d for a deposition period of 80 s, followed by the application of a oxidising current of 75×10^{-9} A (complete depletion), until the potential reached a value that precedes the transition plateau (-0.25 V for Pb and Cd at the TMFE).

  SSCP waves were obtained for Pb(II) (1.19×10^{-7} mol dm^{-3} in NaNO3 0.01 M), in the absence and in the presence of an excess of IDA, for several concentrations of the ligand. Previous to the addition of the ligand, the solution was set at pH 5.5 using MES buffer. For the classical Cd-NTA system, the SSCP waves were constructed for a Cd(II) concentration of 4.75×10^{-7} mol dm^{-3}, in the absence and in the presence of an excess of NTA (2.23×10^{-6} mol dm^{-3}) at pH 8, where MOPS was used as buffer. Also, the association constant k_a was computed for both systems in study. After each SSCP experiment a set of SCP measurements were performed at different rotation speeds of the RDE (500, 1000, 1500, 2000 and 2500 rpm). The deposition potential applied was -0.65 and -0.83 V for lead(II) and cadmium(II), respectively.

6.4. Results and Discussion

6.4.1. Stability of the TMFE prepared in acidic media

The TMF-RDE is subject to mechanical deterioration of the electrode surface during the experimental course. To improve the electrode stability the electrodeposition of mercury was performed in very acidic solutions (pH *ca.* 1.9) as in [17]. The result was the formation of highly homogeneous and reproducible nanometer thin mercury films, displaced over the glassy carbon electrode as a collection of very small radius mercury droplets, as can be seen in the optical microphotographs (Fig. 6.1). The performance, i.e. reproducibility, stability/durability, of the TMF-RDE prepared by this procedure is similar to that achieved for the mercury films, *ex-situ* prepared in thiocyanate media, as reported in chapter 5 [9].
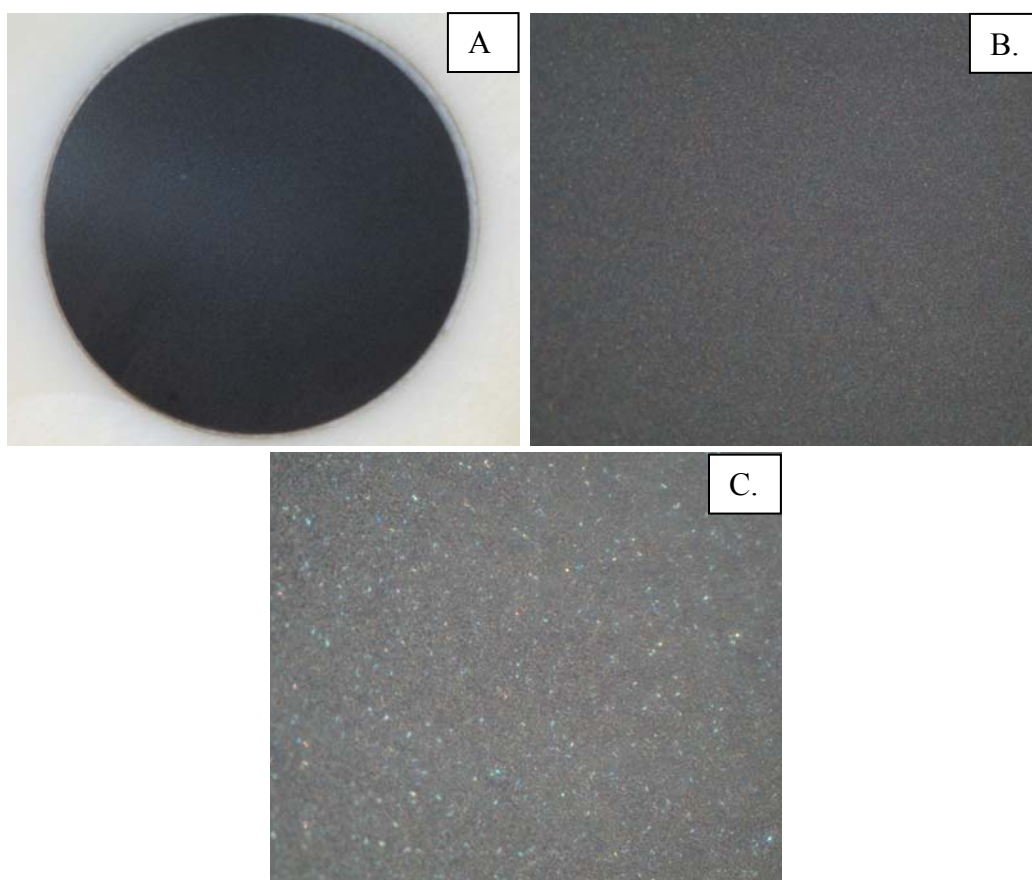

Figure 6.1. Optical micrographs: × 50 (A.), × 100 (B.) and × 500 (C.) of a thin mercury film electrode, 9.1 nm of thickness, plated on a glassy carbon electrode.

One of the crucial features in this study is the repeatability of the SSCP experimental waves in the course of the experiments, especially when higher rotation speeds are applied to the RDE. In order to improve the mechanical stability of the TMF-RDE, a ticker mercury coating (9.1 nm) was used, as compared with the one used on chapter 5 [9], and the TMF-RDE was not used for more than 60 consecutive measurements. Two SSCP experimental waves for lead(II) (calibration 1 and 2) were obtained at 1000 rpm and compared with each other (Fig. 6.2). After the construction of the SSCP wave 1, two replicates of the transition time τ^*, using a single deposition potential (E_d=-0.65 V at t_d=80 s), were recorded for several rotation rates (500, 1000, 1500, 2000 and 2500 rpm). The last set of experiments was repeated after calibration 2.
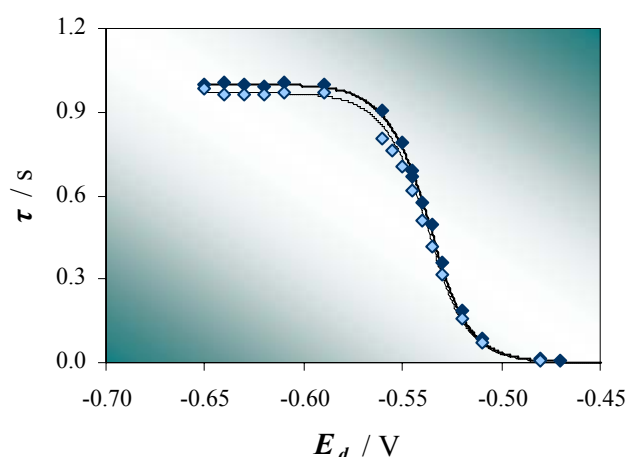
Figure 6.2. Fitted (full and dash line) and experimental ($\blacklozenge$, $\lozenge$) SSCP waves for a Pb(II) concentration of 1.19×10^{-7} mol dm^{-3} at the TMFE (thickness of 9.1 nm). The symbols correspond to different SSCP curves using the same TMFE: ($\blacklozenge$) calibration 1 and ($\lozenge$) calibration 2. The experiments were performed in 0.01 mol dm^{-3} NaNO$_3$ media, using the following SCP experimental parameters: t_d=80 s and I_s=7.5×10^{-8} A. Other parameters: $E^0_{(cal\ 1)}$= –0.381 V, $E^0_{(cal\ 2)}$= –0.382 V, n=2, D_M=9.85×10^{-10} m^2 s^{-1}, δ_M=4.44×10^{-5} m and V_{Hg}=2.82×10^{-14} m^3.

The results reveal that there was a slight decrease in the transition time τ^* (*ca.* 3%) and a small deviation towards negative potentials (1.5 mV) in the second SSCP wave recorded, that reflects only a slight variation in the slope of the log[($\tau^*-\tau$)/τ] *vs* E_d plot in the steepest region (40.0 to 40.1 V^{-1} for SSCP wave 1 and 2, correspondingly). Furthermore, evaluating the variation of the SCP analytical signal, τ^*, with the inverse of the diffusion layer

thickness, $\overline{\delta}^{-1}$ (is related to the rotation speed of the electrode by equation (6.8), where $\overline{D}$ is D_M for the metal only case), the slope obtained was: 1.76×10^{-4} s m and 1.75×10^{-4} s m, after calibration 1 and 2, respectively. Based on these results, we conclude that the mechanical stability and durability of the TMFE was considered suitable for the present experimental demands. The use of the highest rotation rates are not recommended, since it enhances the degradation of the mercury film, due to the coalescence or loss of the constituent Hg droplets.

6.4.2. Experimental lability diagnosis and degree of lability

One of the most valuable features of SSCP is the ability to detect the loss of lability of system. This feature is more evident when the diffusion coefficients of metal and ligand are roughly the same, since it is immediately manifested by a decrease in the limiting wave height τ^*, when compared with the metal only case. For systems that are non-labile this difference is very large, as evidenced in Figure 6.3, which shows the SSCP waves for cadmium(II) in the absence and the presence of an excess of NTA, at pH 8.

In this set of experiments the concentration of cadmium(II) used (4.75×10^{-7} mol dm^{-3}) was four times higher than that used in the case of lead(II) experiments (1.19×10^{-7} mol dm^{-3}), due to the very small signal of the Cd(II)-NTA complex. It is worth to mention that for the present concentration of cadmium(II) and for a deposition time of 80 s, there is no evidence of the saturation of the thin mercury film. The working concentration range of cadmium(II) was set within the interval of $[0\text{-}1.00]\times10^{-6}$ mol dm^{-3}, where the linearity between the SCP signal and the concentration of metal is maintained.

Figure 6.3. Experimental ($\blacklozenge$, $\lozenge$) and fitted (full line) SSCP waves for Cd(II) and Cd(II)-NTA system at pH 8 at the TMFE (thickness of 9.1 nm). Experimental curves were measured for a Cd(II) concentration of 4.75×10^{-7} mol dm^{-3} in the absence ($\blacklozenge$) and presence of 2.23×10^{-6} mol dm^{-3} nitriloacetic acid ($\lozenge$) in 0.1 mol dm^{-3} NaNO$_3$, using the following SCP experimental parameters: t_d=80 s and I_s=7.5$\times$10^{-8} A. Other parameters: E^0 in the interval [-0.376;-0.374] V, n=2, V_{Hg}=2.82$\times$10^{-14} m^3, D_M= D_{ML}=7.19$\times$10^{-10} m^2 s^{-1}, δ_M=4.44$\times$10^{-5} m and v=9.78$\times$10^{-4} m^2 s^{-1}.

For systems which are quasi-labile or where a significant amount of free metal is present this difference will be much smaller. In the present work complete SSCP curves were recorded for different concentrations of IDA. The concentration of ligand was increased, in order to incite the loss of lability of the Pb(II)-IDA complex. Figure 6.4 presents these SSCP waves for the metal only and for the complex Pb(II)-IDA, and displays the calculated fully labile system for comparison (dotted line).

Figure 6.4. Experimental ($\blacklozenge$, $\Diamond$) and fitted (lines) SSCP waves for Pb(II) and Pb(II)-IDA assuming a fully labile (dash line) and quasi-labile system (full line) at pH 5.5 at the TMFE (thickness of 9.1 nm). Experimental curves were measured for a Pb(II) concentration of 1.19×10^{-7} mol dm^{-3} in the absence ($\blacklozenge$) and presence of: (A.) 2.44×10^{-5} mol dm^{-3}, (B.) 3.75×10^{-4} mol dm^{-3} and (C.) 2.82×10^{-3} mol dm^{-3} iminodiacetic acid ($\Diamond$) in 0.01 mol dm^{-3} NaNO$_3$. The SCP experimental parameters used were: t_d=80 s and I_s=7.5×10^{-8} A. Other parameters: E^0 in the interval [-0.386;-0.381] V, n=2, V_{Hg}=2.82×10^{-14} m^3, D_M=9.85×10^{-10} m^2 s^{-1}, δ_M=4.44×10^{-5} m, D_{ML}=7.19×10^{-10} m^2 s^{-1} and v=9.78×10^{-4} m^2 s^{-1}.

The rigorous quantification of the lability degree (ξ) of a ML complex can be calculated from the experimental results and Eq. 6.12. The values obtained for the Pb-IDA system (at different concentration values of IDA) are presented in table 6.1.

Table 6.1. Degree of lability (ξ) of the Pb-IDA complex, at different concentrations of IDA. The other experimental conditions used are the same as indicated in Fig. 6.4.

C_{IDA} / mol dm^{-3}	ξ (%)
2.44×10^{-5}	-0.451
3.75×10^{-4}	0.649
2.82×10^{-3}	0.346

As expected, the degree of lability, ξ, decreases as the ligand concentration increases [15], since the Pb(II)-IDA complex becomes progressively less labile. The negative values obtained for a concentration of IDA of 2.44×10^{-5} mol dm^{-3}, means that $\tau^*_{ML,kin}$ is inferior to τ^*_{freeM}, indicating that there is no excess of ligand with respect to the metal, that is a condition required to use the equations presented in section 6.2.

To be sure that this phenomenon is kinetic in origin and is not due to the irreversibility of the electrochemical reaction or heterogeneity in the chemical speciation, a detailed analyse of the variation $\log[(\tau^*-\tau)/\tau]$ *vs.* E_d in the rising portion at the foot of the wave was made [3,19] for the Pb-IDA system (Fig. 6.5).
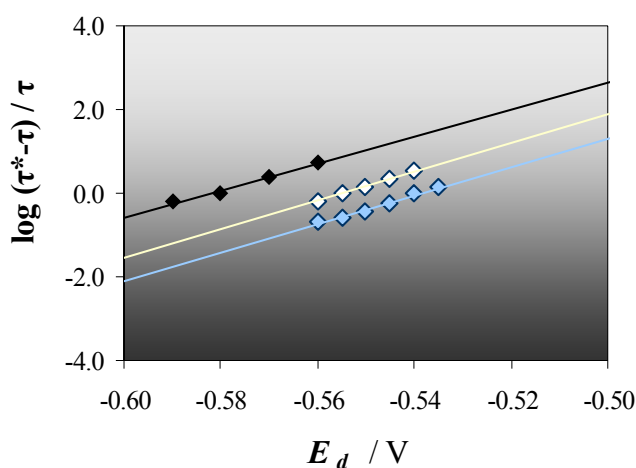

Figure 6.5. Log analysis of the experimental SSCP wave at the TMFE (data presented in Fig. 6.4) for Pb(II) ($\diamond$) and for Pb-IDA complex, using the following ligand concentrations: 3.75×10^{-4} mol dm^{-3} ($\Diamond$) and 2.82×10^{-3} mol dm^{-3} ($\blacklozenge$). Other conditions as indicated in Fig. 6.4.

The reciprocal slope of the corresponding log analysis (log[$(\tau^*-\tau)/\tau$] *vs.* E_d) for the steepest portion (foot) of the wave in the absence and presence and absence of ligand were calculated and the results are presented in table 6.2.

Table 6.2. Slope values and the corresponding standard deviations (σ and 2σ) and the correlation coefficient (r, N = number of experimental points) o the log[$(\tau^*-\tau)/\tau$] *vs* E_d plot in the steepest region of the Pb-IDA experimental SSCP waves, for the several concentration of ligand used.

C_{IDA} / mol dm^{-3}	Slope / V^{-1}	S_{slope} (σ)	S_{slope} (2σ)	R
0.00	34.0	1.4	2.8	0.995 (N=6)
3.75×10^{-4}	34.4	0.7	1.4	0.999 (N=5)
2.82×10^{-3}	32.3	2.2	4.4	0.996 (N=4)

The slope obtained for the complex Pb-IDA (both concentrations of ligand) is in agreement with that of the SSCP experimental wave for the metal only. This is an evidence of kinetic effects in the complexation at the TMFE, since the SSCP depletive wave is not modified. Also this feature, allow us to distinguish this phenomenon from the irreversibility in the electrochemical reaction (in which case reversibility is lost mostly at the top of the wave) and from the chemical heterogeneity in the metal speciation (which spreads the entire wave on the E_d), where the log slopes are highly affected. The same was verified for the HMDE and the Hg-Ir microelectrode, although for a different metal-ligand [3].

6.4.3. Determination of stability constants K in the kinetic current regime

Before proceeding to the determination of dynamic parameters it is necessary to verify the TMF-RDE capability to accurately determine the stability constant of the metal complexes under study. This was already established for the HMDE and Hg-Ir microelectrodes [3] and derives from the validity of the Koutecký-Koryta approximation and the steady-state nature of the transport in the deposition step of SSCP. The results obtained for the Cd(II)-NTA system and the Pb(II)-IDA system are presented in Table 6.3.

Table 6.3. Stability constants (mean values) of the Cd-NTA and Pb-IDA systems, obtained at the TMFE using different experimental conditions: pH, ionic strength (I) and total ligand concentration. All the experiments were performed in $NaNO_3$ media, for concentrations of Cd and Pb of 4.75×10^{-7} mol dm^{-3} and 1.19×10^{-7} mol dm^{-3}, respectively.

M-L system	pH	I / mol dm^{-3}	$C_{L,T}$ / mol dm^{-3}	$log\,K$ / dm^3 mol^{-1}
Cd-NTA	8.01	0.1	2.31×10^{-6}	9.79 ± 0.06 [a]
Pb-IDA	5.50	0.01	3.75×10^{-4}	8.33 ± 0.04 [a]
Pb-IDA	5.50	0.01	2.82×10^{-3}	8.48 ± 0.05 [a]

[a] Mean value of 3 measurements and the corresponding standard deviation (σ);

The log K computed from the shift in the half wave position (by means of Eq. 6.10) at the TMFE was 9.79 ± 0.62 dm^3 mol^{-1} for the Cd-NTA system, that is in conformity with the value of 9.81 dm^3 mol^{-1} obtained at the HMDE in similar experimental conditions (ionic strength and pH) [1] with the value of 9.8 dm^3 mol^{-1} recommended by IUPAC (for a ionic strength of 0.1 mol dm^{-3} and a temperature of 20ºC) [20]. For the Pb-IDA system the log K obtained for 7 measurements was 8.36 ± 0.69 dm^3 mol^{-1} for 0.01 mol dm^{-3} ionic strength, which is in reasonable agreement with the log K value of 8.60 dm^3 mol^{-1}, obtained by extrapolation (using SIT) from the 7.45 dm^3 mol^{-1} reported in the MiniSC Database, Academic software, UK 2000 [20], for an ionic strength of 0.1 mol dm^{-3}.

6.4.4. Determination of kinetic parameters k_a

The sensitivity of SSCP wave to kinetic effects, coupled with the well defined hydrodynamic conditions of the RDE allows the extraction of kinetic parameters, making it possible to calculate the association/dissociation rate constants. At the rotating TMF-RDE the hydrodynamic conditions are well defined and different rotation rates can be applied to the disk electrode, allowing multiple determinations of k_a in a short period of time and different hydrodynamic conditions. Both Cd-NTA and Pb-IDA complexes were used to perform these experiments.

i) Cd-NTA system

The degree of lability of Cd-NTA complex and the experimental association rate constants measured for lead(II), calculated using Eq. 6.18, at different rotation speeds (v_{RDE}) are summarized in table 6.4.

Table 6.4. Degree of lability and association rate constants obtained at the TMF-RDE for the system Cd-NTA. Other conditions as indicated in Fig. 6.3.

v_{RDE} / rpm	ξ (%)	k_a / dm^3 mol^{-1} s^{-1}
500	0.100	3.5×10^9
1000	0.060	2.7×10^9
1500	0.050	2.8×10^9
2000	0.043	2.8×10^9
2500	0.036	2.6×10^9

As expected, the values obtained for the degree of lability values, ξ, are inferior to those obtained for the Pb-IDA system and closer to zero, since the Cd-NTA complex is non-labile. The mean k_a value (5 measurements at different rotation rates) obtained was $(2.9 \pm 0.5) \times 10^9$ dm^3 mol^{-1} s^{-1}, that is in reasonable agreement with a k_a of 4.05×10^9 dm^3 mol^{-1} s^{-1} calculated on the basis of the Eigen mechanism ($k_{-w(Cd)} = 3 \times 10^8$ s^{-1} and $K_{os} = 13.5$ dm^3 mol^{-1}, for $z_M z_L = -4$ and a ionic strength of 0.1 mol dm^{-3}). Although, due to the high degree of non-lability of the Cd(II)-NTA system, the SCP signal of the complex is quite small, occasionally leading to erroneous measurements of the transient time. This might be the cause of the difference verified in the k_a experimental and theoretical values, for the Cd-NTA system.

ii) Pb-IDA system

The theoretical value of k_a calculated for the Eigen mechanism ($k_a=K_{os}\ k_{-w}$) is 2.56×10^{10} dm^3 mol^{-1} s^{-1}, using a dehydration rate constant $k_{-w(Pb)}$ of 7×10^9 s^{-1} and a stability constant for the intermediate outer-sphere complex K_{os} of 3.66 dm^3 mol^{-1} ($z_M z_L$=-2 and a ionic strength of 0.01 mol dm^{-3}). Table 6.5 summarizes the ξ and k_a values for the Pb-IDA system at different rotation speeds and for two IDA concentrations.

Table 6.5. Degree of lability and association rate constants obtained at the TMF-RDE for the system Pb-IDA using different concentrations of the ligand. Other conditions as indicated in Fig. 6.4.

v_{RDE}/ rpm	C_{IDA} / mol dm^{-3}			
	3.75×10^{-4}		2.82×10^{-3}	
	ξ (%)	$k_a{}^a$ dm^3 mol^{-1} s^{-1}	ξ (%)	$k_a{}^a$ dm^3 mol^{-1} s^{-1}
500	0.530	(9.0±1.6)×10^7	0.399	(3.3±0.4)×10^8
1000	0.517	(1.7±0.3)×10^8	0.379	(5.9±0.9)×10^8
1500	0.470	(2.3±0.4)×10^8	0.360	(8.1±1.3)×10^8
2000	0.439	(2.8±0.4)×10^8	0.343	(9.8±1.7)×10^8
2500	0.405	(3.1±0.5)×10^8	0.333	(1.2±0.2)×10^9

[a] Mean value of 3 measurements and the corresponding standard deviation (σ).

A precise determination of k_a requires a non-labile behaviour of the complex, like the case of Cd-NTA. In situations were a significant amount of free metal is present in the test solution or the complex is quasi-labile the effective determination of k_a value becomes very difficult. The measured signal is totally dominated by the free metal with only a small contribution from the complexed species, thus the calculation of ka becomes a matter of identifying small variations on a huge background. As the concentration of ligand in the test solution increases the contribution of the free metal to the SCP signal becomes smaller. At the highest concentration of IDA, according to speciation performed using the log K and protonation parameters from the Mini-SCDatabase Academic Software, UK, 2000 [20], the free metal available is *ca.* 1.1%. In this particular case, the k_a values obtained,

especially at the higher rotation speed (2500 rpm), were closer to the k_a of 2.56×10^{10} dm^3 mol^{-1} s^{-1} calculated by the Eigen mechanism.

Additionally the pH of the test solution was increased, for the highest IDA concentration value (2.82×10^{-3} mol dm^{-3}), in order to promote a higher loss of lability of the system. The results are presented in table 6.6.

Table 6.6. Degree of lability and association rate constants obtained at the TMF-RDE for the system Pb-IDA at pH 6.0 and using a concentration of 2.82×10^{-3} mol dm^{-3}. Other conditions as indicated in Fig. 6.4.

v_{RDE} / rpm	ξ	$k_a{}^a$ / dm^3 mol^{-1} s^{-1}
500	0.307	$(3.4 \pm 0.3) \times 10^9$
1000	0.280	$(5.6 \pm 0.8) \times 10^9$
1500	0.254	$(6.9 \pm 1.2) \times 10^9$
2000	0.240	$(8.3 \pm 1.7) \times 10^9$
2500	0.227	$(9.3 \pm 2.2) \times 10^9$

[a] Mean value of 2 measurements and the corresponding standard deviation (σ).

As expected, there is a decrease in the degree of lability, ξ, of the Pb-IDA system, increasing the pH of the test solution [1], and therefore the complex becomes less labile. Although, the decrease attained by changing the pH from 5.5 to 6.0 was very small and still, the ξ values were not as lower as those obtained for the completely non-labile Cd-NTA system.

The k_a values calculated by means of Eq. 6.18, becomes closer to the theoretical value calculated from the Eigen mechanism, particularly when higher rotation speeds are applied to the carbon disk electrode . Even then, the estimation of k_a under these experimental conditions is not precise, since the Pb-IDA system is not entirely non-labile, as for the Cd-NTA system.

6.5. Conclusions

The major feature of the TMF-RDE in SSCP dynamic studies is the fact that the hydrodynamic conditions at this electrode are well defined. With the application of several rotation rates to the disk electrode, multiple determinations of k_a values can be obtained, in a short period of time and at different hydrodynamic conditions. The results obtained reveal that the TMF-RDE of thickness 9.1 nm proved to be suitable for the present experimental demands, i.e. the use of rotation rates in the range of 500-2500 rpm at the disk electrode, with a satisfactory mechanical stability and durability.

The SSCP experimental lability diagnosis is also valuable at the TMF-RDE, proving that the Pb-IDA complex is non-labile, since the limiting wave height of the SSCP wave fitted using the kinetic current equation is inferior to that expected assuming a fully labile system. As the concentration of IDA in solution increases, the complex loses lability, that is manifested by a decrease in the limiting wave height τ^* and in a deviation of the SSCP experimental wave towards negative potentials.

The TMF-RDE was used for the first time in the determination of speciation parameters, i.e. the stability constant (K) and the association rate constants (k_a), and the results highlighted that:

i) The log K computed from the shift in the half wave position in the kinetic current regime, at this electrode, is in conformity with the theoretical value for the classical system Cd-NTA and, in the case of the Pb-IDA complex, the value obtained is in reasonable agreement with the published values

ii) Some difficulties arise in the determination of k_a experimentally, especially when the analytical signal measured is totally dominated by the free metal with only a small contribution from the complexed species. Even when the contribution of the free metal concentration is very small, the estimation of the k_a values in these experimental conditions is not precise, since the Pb-IDA system is not entirely non-labile. For the Cd-NTA system that is fully non-labile, the k_a mean value obtained was $(2.88\pm0.36)\times10^{-9}$ dm^3 mol^{-1} s^{-1}, that is in reasonable agreement with a k_a of 4.05×10^{-9} dm^3 mol^{-1} s^{-1} calculated on the basis of the Eigen mechanism.

References

[1] J. P. Pinheiro, H. P. van Leeuwen, *J. Electroanal. Chem.* 570 (2004) 69.

[2] H. P. van Leeuwen, R. M. Town, J. Buffle, Rob. F. M. J. Cleven, W. Davison, J. Puy, W. H. van Riemsdijk, L. Sigg, *Environmental Science & Technology* 39-2 (2005) 8545.

[3] H. P. van Leeuwen, R. M. Town, *J. Electroanal. Chem.* 561 (2004) 67.

[4] R. F. Domingos, M. F. Benedetti, J. P. Pinheiro, *Anal. Chim. Acta* 589 (2007) 261.

[5] H. P. van Leeuwen, R. M. Town, *J. Electroanal. Chem.* 536 (2002) 129.

[6] M. Town, H. P. van Leeuwen, *J. Electroanal. Chem.* 541 (2003) 51.

[7] R. M. Town, H. P. van Leeuwen, *Electroanalysis* 16 (2004) 458.

[8] J. Koutecky, J. Koryta, *Electrochim. Acta* 3 (1961) 318.

[9] L.S. Rocha, J. P. Pinheiro, H. M. Carapuça, *J. Electroanal. Chem.* 610 (2007) 37.

[10] V. G. Levich, *Physicochemical Hydrodynamics*, Prentice-Hall, Englewood cliffs, NJ, 1962.

[11] A. J. Bard, L.R. Faulkner, *Electrochemical Methods: Fundamentals and Applications* (2nd ed.), John Wiley & Sons, Inc., New York, 2001, chap. 11-12.

[12] N. Serrano, J. M. Díaz-Cruz, C. Ariño, M. Esteban, *J. Electroanal. Chem.* 560 (2003) 105.

[13] F. M. M. Morel, J. G. Hering, *Principles and Applications of Aquatic Chemistry*, Wiley, New York, 1993, p. 400.

[14] J. Koryta, J. Dvorak, L. Kavan, *Principles of Electrochemistry* (2nd ed.), Wiley, Chichester, 1993

[15] J. Salvador, J. Puy, J. Cecilia, J. Galceran, *J. Electroanal. Chem.* 588 (2006) 33.

[16] S.C.C. Monterroso, H. M. Carapuça, J. E. J. Simão, A. C. Duarte, *Anal. Chim. Acta* 503 (2004) 203.

[17] S. C. C. Monterroso, H. M. Carapuça, A. C. Duarte, *Electroanalysis* 15 (2003) 1878.

[18] L. S. Rocha, H. M. Carapuça, J. P. Pinheiro, *Langmuir* 22 (2006) 8241.

[19] H. P. van Leeuwen, R. M. Town, *Environ. Sci. Technol.* 37 (2003) 3945.

[20] Academic Sofwtare, K. J. Poweel, Mini-SCDatabase, Academic Software, UK, 2000.

CHAPTER 7

Conclusions and Future Work

CHAPTER 7   Conclusions and Future Work

7.1. Conclusions

7.2. Future Work

7.1. Conclusions

In this work the nanometer thin mercury film electrode (TMFE) was successfully applied in the dynamic speciation of trace metals, using two different electroanalytical methods, anodic stripping voltammetry (ASV) and scanning stripping chronopotentiometry (SSCP).

The features of new cation exchange membranes were studied in order to minimize and overcome the typical interferences in the ASV determinations of metal cations. The results highlighted that the use of mixed polymeric coatings prepared from two dissimilar sulfonated polymers, NA and PSS (NA/PSS mass ratio of 5.3), allows the formation of stable thin mercury films for ASV determinations, ensuring a suitable sensitivity, charge selectivity and interesting anti-fouling features. The casting process of these mixed NA/PSS films was reproducible and allows the preparation of reliable and mechanically stable modified electrodes, by a simple preparation procedure (solvent evaporation on a glassy carbon substrate). Therefore, the reproducibility of the coatings, the incorporation of metal cations and the repeatability of the SWASV signals are improved, resembling the features of single coatings of PSS.

In addition the performance of the PSS single coating for ion-exchange voltammetry was evaluated, using different experimental conditions, i.e. the influence of the PSS solution composition, the amount deposited, the molecular weight and of the ionic strength of the external solution electrolyte. The results revealed that the best PSS electrodes were those casted from water, presenting a compact and rigid structure more resistant to solubilisation. Also, the accumulation of lead cation was favoured at a very low ionic strength of the electrolyte, despite of a higher risk of leakage and solubilisation of PSS in this medium. For these electrodes with a high negative charge density within a low volume film, although reproducible and repeatable measurements were obtained, the pre-concentration factors of the divalent metal ion were not as high (2-3 times) as we expected to be (at least 100 times).

The performance of the TMFE in the trace metal speciation by the recently developed SSCP was evaluated. The TMFE was successfully applied in SCP/SSCP measurements of metal cations for 1 day-term. The high sensitivity and resolution obtained at the TMFE and also the low deposition times which in turn are used, made this electrode an excellent complement to the conventional mercury electrodes. The calculated SSCP curves were in excellent agreement with experimental data for Pb(II) at the TMFE. When applied to the determination of complexation parameters, i.e. the stability constant (K), of labile systems (e.g. Pb(II)-PDCA and Pb(II)-carboxylated latex nanospheres), the values calculated from the shift in the SSCP half-wave potential ($\Delta E_{1/2}$), were in accordance with the ones obtained at the HMDE and those predicted by theory. Even with the adsorption of the latex nanoparticles onto the mercury coating, the results achieved highlight the fact that this technique can overcome adsorption complications, the main problem in ASV determinations of trace metals.

When applied to the kinetic current regime, it was found that the SSCP/TMFE couple is very good to detect loss of lability of the system. The log K computed from the shift in the half wave position was in conformity with the theoretical value for the classical system Cd-NTA and in reasonable agreement with the published values for the Pb-IDA complex. The major feature of the TMF-RDE in SSCP dynamic studies is the fact that the hydrodynamic conditions at this electrode are well defined, allowing multiple determinations of the association rate constant (k_a), in a short period of time and at different hydrodynamic conditions. Although, some difficulties arise in the determination of k_a experimentally, namely in situations were a significant amount of free metal is present in the test solution or the complex is quasi-labile the effective determination of k_a value becomes very difficult. For the Pb-IDA complex the accurate determinations of k_a were difficult due to the low signal obtained in true kinetic current regimes and a precise determination of k_a could be only achieved in complexes with a non-labile behaviour of the complex, such as the Cd-NTA system. Even then, this was not entirely possible (an accurate measurement of k_a) since the SCP signal of this last complex is quite small, occasionally leading to erroneous measurements of the transient time.

7.2. Future Work

In the future we would like to extend the applicability of the chemical modification of the TMFE with polyanionic films, in SSCP experiments. The main goal is not only to obtain an electrode surface mechanically more stable and more protected, but also to achieve a higher electrostatic accumulation of metal cations within the polymeric film, thus enlarging the analytical signal. An interesting approach would be the use of different charged polymer films with high charge density but sufficiently rigid in order to resist to the expansion at low ionic strengths.

Also it would be interesting to evaluate the performance of the TMFE to assess the free metal ion concentration by a new electroanalytical technique Absence of gradients and nernstian equilibrium stripping (AGNES). The main objective is the assessment and reduction of the capacitive current, which might be the key problem for lowering the limit of detection of this technique (AGNES). Furthermore, due to the small volume of the amalgam at the TMFE, the accessible area over the volume is larger and for that reason, it is expected that the deposition time needed to reach a certain preconcentration factor, will be much smaller.